



A numerical study of the Dirac Spectrum and Transmission Problems employing the Method of Fundamental Solutions

Francisco Alves Bento

Thesis to obtain the Master of Science Degree in

Applied Mathematics and Computation

Supervisors: Juha Hans Videman
Pedro Ricardo Simão Antunes

Examination Committee

Chairperson: Prof. Pedro Lima
Members of the Committee: Prof. Hugo Tavares
Prof. Pedro Serranho

September 2023

Declaro que o presente documento é um trabalho original da minha autoria e que cumpre todos os requisitos do Código de Conduta e Boas Práticas da Universidade de Lisboa.

I declare that this document is an original work of my own authorship and that it fulfills all the requirements of the Code of Conduct and Good Practices of the Universidade de Lisboa.

“If Stavrogin believes, he does not believe that he believes. And if he does not believe, he does not believe that he does not believe.”

Fyodor Dostoyevsky
Demons

Agradecimentos

À primeira vista, escrever a secção de Agradecimentos quase que toca a formalidade, pequenos parágrafos, uma minuta, curtas linhas sem floreios ou sem a escrita técnica que premeia o resto do trabalho. Porém, como no fim de qualquer etapa, tem o condão de nos levar a reavaliar todo o nosso percurso e toda a gente que tornou este trabalho possível.

Assim, o papel de destaque final vai para os meus orientadores, os professores Juha Videman e Pedro Antunes. Estou-lhes muito grato por aceitarem fazer este percurso comigo, pela disponibilidade que sempre demonstraram, pelas dúvidas esclarecidas, pela experiência e conhecimento que comigo partilharam; e claro, pela motivação e confiança que me deram e tiveram em mim.

Não poderei deixar ainda de agradecer ao Centro de Análise Matemática, Geometria e Sistemas Dinâmicos (CAMGSD), pela bolsa que me foi atribuída e sob a qual tive a oportunidade de efetuar este trabalho.

Claro, aos meus colegas e amigos que me acompanharam, pelas discussões e conversas, pelo apoio que me deram, este que foi sem dúvida importantíssimo em vários pontos, o meu obrigado. Vários houveram que ficaram pelo caminho, outros tantos que nunca souberam que dele fizeram parte, e uns poucos que de um estreita estrada fizeram áleas: a também esses agradeço (e muito!).

Mas quem nunca ficou pelo caminho foi a minha família, aos meus pais, à minha irmã, aos meus avós. Este trabalho não teria sido possível sem o vosso incondicional apoio e pelo que sempre me proporcionaram. O meu grande obrigado.

Abstract

This dissertation studies the application of the Method of Fundamental Solutions (MFS), a meshless technique, to address a duo of Partial Differential Equations (PDEs) problems. Meshless methods provide an alternative to the standard mesh-based approaches, especially suited for intricate geometries. This study is centered on two focal points: firstly, the spectral analysis of the Dirac operator with infinite mass boundary conditions, investigated through large-scale simulations; secondly, the resolution of transmission problems involving the Poisson equation within polygonal and curved domains.

Within the MFS framework, the spectral behavior of the Dirac operator is explored, both verifying existing conjectures and postulating new ones. The study also covers transmission problems with the Poisson equation, utilizing singularity subtraction techniques to improve the accuracy of the method.

This thesis starts by establishing the necessary theory, rigorously introducing and implementing the MFS, and incorporating strategies to address inherent limitations. The results presented underscore the method's validity in addressing challenging PDE problems, showcasing the effectiveness of meshless methods.

Keywords

Meshless methods; Method of Fundamental Solutions; Dirac operator; Transmission problems; Numerical simulations; Singularity subtraction techniques.

Resumo

Esta dissertação estuda a aplicação do Método das Soluções Fundamentais (MSF em português), um método sem malha, aderecendo dois distintos problemas em Equações de Derivadas Parciais (EDPs). Os métodos sem malha são uma alternativa aos clássicos métodos com malha e são particularmente adequados a geometrias mais complexas. Este estudo centra-se em dois pontos principais: primeira-mente, na análise espectral do operador de Dirac com condições de fronteira de massa infinita, que foi investigado usando simulações de larga escala; em segundo lugar, na resolução de problemas de transmissão que envolvem a equação de Poisson, tanto em domínios poligonais como curvos.

Sob a estrutura do MSF, o comportamento espectral do operador de Dirac é explorado sistematicamente, verificando conjecturas existentes e postulando novos resultados. Este estudo cobre também problemas de transmissão com a equação de Poisson, utilizando técnicas de subtração de singularidade que permitem melhorar a precisão do método.

Esta tese começa por estabelecer a teoria necessária, introduz e implementa o MSF rigorosamente, incorporando estratégias que abordam as suas inerentes limitações. Os resultados apresentados sublinham a validade do método em resolver problemas de EDPs complicados, mostrando assim a eficácia de métodos sem malha.

Palavras Chave

Métodos sem malha; Método das Soluções Fundamentais; Operador de Dirac; Problemas de Transmissão; Simulações numéricas; Técnicas de Subtração de Singularidade.

Contents

1	Introduction	1
1.1	On the applications of the Method of Fundamental Solutions	1
1.2	Thesis Overview	2
2	Some Preliminary Results	4
2.1	Some concepts on Banach spaces	4
2.2	Some concepts on Hilbert spaces	8
2.3	Lebesgue and Sobolev Spaces	12
3	From Spectral Theory and Shape Optimization to the Poisson Transmission Problem	18
3.1	The Laplace operator	19
3.1.1	Some shape optimization results	20
3.2	The Dirac operator	23
3.3	A domain decomposition problem	31
4	The Method of Fundamental Solutions	35
4.1	Density and linear independence results	35
4.2	Numerical approach for the Laplace Equation	43
4.2.1	An enrichment technique	45
4.3	Numerical approach for the Helmholtz Equation	47
5	Numerical Results	51
5.1	Dirac equation simulations	51
5.1.1	Numerical validation of the method	52
5.1.2	Quadrilateral results	53
5.1.3	Results for triangles and general polygons	56
5.1.4	Results in smooth domains	59
5.2	Transmission problem	66
5.2.1	Numerical validation of the method	68
5.2.2	Results for the rectangle	69
5.2.3	Results for an L-shape domain with basis functions enrichment	71

6 Conclusions	78
Bibliography	85
A Some details on regular domains and Sobolev spaces	86
B Spectral Decomposition of the Laplace operator	88
C Some useful insights to the Method of Fundamental Solutions	92
C.1 Behavior of the Laplace equation's solutions near a corner.	92
C.2 The Subspace Angle Technique	94
D On Bessel Functions	97

List of Figures

3.1	A wedge-like “shape” with an interior angle Θ	27
3.2	Transmission problem (rectangle example) and its associated equations.	31
4.1	A wedge-like “shape” with an interior angle Θ	46
5.1	Configuration of the boundary, source, and inner points. The number of boundary collocation points used is 1200.	52
5.2	Results obtained by the direct search algorithm for the first three eigenvalues of the disk with $m = 0$. In practice, more accurate approximations are achieved when smaller values of the smallest singular value σ_N of the matrix $Q(k)$ (studied in section C.2) are identified at each minimum.	53
5.3	Plots of the real and imaginary parts of u_1 and u_2 of the first eigenfunction $\mathbf{u} = [u_1 u_2]$. Observe that the imaginary part of u_1 is zero and the artifacts presented are due to precision lost.	54
5.4	Behavior of the first five eigenvalues for rectangles with unit area, width a and $m = 1$	55
5.5	Behavior of the first five eigenvalues for rectangles with unit area, width a and $m = 5$	55
5.6	Behavior of the first five eigenvalues for rectangles with perimeter $L = 4$, width a and $m = 1$	55
5.7	Behavior of the first five eigenvalues for rectangles with perimeter $L = 4$, width a and $m = 5$	55
5.8	Plot of the first three eigenvalues against the perimeter for $m = 1$ for quadrilaterals. The “outliers” marked in black represent the domains in which the third eigenvalue is smaller than the third eigenvalue of the disk.	57
5.9	Ratio between the first two eigenvalues $\frac{\lambda_2}{\lambda_1}$ plotted against the perimeter for $m = 1$ for quadrilaterals, as in Figure 5.8.	57
5.10	Ratio between the third and first eigenvalues $\frac{\lambda_3}{\lambda_1}$ plotted against the perimeter for $m = 1$ for quadrilaterals, as in Figure 5.8.	57
5.11	Configuration space of the admissible triangles. The dashed red line shows a subequilateral triangle; the dashed blue line a superequilateral triangle.	58

5.12 Plot of the first three eigenvalues against the perimeter for triangular domains.	59
5.13 Ratio between the first two eigenvalues $\frac{\lambda_2}{\lambda_1}$ for triangular domains.	59
5.14 Plot of the first eigenvalue $\lambda_1(x, y)$ for each sample point $(x, y) \in R$ for triangular domains.	59
5.15 Plot of the first three eigenvalues against the area with perimeter $L = 15$ for triangular domains.	60
5.16 Numerical simulations in the first eigenvalue of general pentagons.	61
5.17 Numerical simulations in the first eigenvalue of general hexagons.	61
5.18 Numerical simulations in the first eigenvalue of general heptagons.	61
5.19 Numerical simulations in the first eigenvalue of general octagons.	61
5.20 Smooth domain generated by B-splines.	62
5.21 Magnitude of the first three eigenvalues plotted against the perimeter length in smooth domains. The “outliers” marked in black represent the domains in which the third eigenvalue is less than the third eigenvalue of the disk.	63
5.22 Ratio between the first two eigenvalues $\frac{\lambda_2}{\lambda_1}$ for smooth domains.	63
5.23 Ratio between the third and first eigenvalues $\frac{\lambda_3}{\lambda_1}$ for smooth domains.	63
5.24 Optimal domain Ω^* (drawn in orange) and the initial domain (in blue) used in the first iteration of the Nelder-Mead algorithm.	64
5.25 The first three eigenvalues in domains defined by the Minkowski sum Ω_t and plotted for the values of $t \in [0, 1]$ increasing from left to right.	64
5.26 Real and imaginary parts of u_1 and u_2 of the third eigenfunction $\mathbf{u} = [u_1 u_2]$ associated with the optimal domain Ω^*	65
5.27 Configuration of the boundary, source, and interface points. Each domain has 600 boundary points, 377 source points and the common interface has 100 points.	69
5.28 Numerical approximation of the solution u of the Boundary Value Problem (BVP) (5.7) using the configuration presented in Figure 5.27. The colorbar shows the values of u	69
5.29 Numerical simulation with $k_1 = 1$	70
5.30 Numerical simulation with $k_1 = 2$	70
5.31 Numerical simulation with $k_1 = 5$	70
5.32 L-shaped domain with a vertical interface. Configuration of the boundary, source, and interface points.	72
5.33 Numerical approximation of the transmission problem in an L-shaped domain with interface along $x = 0$ and $k_1 = 5$	72
5.34 L-shaped domain with the interface on the symmetry axis. Configuration of the boundary, source, and interface points.	75
5.35 Interface ϵ_γ^0 error.	77

5.36 Interface ϵ_γ^1 error.	77
5.37 Absolute value of the interface errors and numerical approximation for $k_1 = 2$, $p_1 = -2, -1, 0, 1$ and $p_2 = 0, 1$	77
C.1 Rotation of the wedge domain.	94
D.1 Complex plot of the absolute value of the Bessel function $J_\nu(z)$ with $\nu = 0$ in the complex plane from $-2 - 2i$ to $2 + 2i$. The plots are colored by the argument of the function and the colorbar shows its variation from $-\pi$ to π	98
D.2 Complex plot of the absolute value of the Bessel function $Y_\nu(z)$ with $\nu=0$ in the complex plane from $-2 - 2i$ to $2 + 2i$. The plots are colored by the argument of the function and the colorbar shows its variation from $-\pi$ to π	98
D.3 Complex plot of the absolute value of the Hankel function $H_\nu^{(1)}(z)$ with $\nu = 0$ in the complex plane from $-2 - 2i$ to $2 + 2i$. The plots are colored by the argument of the function and the colorbar shows its variation from $-\pi$ to π	99
D.4 Complex plot of the absolute value of the Hankel function $H_\nu^{(2)}(z)$ with $\nu=0$ in the complex plane from $-2 - 2i$ to $2 + 2i$. The plots are colored by the argument of the function and the colorbar shows its variation from $-\pi$ to π	99
D.5 Plot of the real part of $\Phi_k(r)$ with $k = 1.5$ in the disk of radius 10.	102
D.6 Plot of the imaginary part of $\Phi_k(r)$ with $k = 1.5$ in the disk of radius 10.	102

List of Tables

5.1	Eigenvalues for different values of N and the measured absolute error.	53
5.2	Numerical errors at the boundaries $\partial\Omega_1$ and $\partial\Omega_2$ and in the domains Ω_1 and Ω_2	69
5.3	Numerical errors at the interface γ . The condition number of the matrix is also presented.	70
5.4	Consistency errors on the boundary and at the interface γ	71
5.5	Consistency errors on the boundary and in the interface γ	72
5.7	Consistency errors on the boundary and at the interface γ after enriching the basis with particular (angular) solutions.	74
5.8	Consistency errors on the boundary and at the interface γ	74
5.10	Consistency errors on the boundary and at the interface γ after adding particular (angular) solutions to the classical Method of Fundamental Solutions (MFS) basis.	76

List of Algorithms

4.1	Direct Bracketing Algorithm	49
-----	---------------------------------------	----

Acronyms

BFGS	Broyden–Fletcher–Goldfarb–Shanno algorithm
BVP	Boundary Value Problem
MFS	Method of Fundamental Solutions
PDE	Partial Differential Equation
RBF	Radial Basis Function
RMSE	Root Mean Squared Error

1

Introduction

1.1 On the applications of the Method of Fundamental Solutions

Partial Differential Equations (PDEs) serve as fundamental tools for modeling a wide spectrum of phenomena across scientific disciplines, ranging from engineering and physics to biology and finance. Given the complexity and infeasibility of deriving analytical solutions for many cases, accurate numerical solutions have become imperative. While well-established methods like finite differences and finite elements are available for a wide range of PDEs, meshless methods offer an effective alternative, particularly for intricate geometries. This dissertation studies the Method of Fundamental Solutions (MFS), a meshless technique, investigating its applications in solving two distinctive problem domains: the spectral analysis of the Dirac operator under infinite mass boundary conditions, and transmission problems involving the Poisson equation within polygonal and curved domains.

Emerging in the latter part of the previous century, meshless methods provide an alternative to traditional mesh-based approaches, circumventing the challenges of mesh generation in complex geometries. Drawing inspiration from potential and integral equations theory, the more recent Method of Fundamental Solutions approximates solutions by exploiting the fundamental solutions of governing PDEs.

It has garnered attention for solving eigenvalue problems, as seen in [AA13], [Reu06], and [AF11]. We aim to uncover the MFS's capabilities in addressing various PDEs challenges, thereby providing valuable insights into the systems under examination.

The spectral analysis of the Dirac operator under infinite mass boundary conditions, a problem classified as pivotal in shape optimization theory by [KLL19], plays a critical role not only in our comprehension of quantum mechanics and quantum field theory but also in engineering applications, for example in the study of the so-called *Dirac materials* like graphene. Our focus is centered on comprehending the spectral behavior of this operator. By employing the Method of Fundamental Solutions we strive to offer numerical insights that both validate existing conjectures and engender new ones.

Shifting our attention to transmission problems for the Poisson equation, which holds significance in fields like heat conduction, electromagnetism, and contact mechanics, we employ the MFS to investigate solutions within polygonal and curved domains. This study goes into the complexities introduced by interfaces and compatibility conditions in such scenarios. In order to increase the precision of the method, we incorporate methodologies to enhance the MFS, integrating singularity subtraction techniques to heighten accuracy, especially in proximity to the domain's corners. Importantly, this study marks the first instance of utilizing this technique with the Method of Fundamental Solutions for these specific problems.

In subsequent sections, comprising theoretical foundations and numerical methodologies, our objective is to present a straightforward perspective of the MFS's role in addressing complex PDEs problems. This study not only furthers our understanding of meshless approaches but also bridges the gap between numerical simulation and theoretical research, serving as a source of new and challenging problems.

1.2 Thesis Overview

This thesis is structured into six distinct chapters, each organized as follows:

- Chapter 2 introduces foundational concepts in Functional Analysis and Partial Differential Equations. While the majority of these results can be found in classical references and are often covered in graduate courses, they serve as support for the subsequent chapters. Notably, Chapter 4 draws heavily upon these concepts to establish the theoretical framework of the Method of Fundamental Solutions.
- Chapter 3 serves as an introduction to the problems investigated within this thesis and is divided into three distinct sections. In the initial section, some analysis of the Laplace operator is done, presenting established results and conducting a small literature review. Although not directly connected with the study of the Dirac operator, the similarities between the two lead to the conjecture that significant findings of the Laplace operator could extend to the Dirac problem with infinite mass

boundary conditions. This section also serves as a basis for the formulation of new conjectures concerning the Dirac operator's spectrum.

A subsequent portion of this chapter focuses on the exploration of the Dirac operator. It introduces the operator, elucidates some of its properties, and highlights its spectral characteristics. Additionally, a concise yet insightful proof demonstrates the absence of separable solutions in polar coordinates, extending what was previously known for cartesian coordinates. Recent conjectures postulated by field experts are presented, and novel conjectures, influenced by the prior analysis of the Laplace operator, are introduced. These conjectures subsequently become subjects of investigation using the MFS, enabling a comprehensive exploration of their validity and implications.

Finally, the third section of this chapter centers on the Poisson transmission problem in the divergence form. It establishes the problem's context and its relationship with the Poisson equation when featuring a discontinuous source term. This section adopts a modern approach to analyze the relation between the transmission problem and the classical Poisson equation. This examination is important for the subsequent application of the MFS, and it will be needed to theoretically justify the use of the method in Chapter 4.

- Chapter 4 introduces the MFS, and presents density proofs that justify this numerical method for various problems, improving both the rigor and the details. It also presents convergence and stability results, discusses the advantages and disadvantages of the method, and different ways to address its weaknesses, specifically an enrichment technique using particular (angular) solutions responsible for singularity subtraction. Finally, a numerical implementation of the MFS and a direct search algorithm used in finding the eigenvalues are presented.
- In Chapter 5, we present our numerical findings, organized into two distinct sections. The initial section examines the Dirac operator with infinite mass boundary conditions, involving extensive large-scale simulations. Subsequently, outcomes for various domain shapes, including quadrilaterals, triangles, general n -side polygons for $n = 5, 6, 7, 8$, and smooth domains, are outlined, emphasizing the pertinent discoveries. This section concludes by addressing an unconstrained minimization problem aimed at identifying optimal shapes. The second section is dedicated to the transmission problem, focusing on numerical errors and the use of enrichment techniques to enhance the method's accuracy. These results are supplemented with visual aids and concise tables summarizing our findings.
- Finally, Chapter 6, presents the relevant conclusions of this dissertation and proposes future work related to this research topic.

2

Some Preliminary Results

2.1 Some concepts on Banach spaces

This subchapter begins by introducing preliminary concepts on Banach spaces, which play a crucial role in the subsequent numerical methods to be presented. For more details see [Rud91] or [Bré11]. Consider a field \mathbb{F} (\mathbb{R} or \mathbb{C}). We say that a vector space E is a *normed space* if there exists a map $\|\cdot\|$ (called a *norm*) over \mathbb{F} such that for every $x, y \in E$

1. $\|\alpha x\| = |\alpha| \|x\|$, $\alpha \in \mathbb{F}$;
2. $\|x + y\| \leq \|x\| + \|y\|$;
3. $\|x\| \geq 0$;
4. $\|x\| = 0 \iff x = 0$.

In particular, a pivotal notion is of *Banach spaces*, i.e., E is a Banach space if it is a complete normed space.

Definition 2.1.1. Consider a linear operator $T : \text{Dom}(T) \subset E \rightarrow F$, whose domain is represented by $\text{Dom}(T)$, where E and F are Banach spaces with the associated norms $\|\cdot\|_E$ and $\|\cdot\|_F$, respectively. Then

1. The **kernel** (also called the **nullspace**) of T is a subset of E such that

$$\ker(T) = \{x \in E : Tx = 0\}.$$

Accordingly, the **range** (also called the **image**) of T is a subset of F such that

$$R(T) = \{y \in F : \text{there exists some } x \in E \text{ such that } y = Tx\}.$$

2. T is said to be **bounded** (continuous) if there exists $C > 0$ such that $\|Tx\|_F \leq C\|x\|_E$. The operator norm of T is defined as

$$\|T\| = \sup_{\substack{x \in E \\ x \neq 0}} \frac{\|Tx\|_F}{\|x\|_E}.$$

In this case, we write $T \in \mathcal{L}(E, F)$. If $E = F$, we write $T \in \mathcal{L}(E)$;

3. The space of linear and continuous maps from E to \mathbb{R} is the **dual space** of E denoted by E^* . If $S \in E^*$, its norm (the dual norm) is defined in the same manner as the operator norm above, i.e.,

$$\|S\| = \sup_{\substack{x \in E \\ x \neq 0}} \frac{|\langle S, x \rangle|}{\|x\|}$$

where $\langle S, x \rangle_{E^*, E} = Sx$ and denotes the duality pairing between E^* and E . As we will see below, it generalizes the notion of inner product in inner product spaces. Whenever it is obvious what dual pairing is being considered we just write $\langle \cdot, \cdot \rangle$;

4. Assuming that T is bounded, T is said to be **compact** if for any bounded sequence $(u_n)_{n \in \mathbb{N}} \subset E$ there exists a subsequence $(u_{n_k})_{k \in \mathbb{N}}$ such that $(Tu_{n_k})_{k \in \mathbb{N}}$ converges in F ;
5. Assume that $\text{Dom}(T)$ is dense in E . The linear operator $T^* : \text{Dom}(T^*) \subset F^* \rightarrow E^*$ is said to be the **adjoint** of T if

$$\langle v, Tu \rangle_{F^*, F} = \langle T^*v, u \rangle_{E^*, E}, \quad \forall v \in \text{Dom}(T^*),$$

where the domain of T^* is defined by

$$\text{Dom}(T^*) = \{v \in F^* : \exists c \geq 0 \text{ such that } |\langle v, Tu \rangle_{F^*, F}| \leq c\|u\|, \quad \forall u \in \text{Dom}(T)\}.$$

The main result of this section concerns the dual of a normed space. In reality, we do not need to assume that E is a Banach space to present the next results. However, throughout this work, every normed space is also complete. We refer to Chapters 1 and 3 from [Bré11].

Definition 2.1.2 (Reflexive space). *Let E be a normed space and denote its dual by E^* . The bidual space E^{**} is the dual of E^* with the associated norm*

$$\|\xi\| = \sup_{\substack{f \in E^* \\ f \neq 0}} \frac{|\langle \xi, f \rangle|}{\|f\|}.$$

*If the (canonical) map $J : E \rightarrow E^{**}$ defined by*

$$\langle Jx, f \rangle_{E^{**}, E^*} = \langle f, x \rangle_{E^*, E}, \quad \forall x \in E, \forall f \in E^*$$

is surjective then E is said to be reflexive.

The definition above is an important detail in the justification of the Method of Fundamental Solutions. The main ingredient to justify this numerical method is the Hahn-Banach Theorem.

Theorem 2.1.3 (Analytical form of Hahn-Banach Theorem). *Let E be a normed space and $p : E \rightarrow \mathbb{R}$ a functional satisfying*

$$\begin{aligned} p(\lambda x) &= \lambda p(x), \quad \lambda > 0 \\ p(x + y) &\leq p(x) + p(y), \end{aligned}$$

for every $x, y \in E$. Let $G \subset E$ be a linear subspace and $g : G \rightarrow \mathbb{R}$ a linear functional such that

$$g(x) \leq p(x), \quad \forall x \in G.$$

Then, there exists a linear functional $f : E \rightarrow \mathbb{R}$ that extends g to E , coincides with g on G , i.e., $f(x) = g(x)$, $\forall x \in G$ and also satisfies

$$f(x) \leq p(x), \quad \forall x \in E.$$

Remark 2.1.4. *The Theorem mentioned above holds particular significance in Functional Analysis as it demonstrates that the dual E^* of a normed space E possesses interesting properties which can be studied to gain a better understanding of the underlying space E . It can even be utilized to identify, although not uniquely, elements in both E and its dual E^* through duality pairing. This result bears a resemblance to the desirable properties exhibited by Hilbert spaces, which we will explore further in this chapter. Later, it will be used to establish the density of a subset in the whole space when working with the dual pairing between a Banach space and its dual. However, it is important to note that the existence of the functional f is not explicitly provided, as the proof of Theorem 2.1.3 relies on the Axiom of Choice (Zorn's Lemma).*

Under some conditions, an interesting consequence of Theorem 2.1.3 is that two disjoint (and non-empty) convex sets can always be separated by a hyperplane in an infinite-dimensional space.

Definition 2.1.5. Let E be a normed space, f a linear functional on E , and $c \in \mathbb{R}$. A hyperplane H is a subset of E of the form

$$H = \{x \in E : \langle f, x \rangle = c\}.$$

Proposition 2.1.6. Let H be a hyperplane defined by the equation $\langle f, x \rangle = c$, for some linear functional f and $c \in \mathbb{R}$. Then, H is closed if and only if f is continuous.

Notice that if H is a closed hyperplane then the linear functional f that defines the hyperplane is an element of E^* .

Definition 2.1.7. Let A and B be two subsets of E . We say that a hyperplane H defined by the equation $\langle f, x \rangle = c$, for some linear functional f and $c \in \mathbb{R}$, strictly separates A and B if

$$\langle f, x \rangle < c, \forall x \in A,$$

$$\langle f, x \rangle > c, \forall x \in B.$$

Theorem 2.1.8 (Second, geometric, form of the Hahn-Banach Theorem). Let A and B be two disjoint, non-empty, and convex subsets of E such that A is closed and B is compact. Then, there exists a closed hyperplane that strictly separates A and B , i.e., there exists $f \in E^*$ and $c \in \mathbb{R}$ such that for every $a \in A$ and $b \in B$

$$\langle f, a \rangle < c < \langle f, b \rangle.$$

The following Lemma is a consequence of Theorem 2.1.8, and it is a useful tool to prove that some linear subspace $M \subset E$ is dense (in E). We start by introducing the notion of orthogonality in Banach spaces concerning duality pairing, see [Bré11] for more details.

Definition 2.1.9. Let E be a Banach Space and M be a linear subspace of E . We define the orthogonal of M in E in respect to the duality pairing as

$$M^\perp = \{\psi \in E^* : \langle \psi, \varphi \rangle = 0, \forall \varphi \in M\}.$$

Accordingly, if $N \subset E^*$ is a linear subspace, its orthogonal is defined as

$$N^\perp = \{\varphi \in E : \langle \psi, \varphi \rangle = 0, \forall \psi \in N\}$$

Lemma 2.1.10. Let M and N satisfy the same conditions in the definition above. Then

$$(M^\perp)^\perp = \overline{M}$$

and

$$\overline{N} \subset (N^\perp)^\perp.$$

In particular, if E is a reflexive Banach space then

$$(N^\perp)^\perp = \overline{N}.$$

Proof. Since $(M^\perp)^\perp \subset E$ and $(N^\perp)^\perp \subset E^*$ are closed sets and by definition $M \subset (M^\perp)^\perp$ and $N \subset (N^\perp)^\perp$, then the inclusions

$$\overline{M} \subseteq (M^\perp)^\perp, \quad \overline{N} \subseteq (N^\perp)^\perp$$

follow. To check that $(M^\perp)^\perp \subseteq \overline{M}$ we argue by contradiction. Let $x_0 \in (M^\perp)^\perp$ such that $x_0 \notin \overline{M}$. Then, by Theorem 2.1.8 there exists a hyperplane with equation $\langle f, x \rangle = c$ for some $f \in E^*$ and $c \in \mathbb{R}$ that strictly separates the sets $\{x_0\}$ and \overline{M} (both are obviously non-empty convex sets). In particular,

$$\langle f, x \rangle_{E^*, E} < c < \langle f, x_0 \rangle_{E^*, E}, \quad \forall x \in M.$$

Since M is a linear subspace, then $\langle f, x \rangle = 0$, $\forall x \in M$ since, otherwise, given any $x \in M$ we would have that

$$\alpha \langle f, x \rangle_{E^*, E} = \langle f, \alpha x \rangle_{E^*, E} < c, \quad \forall \alpha \in \mathbb{R}$$

which can only be possible if $\langle f, x \rangle_{E^*, E} = 0$. Therefore, $f \in M^\perp$ and $\langle f, x_0 \rangle_{E^*, E} > 0$ but that is a contradiction since, by hypothesis, $x_0 \in (M^\perp)^\perp$ and $\langle f, x_0 \rangle_{E^*, E} = 0$, $\forall f \in M^\perp$.

To prove that $(N^\perp)^\perp = \overline{N}$, we use the same type of argument. Let $f_0 \in (N^\perp)^\perp$ such that $f_0 \notin \overline{N}$. Once again, there exists a hyperplane with equation $\langle \xi, f \rangle = c$ for some $\xi \in E^{**}$ and $c \in \mathbb{R}$ that strictly separates $\{f_0\}$ and \overline{N} , that is

$$\langle \xi, f \rangle < c < \langle \xi, f_0 \rangle, \quad \forall f \in N.$$

Since N is a linear subspace we can also conclude that $\langle \xi, f \rangle = 0$, $\forall f \in N$ and $\langle \xi, f_0 \rangle > 0$. In order to get a contradiction, like in the case above, since E is a reflexive space, then the canonical map J defined in (2.1.2) is surjective, and we can write

$$\langle \xi, f_0 \rangle_{E^{**}, E^*} = \langle Jx_0, f_0 \rangle_{E^{**}, E^*} = \langle f_0, x_0 \rangle_{E^*, E}$$

for some $x_0 \in E$. If we can prove that $\langle f_0, x_0 \rangle_{E^*, E} = 0$, then the contradiction follows. Since $f_0 \in (N^\perp)^\perp$, then $\langle f_0, x_0 \rangle_{E^*, E} = 0$ if $x_0 \in N^\perp$, i.e., $\langle f, x_0 \rangle_{E^*, E} = 0$, $\forall f \in N$. Let $f \in N$. Then, by reflexivity,

$$\langle f, x_0 \rangle_{E^*, E} = \langle Jx_0, f \rangle_{E^{**}, E^*} = \langle \xi, f \rangle_{E^{**}, E^*} = 0, \quad \forall f \in N$$

as we saw above (N is a linear subspace). The desired result follows. \square

Remark 2.1.11. The Lemma 2.1.10 will be used in justifying the Method of Fundamental Solutions. To prove that some subset N of E^* is dense in E and E^* it will suffice to show that its orthogonal N^\perp contains only the trivial element, which belongs to both E and E^* .

2.2 Some concepts on Hilbert spaces

In this section, we introduce some complementary results in Hilbert spaces. Once again, for more details, see [Rud91], [Bré11], or [AU10]. Consider the field \mathbb{F} (\mathbb{R} or \mathbb{C}). We say that a vector space H is

an *inner product space* (or a Pre-Hilbert space) if there exists a map (\cdot, \cdot) (called an *inner product*) over \mathbb{F} such that for every $x, y \in H$

1. $(x, y) = \overline{(y, x)}$ (The bar denotes complex conjugation if $\mathbb{F} = \mathbb{C}$);
2. $(x + y, z) = (x, z) + (y, z)$;
3. $(\alpha x, y) = \alpha(x, y)$, $\alpha \in \mathbb{F}$;
4. $(x, x) \geq 0$;
5. $(x, x) = 0 \iff x = 0$.

Given $x, y \in H$, we say that x and y are orthogonal (denoted by $x \perp y$) if $(x, y) = 0$. Accordingly, given $E, F \subset H$, if $x \perp y$ for every $x \in E, y \in F$ then we say that E and F are orthogonal, and write $E \perp F$. We also denote by E^\perp the set of all $y \in H$ orthogonal to every $x \in E$, i.e., $E^\perp = \{y \in H : (x, y) = 0, \forall x \in E\}$ which we call the orthogonal complement of E . We recall that every inner product space is also a normed space, where the inner product induces the norm

$$\|x\| = \sqrt{(x, x)}$$

satisfying the Cauchy-Schwarz inequality

$$|(x, y)| \leq \|x\| \|y\|, \quad x, y \in H.$$

Finally, if the normed space is complete for the induced norm, then we say that it is a Hilbert space. In what follows, H will always denote a Hilbert space.

Example 2.2.1. A classical Hilbert space, which is used throughout this work, is the space of square-integrable real-valued functions in an open and bounded subset Ω of \mathbb{R}^d . This space is denoted by $L^2(\Omega)$ with the inner product given by

$$(f, g)_{L^2(\Omega)} = \int_{\Omega} f(x)g(x)dx.$$

In Hilbert spaces, proving the density of a subspace $M \subset H$ is more intuitive and can be derived straightforwardly. The following results can be compared with Definition (2.1.9) and Lemma 2.1.10.

Theorem 2.2.2. Consider a closed subspace $M \subset H$. Then,

$$H = M \oplus M^\perp.$$

In other words, every $u \in H$ admits a unique decomposition $u = v + w$, where $v \in M$ and $w \in M^\perp$.

Corollary 2.2.3. Consider a subspace $M \subset H$. Then M is dense in H if and only if $M^\perp = \{0\}$.

Proof. Let $T = \overline{M}$. We want to prove that $T = H$. Using Theorem 2.2.2, it suffices to check that $T^\perp = \{0\}$. Since the inner product is continuous, then $T^\perp = M^\perp = \{0\}$.

On the other hand, since by definition T is closed, by Theorem 2.2.2 we have that $H = T \oplus T^\perp = T \oplus \{0\} = T$ as we wished. \square

A fundamental result in Hilbert spaces is the fact that every linear and continuous function $T : H \rightarrow \mathbb{F}$ can be *represented* by some unique element in H . In what follows we assume that $\mathbb{F} = \mathbb{R}$.

Theorem 2.2.4 (Riesz Representation Theorem). *Let $T : H \rightarrow \mathbb{R}$ be a linear and continuous functional. Then, there exists a unique $u \in H$ such that*

$$Tv = (u, v), \quad \forall v \in H.$$

Moreover, let H^ be the dual space of H . Then the map $H^* \mapsto H$ is an isometric isomorphism (which we denote by \cong) where*

$$\|u\|_H = \|T\|_{H^*}.$$

Remark 2.2.5. *Notice how the inner product in Hilbert spaces has replaced the duality pairing defined in Banach spaces. In fact, Riesz Representation Theorem 2.2.4 allows us to make a stronger statement regarding the dual spaces of Hilbert spaces and work in a more natural framework without ever resorting to the Hahn-Banach Theorem 2.1.3. For example, it is interesting to observe that the definition of orthogonality and orthogonal subspaces in Hilbert spaces (via the inner product) and Banach spaces (via the duality pairing) are essentially the same, with the distinction being an isomorphism between the Hilbert space and its dual. However, in certain cases, working with the definition of orthogonality in Banach spaces can be more useful as it allows for a better generalization, as in proving the density of a closed subspace.*

A generalization of the Theorem 2.2.4 is the Lax-Milgram Theorem.

Definition 2.2.6. *A bilinear form $a : H \times H \rightarrow \mathbb{R}$ is continuous and coercive if there exists some constants $C > 0$ and $\alpha > 0$ such that*

- $|a(u, v)| \leq C \|u\| \|v\|, \quad \forall u, v \in H,$
- $a(u, u) \geq \alpha \|u\|^2, \quad \forall u \in H,$

respectively.

Theorem 2.2.7 (Lax-Milgram Theorem). *Let $a(\cdot, \cdot)$ be a bilinear, continuous, and coercive bilinear form on H . If T is a linear and continuous functional in H , then there exists a unique $u \in H$ such that*

$$a(u, v) = T(v), \quad \forall v \in H.$$

Aiming at stating the well-known Spectral theorem, we will first present some key results and concepts (without proof).

Definition 2.2.8. A sequence $(e_n)_{n \in \mathbb{N}} \in H$ is a Hilbert basis of H if

1. $(e_n, e_m) = \begin{cases} 1, & n = m; \\ 0, & n \neq m \end{cases}$;
2. $\overline{\text{span}\{(e_n)_{n \in \mathbb{N}}\}} = H$.

In a sense, a Hilbert basis resembles a basis in a finite-dimensional vector space.

Proposition 2.2.9. Let $(e_n)_{n \in \mathbb{N}}$ be a Hilbert basis of H . Then, for every $u \in H$, one can write

$$u = \sum_{k \in \mathbb{N}} (u, e_k) e_k \quad \text{and} \quad \|u\|^2 = \sum_{k \in \mathbb{N}} |(u, e_k)|^2.$$

The last equality is known as Parseval's identity.

The proposition 2.2.9 is particularly interesting because it allows us to express every element of H in terms of a countable basis. Theorem 2.2.11 below guarantees the existence of a Hilbert basis.

Definition 2.2.10. We say that H is a separable Hilbert space if there exists a countable subset $M \subset H$ such that $\overline{M} = H$.

Theorem 2.2.11. Every separable Hilbert space admits an orthonormal Hilbert basis.

Definition 2.2.12. Consider a linear operator $T : H_1 \rightarrow H_2$, where H_1 and H_2 are Hilbert spaces.

1. Assume that $H = H_1 = H_2$ and $T \in \mathcal{L}(H)$. T^* is said to be the **adjoint** of T if

$$(y, Tx) = (T^*y, x), \quad \forall x, y \in H;$$

If $T = T^*$, i.e., if the domains (and images) of T and T^* coincide then T is said to be **self-adjoint**.¹

2. Let $T \in \mathcal{L}(H)$ and $\mathbb{F} = \mathbb{R}$. The **resolvent set** of T is defined as

$$\rho(T) = \{\lambda \in \mathbb{R} : T - \lambda I \text{ is bijective from } H \text{ to } H\}$$

and $\sigma(T) = \mathbb{R} \setminus \rho(T)$ is called the **spectrum** of T . One says that $\lambda \in \mathbb{F}$ is an **eigenvalue**² of T if $\ker(T - \lambda I) \neq \{0\}$. Also, u is said to be an **eigenvector** associated with the eigenvalue λ if $u \in \ker(T - \lambda I) \setminus \{0\}$.

¹The existence and uniqueness of T^* may not be obvious, but it follows from Riesz Representation Theorem 2.2.4. In any case, notice the similarities between this definition and the one given in Definition (2.1.1). In fact, in Banach spaces, the existence of the adjoint also follows from the Hahn-Banach Theorem 2.1.3!

²Remarkably, in the infinite-dimensional case, the set of eigenvalues may not coincide with the spectrum $\sigma(T)$. $T - \lambda I$ may fail to be invertible even if $T - \lambda I$ is injective.

Next, we present some important properties regarding the spectrum of a compact operator and of a self-adjoint operator.

Proposition 2.2.13. *Let H be a Hilbert space and consider a compact operator $T \in \mathcal{L}(H)$. Then,*

- $0 \in \sigma(T)$;
- *one of the following holds:*
 - $\sigma(T) = \{0\}$;
 - $\sigma(T) \setminus \{0\}$ *is a finite set*;
 - $\sigma(T) \setminus \{0\}$ *is a sequence converging to 0*.

Proposition 2.2.14. *Let H be a Hilbert space and consider a self-adjoint operator $T \in \mathcal{L}(H)$. Then, $\sigma(T)$ is real and the eigenvectors corresponding to distinct eigenvalues are orthogonal.*

It is now possible to state one of the main results of this section.

Theorem 2.2.15 (Spectral Theorem for compact and self-adjoint operators). *Let H be a separable Hilbert space of infinite dimension and let $T \in \mathcal{L}(H)$ be a compact self-adjoint operator. Then, H admits a Hilbert basis $(e_n)_{n \in \mathbb{N}}$ such that*

$$Te_n = \lambda_n e_n$$

for $\lambda_n \in \mathbb{R}$, $\lambda_n \rightarrow 0$ as $n \rightarrow \infty$, where λ_n can be assumed to be a decreasing sequence.

2.3 Lebesgue and Sobolev Spaces

In this subchapter, we make a brief introduction to Lebesgue and Sobolev spaces theory. The results presented in this section can be found, e.g., in [LM12] and [Eva22]. The lecture notes [Tav] were also consulted. Let $\Omega \subset \mathbb{R}^d$ be an open set. Consider a *multi-index* $\alpha = (\alpha_1, \dots, \alpha_d) \in \mathbb{N}_0^d$, and let $|\alpha| = \alpha_1 + \dots + \alpha_d$. Given a function u defined in Ω , we denote its partial derivatives of order α by

$$D^\alpha u = \frac{\partial^{|\alpha|}}{\partial x_1^{\alpha_1} \dots \partial x_d^{\alpha_d}} u.$$

As usual, we denote the space of test functions with compact support in Ω by

$$\mathcal{D}(\Omega) = C_0^\infty(\Omega) = \{\varphi \in C^\infty(\Omega) : \text{supp } \varphi \text{ is compact in } \Omega\}.$$

Definition 2.3.1 (Lebesgue spaces). *Let $1 \leq p \leq \infty$. We define the Lebesgue space (L^p space)*

$$L^p(\Omega) = \left\{ u : \Omega \rightarrow \mathbb{R} : u \text{ is measurable and } \int_{\Omega} |f|^p dx < \infty \right\}$$

with the associated norm

$$\|f\|_{L^p(\Omega)} = \left(\int_{\Omega} |f|^p dx \right)^{\frac{1}{p}}.$$

If $p = \infty$ we set

$$L^\infty(\Omega) = \left\{ u : \Omega \rightarrow \mathbb{R} : u \text{ is measurable and } \exists C > 0 : |f(x)| \leq C \text{ a.e. on } \Omega \right\}$$

with the associated norm

$$\|f\|_{L^\infty(\Omega)} = \inf \{ C : |f(x)| \leq C \text{ a.e. on } \Omega \}.$$

Definition 2.3.2. We say that $f \in L^1_{\text{loc}}(\Omega)$ if f is integrable in every compact $K \subset \Omega$, i.e.,

$$f\chi_K \in L^1(\Omega), \forall K \subset \Omega \text{ compact},$$

where χ_K is the characteristic function of the set K given by

$$\chi_K(x) = \begin{cases} 1 & \text{if } x \in K \\ 0 & \text{if } x \notin K. \end{cases}$$

This definition can be extended accordingly to every $L^p(\Omega)$ space, with $1 \leq p \leq \infty$.

Before introducing the notion of weak derivative in Sobolev spaces, it will be useful to dive into some Distribution theory. Consider the space of test functions $\mathcal{D}(\Omega) := C_0^\infty(\Omega)$. While we are not interested in defining a topology in this space, we want to characterize linear and continuous functionals acting on $\mathcal{D}(\Omega)$. For now, it suffices to define (sequential) convergence in $\mathcal{D}(\Omega)$.

Definition 2.3.3. For all $n \in \mathbb{N}$, let $(\varphi_n)_n \in \mathcal{D}(\Omega)$ and $\varphi \in \mathcal{D}(\Omega)$. If

1. $\forall n \in \mathbb{N}$ there exists a compact set $K \subseteq \Omega$ such $\text{supp } \varphi_n \subseteq K$;
2. $\forall \alpha \in \mathbb{N}_0^d, \lim_{n \rightarrow \infty} \|D^\alpha \varphi_n - D^\alpha \varphi\|_{L^\infty(\Omega)} = 0$

then we say that φ_n converges to φ in $\mathcal{D}(\Omega)$.

Definition 2.3.4 (Space of distributions). The dual space of $\mathcal{D}(\Omega)$, denoted by $\mathcal{D}^*(\Omega)$, is called the space of distributions, and we say that any element belonging to \mathcal{D}^* is a distribution.

A very illustrative example, with consequences when defining the duality pairing in Sobolev spaces, is that any locally integrable function $u \in L^1_{\text{loc}}(\Omega)$ defines a distribution. It is easy to prove that the operator T_u defined by

$$\begin{aligned} T_u : \mathcal{D}(\Omega) &\rightarrow \mathbb{R} \\ \varphi &\mapsto \int_{\Omega} u\varphi dx \end{aligned}$$

is linear and continuous. Therefore, one can give meaning to the action of a distribution over a test function, whenever the distribution is induced by a locally integrable function u . In this case, we can write

$$\langle u, \varphi \rangle_{D^*(\Omega), D(\Omega)} = \int_{\Omega} u \varphi dx$$

where the duality pairing $\langle \cdot, \cdot \rangle_{D^*(\Omega), D(\Omega)}$ can be seen as a generalization of the $L^2(\Omega)$ inner product.

Definition 2.3.5 (Sobolev Spaces). *For $k \in \mathbb{N}$ and $1 \leq p \leq \infty$ we define the Sobolev space*

$$W^{k,p}(\Omega) = \{u \in L^p(\Omega) : D^\alpha u \in L^p(\Omega), \forall \alpha \in \mathbb{N}_0^d : |\alpha| \leq k\}$$

with the associated norms

- $1 \leq p < \infty$,

$$\|u\|_{W^{k,p}(\Omega)} = \left(\sum_{|\alpha| \leq k} \|D^\alpha u\|_{L^p(\Omega)}^p \right)^{\frac{1}{p}};$$

- $p = \infty$,

$$\|u\|_{W^{k,p}(\Omega)} = \max_{|\alpha| \leq k} \|D^\alpha u\|_{L^\infty(\Omega)}.$$

We say that $D^\alpha u$ is the weak derivative of order α of $u \in L^p(\Omega)$ if $D^\alpha u \in L^p(\Omega)$. The operator D^α is well-defined as a distribution and satisfies

$$\int_{\Omega} D^\alpha u \varphi dx = (-1)^{|\alpha|} \int_{\Omega} u D^\alpha \varphi dx, \quad \forall \varphi \in \mathcal{D}(\Omega).$$

Throughout this work, we are mainly concerned with Sobolev spaces when $p = 2$. In this case, we write $H^k(\Omega) := W^{k,2}(\Omega)$ which is a Hilbert space for the inner product³

$$(u, v) := \sum_{|\alpha| \leq k} (D^\alpha u, D^\alpha v)_{L^2(\Omega)}.$$

One of the main tools used in obtaining the spectral decomposition of the Laplace operator (see Appendix B) is the following Embedding Theorem.

Theorem 2.3.6 (Rellich Theorem). *Assume that Ω is a bounded Lipschitz domain. Then, the embedding $H^1(\Omega) \rightarrow L^2(\Omega)$ is compact, i.e., given a bounded sequence $(u_n)_{n \in \mathbb{N}} \subset H^1(\Omega)$ there exists a convergent subsequence $(u_{n_k})_{k \in \mathbb{N}} \subset L^2(\Omega)$.*

So far we have restricted our definition of Sobolev spaces to $k \in \mathbb{N}$, but it is entirely feasible to extend these spaces to fractional Sobolev spaces using a real exponent $s \in \mathbb{R}_0^+$. While various approaches can be employed for this extension, when $p = 2$ it can be readily achieved through Fourier Transforms.

³Observe that if $k = 0$ then $H^0(\Omega) = L^2(\Omega)$.

Lemma 2.3.7. *Let $u \in L^2(\mathbb{R}^d)$. Then*

$$u \in H^k(\mathbb{R}^d) \iff (1 + |\xi|^k) \hat{u} \in L^2(\mathbb{R}^d)$$

where $\hat{u} = \mathcal{F}u$ denotes the Fourier Transform of u , given by $\mathcal{F}u(\xi) = \hat{u}(\xi) = \int_{\mathbb{R}^d} e^{-2\pi i x \xi} u(x) dx$.

The above characterization of the $H^k(\mathbb{R}^d)$ space motivates the following definition.

Definition 2.3.8. *Let $s \in \mathbb{R}$. The fractional Sobolev space $H^s(\mathbb{R}^d)$ is defined as*

$$H^s(\mathbb{R}^d) = \{u \in L^2(\mathbb{R}^d) : (1 + |\xi|^2)^{\frac{s}{2}} \hat{u} \in L^2(\mathbb{R}^d)\}$$

with the norm

$$\|u\|_{H^s(\mathbb{R}^d)} = \|(1 + |\xi|^2)^{\frac{s}{2}} \hat{u}\|_{L^2(\mathbb{R}^d)}.$$

The definition 2.3.8 only holds for functions defined over the whole space \mathbb{R}^d . In this work, we are mainly concerned with the behavior over a bounded set $\Omega \subset \mathbb{R}^d$. Unfortunately, there are multiple definitions of fractional Sobolev spaces over a bounded set that may not agree between themselves if the boundary of Ω is not smooth enough (if the boundary fails to be parameterized by a continuous function, for example). In any case, the following definition suffices for this work, see [Bog85], [CWHM17] or [HM17].

Definition 2.3.9. *Let $\Omega \subset \mathbb{R}^d$ be a bounded set with a Lipschitz boundary. Define*

$$\dot{H}^s(\Omega) = \{v \in H^s(\mathbb{R}^d) : \text{supp } v \subset \overline{\Omega}\}.$$

Then, the fractional Sobolev space $H^s(\Omega)$ is defined as

$$H^s(\Omega) = H^s(\mathbb{R}^d) \setminus \dot{H}^s(\mathbb{R}^d \setminus \Omega).$$

The norm of a function $u \in H^s(\Omega)$ is given by

$$\|u\|_{H^s(\Omega)} = \inf\{\|\tilde{u}\|_{H^s(\mathbb{R}^d)} : \tilde{u} \in H^s(\mathbb{R}^d), \tilde{u}|_{\Omega} = u\}.$$

Fractional Sobolev spaces are important for our study because they are deeply related to the boundary behavior of a given function. For example, if $u \in H^1(\Omega)$ and Ω is a bounded Lipschitz domain, then $u|_{\partial\Omega} \in H^{\frac{1}{2}}(\partial\Omega)$. However, the statement above must be defined rigorously: not only u is only defined in the open set Ω , but u is only defined *almost everywhere* and the Lebesgue measure of $\partial\Omega$ is zero. Intuitively, we consider the continuous extension of functions from Ω to the boundary $\partial\Omega$ which is only possible if the domain is regular *enough*⁴. This is done in the context of trace theory, cf. [Gey07], [Nec11] or [AF03].

⁴We refer to Appendix A where we briefly study domain regularity and the notion of Sobolev spaces on manifolds, such as the boundary of a Lipschitz domain.

Theorem 2.3.10. *Let Ω be a bounded set with a Lipschitz boundary. Then, there exists a linear and continuous mapping called the trace operator*

$$\gamma_0 : H^1(\Omega) \rightarrow H^{\frac{1}{2}}(\partial\Omega)$$

that admits a bounded right inverse represented by γ_0^{-1} .

In particular, if $u \in H^2(\Omega)$, then $\frac{\partial u}{\partial x_j} \in H^1(\Omega)$ for $j = 1, \dots, d$ and the operator

$$\begin{aligned} \gamma_1 : H^2(\Omega) &\rightarrow L^2(\partial\Omega) \\ u &\mapsto \gamma_0(\nabla u) \cdot n \end{aligned}$$

is linear and continuous⁵ and generalizes the notion of the normal derivative (denoted by $\frac{\partial u}{\partial n}$) on the boundary $\partial\Omega$ for a function $u \in H^2(\Omega)$.

The result above is stated in a very weak form since we are working in Lipschitz domains. If Ω is a smooth domain, then $\gamma_1 : H^2(\Omega) \rightarrow H^{\frac{1}{2}}(\partial\Omega)$, cf. [LM12]. An important (closed) subspace of $H^1(\Omega)$ is the kernel of the trace operator γ_0 ,

$$\ker \gamma_0 = \{u \in H^1(\Omega) : \gamma_0 u = 0\} =: H_0^1(\Omega)$$

which can be equivalently defined as the closure of $\overline{\mathcal{D}(\Omega)}$ in the $H^1(\Omega)$ norm, i.e., $H_0^1(\Omega) := \overline{\mathcal{D}(\Omega)}^{H^1(\Omega)}$. It should be noted that the normal derivative operator γ_1 cannot be defined if we only assume that $u \in H^1(\Omega)$. If such a continuous operator \mathcal{N} existed, then $\mathcal{N}\varphi = 0$ for every $\varphi \in \mathcal{D}(\Omega)$. By continuity, this would imply $\mathcal{N}u = 0$ for all $u \in H_0^1(\Omega)$, leading to a contradiction.

$H_0^1(\Omega)$ is of major importance in the Dirichlet Laplacian problem, since the functions in $H_0^1(\Omega)$ “vanish” on $\partial\Omega$. Next, we state an important result to be used when studying the spectrum of the Dirichlet Laplacian.

Theorem 2.3.11 (Poincaré inequality). *Let $\Omega \subset \mathbb{R}^d$ be a bounded set. Define $W_0^{1,p}(\Omega) := \overline{\mathcal{D}(\Omega)}^{W^{1,p}(\Omega)}$. Then, there exists $C > 0$ such that*

$$\|u\|_{L^p(\Omega)} \leq C \|\nabla u\|_{L^p(\Omega)}, \quad \forall u \in W_0^{1,p}(\Omega).$$

Finally, we shed some light on the dual space of Sobolev spaces (with fractional exponent). In \mathbb{R}^d one can prove the following result, cf. [CZ10] or [Hör15].

Theorem 2.3.12. *Let $s \in \mathbb{R}$ and $u \in H^s(\mathbb{R}^d)$. Then, any linear and continuous functional $T \in (H^s(\mathbb{R}^d))^*$ that acts in $H^s(\mathbb{R}^d)$ can be uniquely represented by some $v \in H^{-s}(\mathbb{R}^d)$ and the duality pairing is given by*

$$\langle T, u \rangle_{(H^s(\mathbb{R}^d))^*, H^s(\mathbb{R}^d)} = \int_{\mathbb{R}^d} \hat{u} \bar{\hat{v}} d\xi = \int_{\mathbb{R}^d} (1 + |\xi|^2)^{\frac{s}{2}} \hat{u} (1 + |\xi|^2)^{-\frac{s}{2}} \bar{\hat{v}} d\xi \leq \|u\|_{H^s(\Omega)} \|v\|_{H^{-s}(\Omega)}$$

⁵One may understand γ_0 here as an elementwise operator, where $\gamma_0(\nabla u) = (\gamma_0(\frac{\partial u}{\partial x_1}), \dots, \gamma_0(\frac{\partial u}{\partial x_d}))$.

where \hat{u} and \hat{v} represent the Fourier Transforms of u and v , respectively. In particular, the dual of $H^s(\mathbb{R}^d)$ is isomorphic to $H^{-s}(\mathbb{R}^d)$.

Remark 2.3.13. Considering the inclusion $\mathcal{D}(\Omega) \subset H^s(\Omega)$, it is straightforward to observe that $(H^s(\Omega))^* \subset D^*(\Omega)$ which implies that $L^2(\Omega) \subset (H^s(\Omega))^* \cong H^{-s}(\Omega)$. Consequently, based on the preceding Theorem, we note that Sobolev spaces with negative exponent s can be regarded as spaces of distributions with the following inclusions:

$$H^s(\Omega) \subset L^2(\Omega) \subset H^{-s}(\Omega).$$

In this case, one can consider $L^2(\Omega)$ as a pivot space, and by virtue of the identification of $L^2(\Omega)$ with its dual, the duality pairing $\langle \cdot, \cdot \rangle_{H^{-s}(\Omega), H^s(\Omega)}$ and the $L^2(\Omega)$ inner product coincide for every $u \in H^s(\Omega)$ and

$$\langle v, u \rangle_{H^{-s}(\Omega), H^s(\Omega)} = \int_{\Omega} uv dx \quad (2.1)$$

whenever it makes sense, i.e., when $v \in L^2(\Omega)$.

Theorem 2.3.10 allows to give some meaning to the space $H^{-\frac{1}{2}}(\Omega)$. Let $u \in H^2(\Omega)$ and $v \in H^{\frac{1}{2}}(\partial\Omega)$. Then, $\gamma_0^{-1}v \in H^1(\Omega)$ and by Green's formula (see the Appendix B)

$$\langle \gamma_1 u, v \rangle_{H^{-\frac{1}{2}}(\partial\Omega), H^{\frac{1}{2}}(\partial\Omega)} = \int_{\Omega} \Delta u \gamma_0^{-1} v dx + \int_{\Omega} \nabla u \cdot \nabla \gamma_0^{-1} v dx$$

we have $\gamma_1 u \in H^{-\frac{1}{2}}(\Omega)$.

3

From Spectral Theory and Shape Optimization to the Poisson Transmission Problem

Until otherwise indicated, let $\Omega \subset \mathbb{R}^d$ be an open and bounded domain with C^2 boundary, with $d \geq 2$.

Let $p(x)$ be a polynomial in the variables $x = (x_1, \dots, x_d)$, and $p(\partial)$ be the partial differential operator obtained by substituting $\frac{\partial}{\partial x_i}$ for x_i in $p(x)$. We start by introducing the definition of a fundamental solution of a partial differential operator:

Definition 3.0.1. Consider the polynomial $p(\partial)$. A distribution $\Phi \in \mathcal{D}'(\mathbb{R}^n)$ is said to be a fundamental solution of the partial differential operator $p(\partial)$ if

$$p(\partial)\Phi = \delta,$$

where δ is the Dirac Delta distribution.

In particular, given Φ satisfying the above conditions, we have that $p(\partial)\Phi(x) = 0$ for $x \in \mathbb{R}^d \setminus \{0\}$.

Then, it is easy to see that the fundamental solution of a partial differential operator is not unique: if v is such that $p(\partial)v(x) = 0$ for all $x \in \mathbb{R}^d$, then $p(\partial)(\Phi + v) = \delta$. However, the fundamental solutions given below are chosen because they exhibit an important asymptotic behavior, which is needed for the numerical method presented in Chapter 4.

An important result in this context is the Malgrange-Ehrenpreis Theorem, which is also based on the Hahn-Banach Theorem 2.1.3.

Theorem 3.0.2 (Malgrange-Ehrenpreis). *Every partial differential operator $p(\partial)$ with constant coefficients has a fundamental solution $\Phi \in \mathcal{D}^*(\mathbb{R}^d)$.*

Proof. See [RS75]. □

Below the fundamental solution of the Laplace operator and some major results concerning Laplace and Helmholtz equations are presented.

3.1 The Laplace operator

In what follows, consider the Laplace operator $-\Delta = -\sum_{i=1}^d \frac{\partial^2}{\partial x_i^2}$ associated with the well-known Laplace equation

$$-\Delta u = 0. \tag{3.1}$$

Throughout this first part, we are mostly concerned about its spectrum which is associated with the Helmholtz equation

$$-(\Delta + \lambda)u = 0 \iff -\Delta u = \lambda u. \tag{3.2}$$

A precise definition of an eigenvalue of equation (3.2) is stated in B.0.3, where the existence proof of those eigenvalues is presented, as well as their variational form in B.0.4.

Remark 3.1.1. *In some literature, it is common to write the Helmholtz equation as $-\Delta u = k^2 u$, where k is known as an eigenfrequency (or wave number), and $k^2 = \lambda$. This terminology is a consequence of the fact that the Helmholtz equation can be derived from the wave equation, where a constant c^2 , $c \in \mathbb{R}$, is used.*

By Theorem 3.0.2 we know that both equations (3.1) and (3.2) admit fundamental solutions that are given below.

Proposition 3.1.2. *The function $\Phi : \mathbb{R}^d \setminus \{0\} \rightarrow \mathbb{R}$ given by*

$$\Phi(x) = \begin{cases} -\frac{1}{2\pi} \log |x|, & d = 2 \\ \frac{1}{(d-2)|\partial B_1|} \frac{1}{|x|^{d-2}}, & d > 2 \end{cases}$$

is the fundamental solution of equation (3.1), where $|\partial B_1|$ denotes the surface area of the unitary ball.

Proposition 3.1.3. *The function $\Phi_\lambda : \mathbb{R}^d \setminus \{0\} \rightarrow \mathbb{R}$ given by*

$$\Phi_\lambda(x) = \begin{cases} \frac{i}{4} H_0^{(1)}(\sqrt{\lambda} \|x\|), & d = 2 \\ \frac{e^{i\sqrt{\lambda} \|x\|}}{4\pi \|x\|}, & d = 3 \end{cases}$$

is the fundamental solution of equation (3.2), where $H_0^{(1)}$ is the Hankel function of the first kind and order 0, given by

$$H_0^{(1)}(x) = J_0(x) + iY_0(x),$$

where J_0 and Y_0 are the Bessel functions of the first and second kind with order zero, respectively¹.

If one considers the eigenfrequency form of the Laplace equation, then the fundamental solution in Proposition 3.1.3 would change accordingly.

3.1.1 Some shape optimization results

In this subsection, some important results regarding shape optimization are presented. More precisely, we are interested in problems of the form

$$\min\{F(\lambda_1(\Omega), \dots, \lambda_k(\Omega)) : |\Omega| = c, \Omega \subset \mathbb{R}^d\}, \quad (3.3)$$

where F is a function of the first k eigenvalues of the Laplace operator and $c > 0$. We point the reader to [Hen06] and [Hen17] for more details.

Theorem 3.1.4 (Faber-Krahn inequality). *Let $B \subset \mathbb{R}^d$ be a ball of volume c . Then, among all open domains $\Omega \subset \mathbb{R}^d$ of volume c we have that,*

$$\lambda_1(B) = \min\{\lambda_1(\Omega) : |\Omega| = c\}.$$

In particular, as proved by Krahn in [Kra26], the corresponding isoperimetric inequality

$$\lambda_1(\Omega) \geq \left(\frac{C_d}{c}\right)^{\frac{d}{2}} j_{d/2-1,1},$$

where C_d is the volume of the d -dimensional unit ball and $j_{p,1}$ is the first positive zero of the Bessel function J_p , holds.

Theorem 3.1.4 is a classic form of an isoperimetric inequality, conjectured for the first time by Lord Rayleigh. More recently, a reverse of the Faber-Krahn inequality was proven in [FK08].

Theorem 3.1.5. *Let $\Omega \subset \mathbb{R}^d$ be an open bounded convex domain and denote the inradius of Ω (radius of the largest ball contained in Ω) by ρ_Ω . Then,*

$$\lambda_1(\Omega) \leq \frac{|\partial\Omega|}{d\rho_\Omega|\Omega|} \lambda_1(\mathbb{D}),$$

where \mathbb{D} is the unit disk of \mathbb{R}^d .

¹ See Appendix D for more information on Bessel functions.

While Faber-Krahn inequality deals with the first eigenvalue of the Laplace operator, other results have been uncovered for the second and third eigenvalues:

Theorem 3.1.6 (Krahn-Szegő). *The open domain which solves the problem*

$$\min\{\lambda_2(\Omega) : |\Omega| = c\}$$

consists of two equal and disjoint balls of volume $\frac{c}{2}$.

The following results are in the context of quasi-open sets, generalizing the above results for a general functional F considered in (3.3) (see [Hen06] for more details and definition of a quasi-open set). A result regarding the topology of a given domain Ω and its connection with the minimization of each eigenvalue was given by Wolf and Keller in [WK94]. Among the class of quasi-open sets, denote by Ω_n^* the quasi-open set which minimizes λ_n , which we denote by $\lambda_n^* := \lambda_n(\Omega_n^*)$ for $n \in \mathbb{N}$.

Theorem 3.1.7 (Wolf-Keller). *Let Ω_k^* be the union of (at least two) disjoint domains, each of them with positive volume. Then,*

$$(\lambda_k^*)^{\frac{d}{2}} = (\lambda_i^*)^{\frac{d}{2}} + (\lambda_{k-i}^*)^{\frac{d}{2}} = \min_{1 \leq j \leq \frac{k-1}{2}} ((\lambda_j^*)^{\frac{d}{2}} + (\lambda_{k-j}^*)^{\frac{d}{2}}),$$

where i is a value of $j \leq \frac{k-1}{2}$ that minimizes $(\lambda_i^)^{\frac{d}{2}} + (\lambda_{k-i}^*)^{\frac{d}{2}}$. Furthermore, the disjoint union*

$$\Omega_k^* = \left[\left(\frac{\lambda_i^*}{\lambda_k^*} \right)^{\frac{1}{2}} \Omega_i^* \right] \cup \left[\left(\frac{\lambda_{k-i}^*}{\lambda_k^*} \right)^{\frac{1}{2}} \Omega_{k-i}^* \right]$$

holds, where $c\Omega$ is seen as a dilation of Ω by a factor of scale $c > 0$.

Roughly speaking, Theorem 3.1.7 states that if Ω_k^* is not connected and minimizes λ_k , then each connected component must be a minimizer for a lower eigenvalue.

Generalizations of Theorems 3.1.4 and 3.1.6 become harder to prove for high-order eigenvalues. Bucur and Henrot proved in [HB00] that there exists a domain Ω that minimizes λ_3 , and it is conjectured to be the disk². In [Buc12], Bucur was able to assert the existence of, at least, one solution to problem (3.3).

Theorem 3.1.8 (Bucur). *For every $k \in \mathbb{N}$ the problem*

$$\min\{\lambda_k(\Omega) : |\Omega| = c\}$$

has at least one solution. Moreover, every solution is bounded and has a finite perimeter.

²Notice that Ω_3 must be connected in dimension 2. Otherwise, by Theorem 3.1.7, Ω_3 would be the union of the domains that minimize λ_1 and λ_2 (see Theorems 3.1.4 and 3.1.6), where one can explicitly compute $\lambda_3 = \lambda_1 + \lambda_2 \approx 51.504$. However, this would be a contradiction since the eigenvalue of the unit disk is $\lambda_3(\mathbb{D}) \approx 46.125$ when considering unitary measure $c = 1$. For three dimensions the result is the same, but for $d \geq 4$ one cannot conclude anything.

Theorem 3.1.9 (Mazzoleni-Pratelli). *Let $k \in \mathbb{N}$ and suppose that $F : \mathbb{R}^k \rightarrow \mathbb{R}$ in (3.3) is lower semicontinuous, increasing in each variable. Then, among quasi-open sets, there exists a bounded minimizer Ω for problem (3.3). More precisely, a minimizer Ω is contained in a cube of side R , where R depends on k and on the dimension of the space d , but not on F .*

A significant observation related to triangular and quadrilateral domains involves their invariance under *Steiner symmetrizations*. This symmetry property ensures that when a triangle or a quadrilateral undergoes a Steiner symmetrization, it remains a triangle or a quadrilateral, respectively. This transformation conserves the area of the domain while reducing both its perimeter and the value of its first eigenvalue. As a consequence of this transformation, we can establish the following result.

Theorem 3.1.10 (Pólya-Szegő). *The equilateral triangle minimizes λ_1 among all triangles with fixed area. In particular, the inequality*

$$\frac{4\pi^2}{\sqrt{3}|T|} \leq \lambda_1(T)$$

holds for every triangle T of area $|T|$. Analogously, λ_1 is minimized for the square among all quadrilaterals.

However, an analogous result for the n -side polygon is still an open problem conjectured by Pólya and Szegő in [PS51].

Conjecture 3.1.11. *Let $n \geq 5$ and consider the class of n -side polygons. Then, the regular n -side polygon has the least first eigenvalue among all n -side polygons with fixed area.*

Very recently, Bogosel and Bucur proved in [BB22] that Conjecture (3.1.11) can be reduced to a finite number of certified numerical computations with machine precision and performed them for $n = 5, 6, 7, 8$. More precisely, they studied perturbations of the Hessian matrix³ of the first eigenvalue as a function of the vertices coordinates, numerically checked that it is a positive definite matrix for regular polygons (therefore they are local minimizers) and found an estimate for the maximal diameter of an optimal polygon, which was used to reduce the conjecture to a finite number of numerical computations.

Related to triangles, we can also cite the recent work of Gómez-Serrano and Orriols in [GSO21], which was based on the previous work of Antunes and Freitas [AF11] who conjectured that the first three eigenvalues are enough to define the shape of a triangle (such result resembles the famous Marc Kac question if one can “hear the shape of a drum” in [Kac66], that is, if given the frequencies produced by a drum one could identify the drum’s shape, which has proven to be false, see [GWW92] for more details). In any case, Gómez-Serrano and Orriols were able to show that knowing any three eigenvalues is not enough to fully characterize the shape of a triangle.

Theorem 3.1.12 (Serrano-Orriols). *There exist two triangles T_A and T_B not isometric to each other such that $\lambda_i(T_A) = \lambda_i(T_B)$, for $i = 1, 2, 4$.*

³Such topic is outside of the scope of this work. However, the concept of shape derivative is briefly explained in 5.1.4.

Another important result in this field is related to the ratio between the first and the second eigenvalues.

Theorem 3.1.13 (Ashbaugh-Benguria). *The solution to the maximization problem*

$$\max \left\{ \frac{\lambda_2(\Omega)}{\lambda_1(\Omega)} : \Omega \subset \mathbb{R}^d, \Omega \text{ open} \right\}$$

is the ball in \mathbb{R}^d . In particular, it can be shown that

$$\frac{\lambda_2(\Omega)}{\lambda_1(\Omega)} \leq \frac{j_{\frac{d}{2},1}^2}{j_{\frac{d}{2}-1,1}^2},$$

where $j_{p,1}$ is the first positive zero of the Bessel function J_p .

Remark 3.1.14. *Note that in Theorem 3.1.13 we do not fix the volume of our domain and only assume that it has a finite measure. This is a consequence of the homogeneity proven in Corollary (B.0.6) and of the fact that we are now considering a ratio between two eigenvalues in the same domain.*

3.2 The Dirac operator

Due to recent advancements in nuclear, and molecular physics and the discovery of very interesting electrical, mechanical, and thermal properties of Dirac materials (graphene, for example), a lot of attention has been put on the Dirac equation. Presented by Paul Dirac in his 1928 article [Dir28], the Dirac equation was able to successfully merge the famous Schrödinger equation with special relativity, explain the phenomenon that today is known as *spin* and predict the existence of *antimatter*. It describes the relativistic dynamics of spin- $\frac{1}{2}$ particles (like the electron), whose energy states can be determined by studying the spectrum of the Hamiltonian (Dirac) operator \hat{H} in $L^2(\Omega, \mathbb{C}^2)$ for any $x \in \Omega \subset \mathbb{R}^2$,

$$\hat{H}\mathbf{u} = E\mathbf{u} \quad \text{with} \quad \hat{H} = -i(\sigma \cdot \nabla) + (m + V(x))\mathbb{I}_2, \quad (3.4)$$

where $\nabla = (\partial_1, \partial_2)$ is the gradient operator, m is the mass and E the energy of the particle, $V(x)$ is some external potential, \mathbb{I}_2 is the 2×2 identity matrix and $\mathbf{u} \in L^2(\Omega, \mathbb{C}^2)$ is a two-component spinor. One of the major problems regarding the study of Dirac's equation is the fact that, unlike Schrödinger's equation, it has a matrix structure that is given by the Pauli's matrices

$$\sigma_1 = \begin{bmatrix} 0 & 1 \\ 1 & 0 \end{bmatrix} \quad \sigma_2 = \begin{bmatrix} 0 & -i \\ i & 0 \end{bmatrix}$$

which can be incorporated in $\sigma = (\sigma_1, \sigma_2)$.

Setting the potential $V(x) = 0$ and considering $\Omega \subset \mathbb{R}^2$ to be a bounded and open domain with C^3 boundary, we can rewrite equation (3.4) in the form

$$\begin{bmatrix} m & -i(\partial_1 - i\partial_2) \\ -i(\partial_1 + i\partial_2) & -m \end{bmatrix} \begin{bmatrix} u_1(x) \\ u_2(x) \end{bmatrix} = E \begin{bmatrix} u_1(x) \\ u_2(x) \end{bmatrix} \quad (3.5)$$

where we let $\mathbf{u}(x) = \begin{bmatrix} u_1(x) \\ u_2(x) \end{bmatrix}$. In particular, we are interested in studying it under the so-called *infinite mass boundary conditions*. We point the reader to [LOB19], [BK22], and [ABLOB21] for more details about this type of boundary conditions and the results below. For a point $x \in \Gamma = \partial\Omega$, we denote by $\mathbf{n}(x) = (n_1(x), n_2(x))^T$ the outward unitary vector to Γ , and define the domain of \hat{H} as

$$\text{Dom}(\hat{H}) = \{\mathbf{u} \in H^1(\Omega, \mathbb{C}^2) : u_2 = i(n_1 + in_2)u_1 \text{ on } \Gamma\}.$$

Let $\boldsymbol{\tau}(x) = (n_2(x), -n_1(x))^T$ be the unit tangent vector at point $x \in \Gamma$ such that $(\boldsymbol{\tau}(x), \mathbf{n}(x))$ is a positively-oriented orthonormal basis in \mathbb{R}^2 . Considering the arc-length parametrization of Γ given by the map

$$s : [0, L] \rightarrow \mathbb{R}^2, \quad s(t) = \int_0^t \|r'(\sigma)\| d\sigma$$

where L represents the arc-length of Γ and r is a parametrization of Γ , we denote by $\kappa : \Gamma \rightarrow \mathbb{R}$ the signed curvature of Γ where the *Frenet-Serret* formula (with the dependency on t in s dropped)

$$\frac{\partial \boldsymbol{\tau}}{\partial s} = \kappa(s) \mathbf{n}(s) \quad (3.6)$$

holds. We will now state some general results regarding the spectrum of the Dirac operator, c.f. Theorem B.0.4 for the proof of a similar result for the Laplace operator.

Proposition 3.2.1. *Consider the eigenvalue problem (3.5). Then, the following results hold,⁴*

- *The eigenvalues are real and the spectrum of the Dirac operator is discrete. Also, the spectrum is symmetric, and the eigenvalues can be arranged as follows*

$$-\infty \leftarrow \dots \leq -\lambda_3 \leq -\lambda_2 \leq -\lambda_1 < 0 < \lambda_1 \leq \lambda_2 \leq \lambda_3 \leq \dots \rightarrow \infty;$$

- *The principal (first) eigenvalue can be described using the variational form*

$$\lambda_1^2 = \min_{0 \neq \mathbf{u} \in \text{Dom}(\hat{H})} \frac{\|\nabla \mathbf{u}\|_{L^2(\Omega)}^2 + m^2 \|\mathbf{u}\|_{L^2(\Omega)}^2 + m \|\gamma_0 \mathbf{u}\|_{L^2(\Gamma)}^2}{\|\mathbf{u}\|_{L^2(\Omega)}^2},$$

where γ_0 denotes the trace operator studied in Theorem 2.3.10;

- *Let $m = 0$ and Ω be the unit disk \mathbb{D} . Then, we have that the first eigenvalue is the smallest positive solution to the equation*

$$J_0(\lambda_1) = J_1(\lambda_1),$$

and the associated eigenfunction is (in polar coordinates)

$$\mathbf{u}(r, \theta) = \begin{pmatrix} J_0(\lambda_1 r) \\ ie^{i\theta} J_1(\lambda_1 r) \end{pmatrix}$$

⁴Notice that we have defined the eigenvalue E as λ . Not only for consistency reasons, but also because we are mainly interested in the mathematical description of the problem, and not in the physical intuition behind it.

where J_p is the Bessel function of first kind of order p . For future comparison, the numerical approximation of the first eigenvalue is $\lambda_1 \approx 1.434695650819$

Proposition 3.2.3 below, regarding the lack of separable solutions of the Dirac operator, will have interesting consequences in the numerical approach to solve the Dirac equation. We start by stating and proving the following auxiliary lemma:

Lemma 3.2.2. *Let $\mathbf{u} \in H^2(\Omega)$ be a solution of (3.5) such that $u \in \text{Dom}(\hat{H})$. Then,*

$$\|\hat{H}\mathbf{u}\|_{L^2(\Omega)}^2 = \|\nabla\mathbf{u}\|_{L^2(\Omega)}^2 + m^2\|\mathbf{u}\|_{L^2(\Omega)}^2 + m\|\gamma\mathbf{u}\|_{L^2(\Gamma)}^2 - \frac{1}{2} \int_{\Gamma} \kappa |\mathbf{u}|^2 d\sigma \quad (3.7)$$

Proof. Recalling the $L^2(\Omega)$ inner product for complex functions

$$(f, g)_{L^2(\Omega)} = \int_{\Omega} f \bar{g} dx,$$

one obtains, see the left side of (3.5)

$$\|\hat{H}\mathbf{u}\|_{L^2(\Omega)}^2 = m^2\|u_1\|_{L^2(\Omega)}^2 + m^2\|u_2\|_{L^2(\Omega)}^2 \quad (3.8)$$

$$+ im \int_{\Omega} u_1(\partial_1 + i\partial_2)\bar{u}_2 dx - im \int_{\Omega} \bar{u}_1(\partial_1 - i\partial_2)u_2 dx \quad (3.9)$$

$$+ im \int_{\Omega} \bar{u}_2(\partial_1 + i\partial_2)u_1 dx - im \int_{\Omega} u_2(\partial_1 - i\partial_2)\bar{u}_1 dx \quad (3.10)$$

$$+ \|(\partial_1 - i\partial_2)u_2\|_{L^2(\Omega)}^2 + \|(\partial_1 + i\partial_1)u_1\|_{L^2(\Omega)}^2. \quad (3.11)$$

Addressing each line of the expression above individually:

- For (3.8) one directly has

$$m^2\|u_1\|_{L^2(\Omega)}^2 + m^2\|u_2\|_{L^2(\Omega)}^2 = m^2\|\mathbf{u}\|_{L^2(\Omega)}^2.$$

- For (3.9) one integrates by parts the first term

$$\int_{\Omega} u_1(\partial_1 + i\partial_2)\bar{u}_2 dx = \int_{\Gamma} u_1\bar{u}_2(1+i)d\sigma - \int_{\Omega} \bar{u}_2(\partial_1 + i\partial_2)u_1 dx$$

where the last term cancels with the first term of (3.10).

- Analogously, for (3.10) one obtains a similar result for the last term

$$\int_{\Omega} u_2(\partial_1 - i\partial_2)\bar{u}_1 dx = \int_{\Gamma} u_2\bar{u}_1(1-i)d\sigma - \int_{\Omega} \bar{u}_1(\partial_1 - i\partial_2)u_2 dx$$

where the last term cancels with the last term of (3.9).

- For (3.11), firstly the following property was deduced

$$\text{Im} \left(\int_{\Omega} \partial_1 v \partial_2 \bar{v} dx \right) = \frac{1}{2i} \int_{\Gamma} \bar{v} \partial_{\tau} v d\sigma, \quad \forall v \in H^2(\Omega), \quad (3.12)$$

where $\partial_\tau v = \tau \cdot \nabla v$, which can be obtained using integration by parts. Then, for each term

$$\begin{aligned} \|(\partial_1 - i\partial_2)u_2\|_{L^2(\Omega)}^2 &= \|\nabla u_2\|_{L^2(\Omega)}^2 + i\left(\int_{\Omega} \partial_1 u_2 \partial_2 \bar{u}_2 dx - \int_{\Omega} \partial_2 u_2 \partial_1 \bar{u}_2 dx\right) \\ &= \|\nabla u_2\|_{L^2(\Omega)}^2 + i\int_{\Gamma} \bar{u}_2 \partial_\tau u_2 d\sigma \\ \|(\partial_1 + i\partial_2)u_1\|_{L^2(\Omega)}^2 &= \|\nabla u_1\|_{L^2(\Omega)}^2 - i\left(\int_{\Omega} \partial_1 u_1 \partial_2 \bar{u}_1 dx - \int_{\Omega} \partial_2 u_1 \partial_1 \bar{u}_1 dx\right) \\ &= \|\nabla u_1\|_{L^2(\Omega)}^2 - i\int_{\Gamma} \bar{u}_1 \partial_\tau u_1 d\sigma \end{aligned}$$

where the property 3.12 was used.

As such, one can write everything as

$$\begin{aligned} \|\hat{H}\mathbf{u}\|_{L^2(\Omega)}^2 &= m^2\|\mathbf{u}\|_{L^2(\Omega)}^2 + im\left(\int_{\Gamma} u_1 \bar{u}_2 (1+i)d\sigma - \int_{\Gamma} u_2 \bar{u}_1 (1-i)d\sigma\right) \\ &\quad + \|\nabla \mathbf{u}\|_{L^2(\Omega)}^2 + i\left(\int_{\Gamma} \bar{u}_2 \partial_\tau u_2 d\sigma - \int_{\Gamma} \bar{u}_1 \partial_\tau u_1 d\sigma\right). \end{aligned}$$

Finally, using the boundary conditions $u_2 = i(n_1 + in_2)u_1$, one concludes that

$$im\left(\int_{\Gamma} u_1 \bar{u}_2 (1+i)d\sigma - \int_{\Gamma} u_2 \bar{u}_1 (1-i)d\sigma\right) = \|\gamma \mathbf{u}\|_{L^2(\Gamma)}^2$$

while

$$i\int_{\Gamma} \bar{u}_2 \partial_\tau u_2 d\sigma - i\int_{\Gamma} \bar{u}_1 \partial_\tau u_1 d\sigma = -\frac{1}{2}\int_{\Gamma} \kappa |\mathbf{u}|^2 d\sigma$$

where was used the Frenet-Serret formula (3.6) and the fact that on Γ one has $|u_1|^2 = |u_2|^2$. \square

A Partial Differential Equation is said to be separable if its solution can be written as the product of functions on each coordinate, i.e., if its solution $u(q)$, $q = (q_1, \dots, q_d) \in \mathbb{R}^d$ can be written as $u(q) = \prod_{i=1}^d S_i(q_i)$, where the functions S_i only depend on the (scalar) variable q_i , $i = 1, \dots, d$.

Proposition 3.2.3. *Let $\mathbf{u} \in H^2(\Omega)$ be a solution of (3.5) such that $\mathbf{u} \in \text{Dom}(\hat{H})$. Then \mathbf{u} cannot be written using separable solutions, neither in cartesian coordinates in a rectangular domain nor polar coordinates near a corner.*

Proof. One starts by showing that $|\lambda| > m$ for any eigenvalue λ if $\kappa = 0$ a.e.. Assuming that there exists an eigenvalue λ associated with an eigenfunction \mathbf{u} such that $|\lambda| \leq m$, by Lemma 3.2.2 one finds that

$$\|\nabla \mathbf{u}\|_{L^2(\Omega)}^2 + m\|\gamma \mathbf{u}\|_{L^2(\Gamma)}^2 \leq 0 \implies \|\nabla \mathbf{u}\|_{L^2(\Omega)} = 0 \wedge m\|\gamma \mathbf{u}\|_{L^2(\Gamma)} = 0$$

and \mathbf{u} must be a constant, which does not satisfy the boundary conditions (unless $\mathbf{u} = 0$, which would satisfy the conditions above, but it is not considered).

Since $\mathbf{u} \in H^2(\Omega)$, using (3.5), one can express u_2 as

$$u_2 = \frac{-i(\partial_1 + i\partial_2)u_1}{\lambda + m}$$

allowing to rewrite the Dirac equation (3.5) using the Helmholtz equation with Cauchy–Riemann oblique boundary conditions:

$$\begin{cases} -\Delta u_1 = (\lambda^2 - m^2)u_1, & \text{in } \Omega \\ i(\partial_1 + i\partial_2)u_1 + (\lambda + m)i(n_1 + in_2)u_1 = 0, & \text{on } \Gamma. \end{cases} \quad (3.13)$$

In the rest of the proof, we will take into consideration polar coordinates, where one studies the behavior of separable solutions near a corner, locating the origin of coordinates at the corner.

1. Assume that Ω has at least one corner where the domain has a *wedge-like* shape with maximum amplitude Θ (see Figure 3.1).

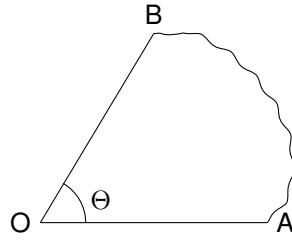


Figure 3.1: A wedge-like “shape” with an interior angle Θ .

In this case, since the outward unit normal on \overline{OA} is $\mathbf{n} = \begin{pmatrix} 0 \\ -1 \end{pmatrix}$ and on \overline{OB} is $\mathbf{n} = \begin{pmatrix} -\sin \theta \\ \cos \theta \end{pmatrix}$, using polar coordinates the system (3.13) transforms into

$$\begin{cases} \left(\partial_r^2 + \frac{1}{r} \partial_r + \frac{1}{r^2} \partial_\theta^2 \right) u_1 = (\lambda^2 - m^2)u_1, & \text{in } \Omega \\ i(\cos \theta \partial_r - \frac{1}{r} \sin \theta \partial_\theta + i(\sin \theta \partial_r + \frac{1}{r} \cos \theta \partial_\theta))u_1 + (\lambda + m)u_1 = 0, & \text{on } \overline{OA} \cdot \\ i(\cos \theta \partial_r - \frac{1}{r} \sin \theta \partial_\theta + i(\sin \theta \partial_r + \frac{1}{r} \cos \theta \partial_\theta))u_1 + (\lambda + m)i(-\sin \theta + i \cos \theta)u_1 = 0, & \text{on } \overline{OB} \end{cases} \quad (3.14)$$

Assume that there exists a solution $u(r, \theta) = R(r)T(\theta)$ of (3.14). Then, from the PDE in the interior Ω one has

$$u(r, \theta) = J_k \left(r \sqrt{\lambda^2 - m^2} \right) (A \cos(k\theta) + B \sin(k\theta))$$

for some $A, B, k \in \mathbb{C}$, were A and B are not simultaneously zero. Applying the condition on \overline{OA} , with $\theta = 0$, one finds that

$$\begin{aligned} & \frac{J_k \left(r \sqrt{\lambda^2 - m^2} \right) (r(m + \lambda)A - kB)}{r} \\ & + \frac{1}{2} i \sqrt{\lambda^2 - m^2} A \left(J_{-1+k} \left(r \sqrt{\lambda^2 - m^2} \right) - J_{1+k} \left(r \sqrt{\lambda^2 - m^2} \right) \right) = 0 \end{aligned} \quad (3.15)$$

Using the recurrence relation for the derivatives of Bessel functions⁵

$$2 \frac{dJ_\alpha(r)}{dr} = J_{\alpha-1}(r) - J_{\alpha+1}(r),$$

⁵Once again, we refer to Appendix D.

equation (3.15) can be rewritten as

$$\frac{J_k(r\sqrt{\lambda^2 - m^2})(r(m + \lambda)A - kB)}{r} + iA \frac{d}{dr} \left[J_k(r\sqrt{\lambda^2 - m^2}) \right] = 0$$

where $J_k(r\sqrt{\lambda^2 - m^2})$ is the solution of the differential equation

$$\frac{\tilde{R}(r)(r(m + \lambda)A - kB)}{r} + iA \frac{d}{dr} \tilde{R}(r) = 0,$$

whose solutions are of the form

$$\tilde{R}(r) = Ce^{ir(m+\lambda)r - ik\frac{B}{A}}$$

for every $C \in \mathbb{C}$. Since they form a basis of solutions, there must be some $C \neq 0$ such that

$$J_k(r\sqrt{\lambda^2 - m^2}) = Ce^{ir(m+\lambda)r - ik\frac{B}{A}}.$$

Analogously, considering the condition on \overline{OB} , one must have

$$\begin{aligned} & ir \left(A \cos(k\Theta) + B \sin(k\Theta) \right) \frac{d}{dr} J_k(r\sqrt{\lambda^2 - m^2}) \\ & - J_k(r\sqrt{\lambda^2 - m^2}) \left(\cos(k\Theta)(Bk + Amr + A\lambda r) + \sin(k\Theta)(Br(\lambda + m) - Ak) \right) = 0. \end{aligned}$$

Once again, $J_k(r\sqrt{\lambda^2 - m^2})$ is the solution of the differential equation

$$\begin{aligned} & ir \left(A \cos(k\Theta) + B \sin(k\Theta) \right) \frac{d}{dr} \tilde{\tilde{R}}(r) \\ & - \tilde{\tilde{R}}(r) \left(\cos(k\Theta)(Bk + Amr + A\lambda r) + \sin(k\Theta)(Br(\lambda + m) - Ak) \right) = 0, \end{aligned}$$

whose solutions are given by

$$\tilde{\tilde{R}}(r) = De^{-ir(\lambda+m)r - \frac{ik(B \cos(k\Theta) - A \sin(k\Theta))}{A \cos(k\Theta) + B \sin(k\Theta)}}, \quad \forall D \in \mathbb{C}.$$

Then, for some $D \neq 0$,

$$J_k(r\sqrt{\lambda^2 - m^2}) = De^{-ir(\lambda+m)r - \frac{ik(B \cos(k\Theta) - A \sin(k\Theta))}{A \cos(k\Theta) + B \sin(k\Theta)}}$$

which implies that

$$Ce^{ir(m+\lambda)r - ik\frac{B}{A}} = De^{-ir(\lambda+m)r - \frac{ik(B \cos(k\Theta) - A \sin(k\Theta))}{A \cos(k\Theta) + B \sin(k\Theta)}}.$$

Since C and D are non-zero \mathbb{C} constants, this implies that

$$\begin{cases} -2ir(m + \lambda) = 0 \\ -ik \left(-\frac{(B \cos(k\Theta) - A \sin(k\Theta))}{A \cos(k\Theta) + B \sin(k\Theta)} - \frac{A}{B} \right) = 0 \end{cases} \implies \begin{cases} \lambda = -m \\ k = 0, \end{cases}$$

thus $u = 0$, a contradiction.

2. For cartesian coordinates (in rectangular domains), we refer to the proof in [BK22].

□

Remark 3.2.4. We note that two important details are being overlooked: domains with corners do not have the smoothness required for formula (3.7) (and signed curvature is not defined everywhere, only on each edge where $\kappa = 0$), neither u has enough regularity to be integrated by parts while expanding (3.11). We refer to [Vu23], where such details can be found for any two-dimensional polygon.

Let $m \geq 0$. We now present some open problems regarding the spectrum of equation (3.5) that we try to address numerically in this work.

Conjecture 3.2.5 (A Faber-Krahn type inequality). *Let $\Omega \subset \mathbb{R}^2$ be an open Lipschitz domain. Then,*

$$\lambda_1(\Omega) \geq \lambda_1(\Omega^*)$$

where Ω^* is the disk of the same area or perimeter as Ω .

The conjecture above is regarded as a hot problem in spectral geometry [KLL19]. In [BFSVDB17] a geometric lower bound for the first (non-negative) eigenvalue was found, while in [LOB19] a sharp upper bound (a reverse Faber-Krahn type inequality, like in Theorem 3.1.5) was proved to hold for convex domains with C^3 boundary. One of the objectives of this work is to give some numerical evidence for the conjecture above, although it is (obviously) impossible to test every possible domain and every possible mass m . However, some types of domains can be systematically approached and one can try to rule them out, so that if the conjecture fails it probably has to fail for some non-conventional shape. Another conjecture we are interested in is the Ashbaugh-Benguria Theorem for the Dirac operator with infinite mass boundary conditions.

Conjecture 3.2.6 (An Ashbaugh-Benguria type result). *Let $\Omega \subset \mathbb{R}^2$ be an open Lipschitz domain. Then, the solution to the maximization problem*

$$\max \left\{ \frac{\lambda_2(\Omega)}{\lambda_1(\Omega)} : \Omega \subset \mathbb{R}^2 \right\}$$

is the ball in \mathbb{R}^2 .

Due to the difficulty of proving these conjectures, simpler versions restricted to triangles and rectangles were considered. For example, in [BK22] a study for rectangles was conducted, where the conjectures below were proved under some extra hypothesis:

Conjecture 3.2.7 (Shape optimization in rectangles). *Let $\lambda_1(a, b) = \lambda_1(\Omega_{a,b})$ denote the first eigenvalue of the Dirac operator with infinite mass boundary conditions in a rectangle with sides a and b . Then,*

1. *Area constraint (unitary area): $\lambda_1(a, \frac{1}{a}) \geq \lambda_1(1, 1)$, $\forall a > 0$;*
2. *Perimeter constraint (perimeter equal to 4): $\lambda_1(a, 2 - a) \geq \lambda_1(1, 1)$, $\forall a \in (0, 2)$.*

Point 1 holds under any of the following assumptions

1. Large eccentricity constraint: $|a^2 - 4| > \sqrt{15}$;
2. Heavy masses constraint: $m\left(\frac{1}{a^2} + a^2 - 2\right) \geq 56$,

and point 2 also holds under any of the following assumptions

1. Large eccentricity constraint: $|a^2 - 1| > \frac{9-\sqrt{33}}{8}$;
2. Heavy masses constraints: $m\left(\frac{1}{a^2} + \frac{1}{(2-a)^2} - 2\right) \geq 56$.

In the same vein, in [Vu23] very similar results were conjectured for isosceles right triangles, in this case for any fixed area or perimeter:

Conjecture 3.2.8 (Shape optimization in triangles). *Consider the triangle $\Omega_{a,b}$ defined by the points $O = (0, 0)$, $A = (a, 0)$, $B = (0, b)$ for $a, b > 0$ and let $\lambda_1(a, b) = \lambda_1(\Omega_{a,b})$. Then,*

1. Area constraint: $\lambda_1(a, b) \geq \lambda_1(k, k)$, $\forall a, b > 0$ for any positive k such that $ab = k^2$;
2. Perimeter constraint: $\lambda_1(a, b) \geq \lambda_1(k, k)$, $\forall a \in (0, (2 + \sqrt{2})k)$ and $\forall b > 0$ such that $a + b + \sqrt{a^2 + b^2} = (2 + \sqrt{2})k$, for any positive k .

Point 3.2.8 holds under any of the assumptions

1. $a \geq 9k$;
2. $a \leq \frac{k}{9}$,

and point 3.2.8 also holds under any of the following assumptions

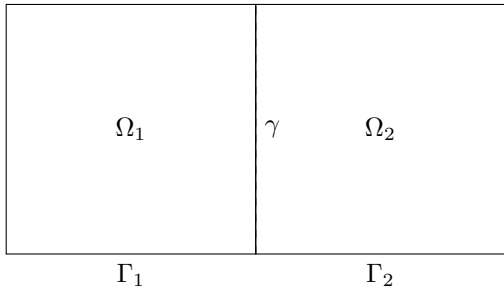
1. $a \geq 3.5k$;
2. $a \leq \frac{k}{9}$.

In this work, both Conjectures 3.2.7 and 3.2.8 are individually studied and Conjecture 3.2.6 is considered for triangles and quadrilaterals. Conjecture 3.2.5 is also studied for regular n -sided polygons with unit area, as in the Pólya-Szegő Conjecture 3.1.11.

Conjecture 3.2.9. *Let $\Omega \subset \mathbb{R}^2$ be an open Lipschitz domain, $n \geq 5$ and consider the class of n -sided polygons. Then, the regular n -sided polygon has the least first eigenvalue among all n -sided polygons with fixed area.*

3.3 A domain decomposition problem

As studied in [GSV19], consider a polygonal domain $\Omega \subset \mathbb{R}^2$ which we divide into two non-overlapping regions Ω_1 and Ω_2 such that $\overline{\Omega} = \overline{\Omega_1} \cup \overline{\Omega_2}$. We denote their common boundary by $\gamma = \partial\Omega_1 \cap \partial\Omega_2$ and denote by $\Gamma_i = \partial\Omega_i \setminus \gamma$ the boundary of each domain Ω_i minus the common boundary, see Figure 3.2. The problem we address in this section is to find functions u_1, u_2 which satisfy the equations (3.16), where $k_1 \geq k_2 > 0$ are constants, $f_i \in L^2(\Omega_i)$ is a source function on each domain, and \mathbf{n}_i is the (normalized) outward normal to each subdomain $\Omega_i, i = 1, 2$. Finally, we write $\mathbf{n} = \mathbf{n}_1 = -\mathbf{n}_2$ when \mathbf{n} is restricted to the interface γ .



$$\begin{cases} -\nabla \cdot (k_i \nabla u_i) = f_i, & \text{in } \Omega_i \\ u_1 - u_2 = 0, & \text{on } \gamma \\ k_1 \frac{\partial u_1}{\partial \mathbf{n}_1} + k_2 \frac{\partial u_2}{\partial \mathbf{n}_2} = 0, & \text{on } \gamma \\ u_i = 0, & \text{on } \Gamma_i \end{cases} \quad (3.16)$$

Figure 3.2: Transmission problem (rectangle example) and its associated equations.

In what follows, we mainly follow the reference [QV99]. Equations (3.16) can be used in studying a system of two bodies with different material parameters (contact resistance or thermal conductivity) connected through an interface γ . If we set

$$k(x) = \begin{cases} k_1, & x \in \Omega_1 \\ k_2, & x \in \Omega_2 \end{cases}, \quad f = \begin{cases} f_1, & \text{in } \Omega_1 \\ f_2, & \text{in } \Omega_2 \end{cases},$$

then problem (3.16) can be seen as a natural reformulation of the Poisson equation with variable coefficients

$$\begin{cases} -\nabla \cdot (k(x) \nabla u) = f, & \text{in } \Omega \\ u = 0, & \text{on } \partial\Omega \end{cases} \quad (3.17)$$

where f is (possibly) discontinuous through the interface γ and

$$u = \begin{cases} u_1, & \text{in } \Omega_1 \\ u_2, & \text{in } \Omega_2 \end{cases}.$$

Equivalence between problems (3.16) and (3.17) (in the appropriate spaces defined below), follows from the transmission conditions in (3.16) which enforce the continuity of the solutions and its normal derivative on γ . To show the equivalence between the two problems, we write the variational (weak) form associated with problems (3.16) and (3.17). The weak form of (3.17) is given by

$$a(u, v) = \int_{\Omega} k(x) \nabla u \cdot \nabla v dx = \int_{\Omega} f v dx$$

where we defined the associated bilinear form a in the Sobolev Space $H_0^1(\Omega)$, and the problem can be rewritten as

$$\text{find } u \in H_0^1(\Omega) : a(u, v) = (f, v), \forall v \in H_0^1(\Omega), \quad (3.18)$$

where (f, v) denotes the $L^2(\Omega)$ inner product between f and v , which has a unique solution in $H_0^1(\Omega)$ by virtue of Lax-Milgram lemma 2.2.7.

For (3.16) the process is not so direct. In what follows, the L^2 inner product in Ω_i is also denoted by (\cdot, \cdot) , since it is clear from the context. Given the subdomain Ω_1 , one multiplies the first equation by $v_1 \in H_0^1(\Omega_1)$ and integrates by parts to obtain the bilinear form

$$a_1(u_1, v_1) = \int_{\Omega_1} k_1 \nabla u_1 \cdot \nabla v_1 dx = (f_1, v_1),$$

and analogously for the subdomain Ω_2 , considering $v_2 \in H_0^1(\Omega_2)$ one finds that

$$a_2(u_2, v_2) = \int_{\Omega_2} k_2 \nabla u_2 \cdot \nabla v_2 dx = (f_2, v_2),$$

To (weakly) impose the continuity of the normal derivative at γ , consider the functional space

$$V_i = \{v \in H^1(\Omega_i) : v|_{\partial\Omega \cap \partial\Omega_i} = 0\},$$

and let $v_1 \in V_1$ and $v_2 \in V_2$. This allows us to write

$$\begin{aligned} - \int_{\Omega_1} k_1 \Delta u_1 v_1 dx - \int_{\Omega_2} k_2 \Delta u_2 v_2 dx &= \int_{\Omega_1} k_1 \nabla u_1 \cdot \nabla v_1 dx + \int_{\Omega_2} k_2 \nabla u_2 \cdot \nabla v_2 dx \\ &\quad - k_1 \int_{\gamma} \frac{\partial u_1}{\partial n_1} v_1 dx - k_2 \int_{\gamma} \frac{\partial u_2}{\partial n_2} v_2 dx \end{aligned}$$

Observe that if $v_1|_{\gamma} = v_2|_{\gamma} = \eta$, then using the condition on the normal derivative one would find that

$$\int_{\Omega_1} k_1 \nabla u_1 \cdot \nabla v_1 dx + \int_{\Omega_2} k_2 \nabla u_2 \cdot \nabla v_2 dx = (f_1, v_1) + (f_2, v_2).$$

As such, consider a continuous extension operator P_i from the interface to the domain Ω_i such that $(P_i \eta)|_{\gamma} = \eta$. In that case, given a function⁶ μ defined in γ , the identity above holds by rewriting it in the form

$$\int_{\Omega_1} k_1 \nabla u_1 \cdot \nabla P_1 \mu dx + \int_{\Omega_2} k_2 \nabla u_2 \cdot \nabla P_2 \mu dx = (f_1, P_1 \mu) + (f_2, P_2 \mu).$$

Finally, for the continuity on the interface, we assume that $u_1 = u_2$ on γ . The process above allows us to state the weak form of problem (3.16) as follows⁷.

⁶A description of such function will be given below when we formalize the weak form of the problem. For now, assume that such an extension has the regularity that we need.

⁷Analogous characterizations can be derived. This characterization is particularly useful when using decomposition methods which discretize the operators P_1 and P_2 .

Definition 3.3.1. Consider the set of equations (3.16). For $i = 1, 2$, let

$$\begin{aligned} V_i &= \{v_i \in H^1(\Omega_i) : v_i|_{\partial\Omega \cap \partial\Omega_i} = 0\}, \\ \Lambda &= \{\eta \in H^{\frac{1}{2}}(\gamma) : \eta = v|_\gamma \text{ for some } v \in H_0^1(\Omega)\}, \\ a_i(u_i, v_i) &= \int_{\Omega_i} k_i \nabla u_i \cdot \nabla v_i dx. \end{aligned}$$

Then the weak formulation of (3.16) reads as

$$\text{find } u_1 \in V_1, u_2 \in V_2 \text{ such that } \begin{cases} a_1(u_1, v_1) = (f_1, v_1), & \forall v_1 \in H_0^1(\Omega_1) \\ a_2(u_2, v_2) = (f_2, v_2), & \forall v_2 \in H_0^1(\Omega_2) \\ u_1 = u_2, & \text{on } \gamma \\ a_1(u_1, P_1\mu) + a_2(u_2, P_2\mu) = (f_1, P_1\mu) + (f_2, P_2\mu), & \forall \mu \in \Lambda \end{cases} \quad (3.19)$$

where the operator $P_i : \Lambda \rightarrow V_i$ is continuous for $i = 1, 2$.

We are now ready to prove the equivalence between the weak formulations of problems (3.16) and (3.17).

Theorem 3.3.2. Problem (3.18) is equivalent to (3.19).

Proof. (\implies) :

Let $u \in H_0^1(\Omega)$ be a solution of problem (3.18). Define $u_1 = u|_{\Omega_1}$ and $u_2 = u|_{\Omega_2}$. In order to check that u_1 satisfies the first equation in (3.19), let $v_1 \in H_0^1(\Omega_1)$. Considering the extension

$$\tilde{v}_1 = \begin{cases} v_1, & \text{in } \Omega_1 \\ 0, & \text{in } \Omega_2 \end{cases},$$

$\tilde{v}_1 \in H_0^1(\Omega)$ and by assumption $a_1(u_1, v_1) = a(u, \tilde{v}_1) = (f, \tilde{v}_1) = (f_1, v_1)$, as expected. For the second equation in (3.19) the process is analogous. For equation 3 in (3.19), we use the fact that $u \in H_0^1(\Omega)$ and therefore u is Hölder continuous by the De Giorgi Theorem, see Theorem 8.22 in [GTGT77]. As such, u is continuous on the interface and $u_1 = u_2$ on γ .

Finally, given $\mu \in \Lambda$, one defines

$$P\mu = \begin{cases} P_1\mu, & \text{in } \Omega_1 \\ P_2\mu, & \text{in } \Omega_2 \end{cases}$$

which satisfies $P\mu \in H_0^1(\Omega)$ and the equality 4 in (3.19).

(\impliedby) :

Let $u_1 \in V_1, u_2 \in V_2$ solve (3.19) in each subdomain and set

$$u = \begin{cases} u_1, & \text{in } \Omega_1 \\ u_2, & \text{in } \Omega_2 \end{cases}$$

as before. To check that $u \in H_0^1(\Omega)$, let $v \in \mathcal{D}(\Omega)$. Using integration by parts and the fact that $u_1 = u_2$ on the interface γ we have

$$\int_{\Omega} u \frac{\partial v}{\partial x_j} dx = \int_{\Omega_1} u_1 \frac{\partial v}{\partial x_j} dx + \int_{\Omega_2} u_2 \frac{\partial v}{\partial x_j} dx = - \int_{\Omega_1} \frac{\partial u_1}{\partial x_j} v dx - \int_{\Omega_2} \frac{\partial u_2}{\partial x_j} v dx,$$

where the weak derivatives of u exist and are given by

$$\frac{\partial u}{\partial x_j} = \begin{cases} \frac{\partial u_1}{\partial x_j}, & \text{in } \Omega_1 \\ \frac{\partial u_2}{\partial x_j}, & \text{in } \Omega_2, \end{cases}$$

for each $j = 1, 2$. Defining $P\mu$ as above, take $\mu \in \Lambda$ such that for some $v \in H_0^1(\Omega)$ one has $\mu = v|_{\gamma}$ and let $v_i = v|_{\Omega_i}$. Thus, the difference $(v_i - P_i\mu) \in H_0^1(\Omega_i)$ for each $i = 1, 2$ and

$$\begin{aligned} a(u, v) &= \int_{\Omega} k(x) \nabla u \cdot \nabla v dx = \int_{\Omega_1} k_1 \nabla u_1 \cdot \nabla v_1 dx + \int_{\Omega_2} k_2 \nabla u_2 \cdot \nabla v_2 dx \\ &= \int_{\Omega_1} k_1 \nabla u_1 \cdot \nabla (v_1 - P_1\mu) dx + \int_{\Omega_1} k_1 \nabla u_1 \cdot \nabla P_1\mu dx + \int_{\Omega_2} k_2 \nabla u_2 \cdot \nabla (v_2 - P_2\mu) dx + \int_{\Omega_2} k_2 \nabla u_2 \cdot \nabla P_2\mu dx \\ &= \int_{\Omega_1} f_1 (v_1 - P_1\mu) dx + \int_{\Omega_2} f_2 (v_2 - P_2\mu) dx + \int_{\Omega_1} f_1 P_1\mu dx + \int_{\Omega_2} f_2 P_2\mu dx \\ &= \int_{\Omega_1} f_1 v_1 dx + \int_{\Omega_2} f_2 v_2 dx = \int_{\Omega} f v dx = (f, v), \end{aligned}$$

where $f = \begin{cases} f_1, & \text{in } \Omega_1 \\ f_2, & \text{in } \Omega_2 \end{cases}$ as defined above, and we used the first, the second and the fourth equations in (3.19). □

4

The Method of Fundamental Solutions

4.1 Density and linear independence results

The Method of Fundamental Solutions is the base method to be implemented throughout this work. As a meshless method, it does not involve any kind of domain discretization (into some mesh) like in finite differences or finite elements methods. Instead, one faces a point placement problem. Considering that mesh generation constitutes a computationally intensive aspect of the aforementioned methods, the MFS stands out due to its distinct advantage of circumventing this necessity.

As the name implies, the MFS is based on the fundamental solution of a given elliptic PDE. Consider the elliptic linear differential operator \mathcal{L} , with a fundamental solution Φ such that $\mathcal{L}\Phi(x) = \delta$ for all $x \in \mathbb{R}^d$. In essence, we utilize this fundamental solution to construct the approximation

$$\tilde{u}(x) = \sum_{j=1}^N \alpha_j \Phi(x - y_j), \quad (4.1)$$

to the Boundary Value Problem (BVP)

$$\begin{cases} \mathcal{L}u(x) = 0, & \text{for } x \in \Omega \\ \mathcal{B}u(x) = 0, & \text{for } x \in \partial\Omega, \end{cases}$$

where \mathcal{B} is a linear boundary operator.

In equation (4.1), $y_j \in \mathbb{R}^d \setminus \overline{\Omega}$ for $j = 1, \dots, N$ are the so-called source points, which we deliberately place outside the domain, since, under translation, the fundamental solutions exhibit singularities at each y_j . Otherwise, our approximation would introduce singularities within Ω . By definition and using the linearity of the operator \mathcal{L} , \tilde{u} satisfies the equation within Ω , and we can determine the coefficients α_j by imposing the boundary conditions

$$\mathcal{B}\tilde{u}(x) = \sum_{j=1}^N \alpha_j \mathcal{B}\Phi(x - y_j) = 0.$$

Remark 4.1.1. While the motivation above might seem far-fetched, it's worth noting that the approximation \tilde{u} resembles a convolution between some density function $\alpha(x)$ and the fundamental solution Φ . As we will see below, it can be proven that the fundamental solutions of the operator \mathcal{L} are dense in the functional space defined on $\partial\Omega$ (which is sufficient since, as already discussed, the PDE is satisfied by construction). For example, for Dirichlet boundary conditions, one sets $\mathcal{B} = I$ and utilizes the single layer potential

$$u(x) = \int_{\hat{\Gamma}} \Phi(x - y) \varphi(y) d\sigma(y), \text{ for } x \in \mathbb{R}^2 \setminus \hat{\Gamma},$$

which is continuous in \mathbb{R}^2 , where $\varphi(y)$ is a layer density to be determined and $\hat{\Gamma}$ is some (source) set placed outside Ω (in Definition 4.1.2 below we formalize this concept rigorously). Through a discretization approach, one can consider the approximation

$$u(x) \approx \sum_{j=1}^N w_j \varphi(y_j) \Phi(x - y_j) = \tilde{u}(x), \quad (4.2)$$

where $y_j \in \hat{\Gamma}$ and w_j are the nodes and weights of some quadrature, respectively. By setting $\alpha_j = w_j \varphi(y_j)$, we recover the earlier approximation.

First, we introduce the notion of *artificial boundary* (or *pseudo-boundary*), which is analyzed in [Alv09].

Definition 4.1.2. A source set $\hat{\Gamma}$ is said to be admissible if

1. $\hat{\Gamma} \subset \mathbb{R}^d \setminus \overline{\Omega}$ is an open set with components in each external part of Ω ;
2. $\hat{\Gamma} = \partial\hat{\Omega}$ is the boundary of $\hat{\Omega}$, where $\hat{\Omega} \subset \mathbb{R}^d \setminus \overline{\Omega}$ is an open set with components in each external part of Ω . Note that the problem must be well-posed in $\hat{\Omega}$;
3. $\hat{\Gamma} \subset \partial\hat{\Omega}$, when $\partial\hat{\Omega}$ is an analytical boundary set verifying (2.) and $\hat{\Gamma}$ is open in the $\partial\hat{\Omega}$ topology.

We denote the set of chosen source points by $\mathcal{Y} = \{y_j \in \hat{\Gamma} : j = 1, \dots, N\}$.

Throughout this work, we will exclusively use the source set described in point 2 of Definition 4.1.2. We make this choice as it consistently yields superior numerical results. However, it's worth noting that the density results presented remain applicable even when considering different types of admissible source sets.

Assuming that $\mathcal{L} = -\Delta$ and Φ is the fundamental solution of the Laplace equation, we are working with Dirichlet boundary conditions unless stated otherwise. It's important to highlight that the results stated below are also valid with different boundary conditions. In the appropriate functional space and given an admissible source set $\hat{\Gamma}$, consider the approximation space

$$\mathcal{S}(\Gamma, \hat{\Gamma}) = \text{span}\{\Phi(x - y)|_{x \in \Gamma} : y \in \hat{\Gamma}\}.$$

Some preliminary results are going to be needed in order to present the desired density proofs. We start by introducing the concept of analytic continuation. We refer to [NN12] for more details.

Definition 4.1.3. *Let f be a complex-valued function defined on $\Omega \subset \mathbb{C}$. We say that f is holomorphic on Ω if for every $a \in \Omega$, there exists a neighborhood U of a and $(c_n)_{n \in \mathbb{N}} \subset \mathbb{C}$ such that the power series*

$$\sum_{n=0}^{\infty} c_n (z - a)^n$$

converges to $f(z)$ for every $z \in U$.

Theorem 4.1.4 (Analytic continuation). *Let f be a holomorphic function in the connected subset $\Omega \subset \mathbb{C}$. If there exists a non-empty $U \subset \Omega$ such that $f = 0$ in U , then $f = 0$ in Ω .*

As evident from the Remark 4.1.1 above, the examination of layer potentials plays a pivotal role in the Method of Fundamental Solutions. Due to the depth of this topic, we refer to [CZ10], [Kre13], and [CK13] for a more comprehensive understanding.

Definition 4.1.5. *Let $\Omega \subset \mathbb{R}^d$ be a bounded domain of class C^2 and $\varphi \in H^{\frac{1}{2}}(\partial\Omega)$. For $x \in \partial\Omega$, the functions*

$$S\varphi(x) = \int_{\partial\Omega} \Phi(x - y) \varphi(y) d\sigma(y)$$

and

$$M\varphi(x) = \int_{\partial\Omega} \frac{\partial\Phi(x - y)}{\partial n_y} \varphi(y) d\sigma(y)$$

are called the single and double layer potentials associated with the operators S and M with density φ , respectively.

Proposition 4.1.6. *Let $\Omega \subset \mathbb{R}^d$ be a bounded domain of class C^2 and $\varphi \in H^{\frac{1}{2}}(\partial\Omega)$. Then the single layer potential is harmonic in $\mathbb{R}^d \setminus \overline{\partial\Omega}$, continuous across $\partial\Omega$, and for every $x \in \partial\Omega$ we have the following jump relations for the normal derivative:*

$$\frac{\partial S\varphi_{\pm}}{\partial n}(x) = \int_{\partial\Omega} \frac{\partial\Phi(x - y)}{\partial n_x} \varphi(y) d\sigma(y) \mp \frac{1}{2}\varphi(x),$$

where

$$\frac{\partial S\varphi_{\pm}}{\partial n}(x) := \lim_{h \rightarrow 0} n(x) \cdot \nabla S\varphi(x \pm hn(x))$$

is to be understood in the sense of uniform convergence on $\partial\Omega$ and where the integral exists as an improper integral. In particular, we have

$$\varphi(x) = \frac{\partial S\varphi_+}{\partial n}(x) - \frac{\partial S\varphi_-}{\partial n}(x), \quad \forall x \in \partial\Omega.$$

Analogously, the double layer potential is harmonic in $\mathbb{R}^d \setminus \overline{\partial\Omega}$, its normal derivative is continuous across $\partial\Omega$, and for every $x \in \partial\Omega$ we have the following jump relations:

$$M\varphi_{\pm}(x) = \int_{\partial\Omega} \frac{\partial \Phi(x-y)}{\partial n_y} \varphi(y) d\sigma(y) \pm \frac{1}{2} \varphi(x),$$

where

$$M\varphi_{\pm}(x) := \lim_{h \rightarrow 0} M\varphi(x \pm hn(x)).$$

In particular, we have

$$\varphi(x) = M\varphi(x)_+ - M\varphi(x)_-, \quad \forall x \in \partial\Omega.$$

Lastly, it will be useful to study the well-posedness of the exterior Dirichlet problem for the Laplace Equation, e.g. [Sal16].

Theorem 4.1.7 (Well-Posedness of the Exterior Dirichlet problem). *Let Ω be a bounded and open subset of \mathbb{R}^2 . Then, there exists a unique solution $u \in C^2(\Omega^c) \cap C(\overline{\Omega^c})$ of the exterior Dirichlet Laplacian problem with boundary data $g \in C(\partial\Omega)$ given by*

$$\begin{cases} \Delta u = 0, & \text{in } \mathbb{R}^2 \setminus \overline{\Omega} \\ u = g, & \text{on } \partial\Omega \\ u(x) = \mathcal{O}(1), & \text{for } |x| \rightarrow \infty. \end{cases}$$

Remark 4.1.8. Notice that the condition at infinity must be enforced to ensure uniqueness. For example, if considering null Dirichlet boundary conditions, one could easily find a family of solutions up to a multiplicative constant (if $u(x)$ is a solution, then $\alpha u(x)$ would also be a solution for any $\alpha \in \mathbb{R}$).

The main result which justifies the MFS for the Laplace equation is now stated. The proof given here is slightly different from the ones in [Bog85], [Alv09] and [Smy09]. It is also influenced by the proofs in [Val08].

Theorem 4.1.9. *Let Ω be an open and bounded set with C^2 boundary $\Gamma = \partial\Omega$ such that $\overline{\Omega} \subset \hat{\Omega} \subset \mathbb{R}^2$, where $\hat{\Omega}$ is an open and bounded set and $\hat{\Gamma} = \partial\hat{\Omega}$ is an admissible source set. Then, $\mathcal{S}(\Gamma, \hat{\Gamma}) \oplus \mathbb{R}$ is dense in $H^{\frac{1}{2}}(\Gamma)$.*

Proof. Using the notation from Lemma 2.1.10, consider $E = H^{\frac{1}{2}}(\Gamma)$. For every (fixed) $y \in \hat{\Gamma}$, the maps ¹

$$\begin{aligned}\Phi(\cdot - y) : \varphi &\mapsto \int_{\Gamma} \Phi(x - y) \varphi(x) d\sigma(x) \\ 1 : \varphi &\mapsto \int_{\Gamma} \varphi(x) d\sigma(x)\end{aligned}$$

are linear and continuous in $H^{\frac{1}{2}}(\Gamma)$, and $1, \Phi(\cdot - y) \in H^{-\frac{1}{2}}(\Gamma)$ (notice that $1, \Phi(\cdot - y) \in L^1_{\text{loc}}(\mathbb{R}^2)$ and $1, \Phi(\cdot - y) \in L^2(\Gamma)$).

Let $N = S(\Gamma, \hat{\Gamma}) \oplus \mathbb{R} \subset H^{-\frac{1}{2}}(\Gamma)$. Using the Definition 2.1.9, consider the set

$$N^{\perp} = \{\varphi \in H^{\frac{1}{2}}(\Gamma) : \langle \psi, \varphi \rangle = 0, \forall \psi \in N\},$$

where the duality pairing $\langle \cdot, \cdot \rangle$ generalizes the L^2 inner product as explained in Remark 2.3.13 and defined in (2.1). By Remark 2.1.11, it suffices to prove that $N^{\perp} = \{0\}$. Let $\varphi \in N^{\perp}$ and define

$$w(y) = \int_{\Gamma} \Phi(x - y) \varphi(x) d\sigma(x), \quad y \in \mathbb{R}^2.$$

Since $\varphi \in N^{\perp}$, then

$$\int_{\Gamma} \Phi(x - y) \varphi(x) d\sigma(x) = 0, \quad \forall y \in \hat{\Gamma} \quad (4.3)$$

and

$$\int_{\Gamma} \varphi(x) d\sigma(x) = 0. \quad (4.4)$$

In order to verify that $w(y)$ satisfies the exterior Laplace problem with Dirichlet boundary conditions, one uses the fact that w exhibits the asymptotic behavior (see Chapter 6 of [Kre13])

$$w(y) = -\frac{1}{2\pi} \int_{\Gamma} \varphi(x) d\sigma(x) \log |y| + \mathcal{O}(1), \quad |y| \rightarrow \infty$$

and condition (4.4), to check that w is bounded at infinity. Therefore, by condition (4.3)

$$\begin{cases} \Delta w = 0, & \text{in } \mathbb{R}^2 \setminus \hat{\Omega} \\ w(y) = 0, & \text{on } \hat{\Gamma} \\ w(y) = \mathcal{O}(1), & |y| \rightarrow \infty. \end{cases}$$

Since the problem above is well-posed, it has a unique solution $w(y) = 0, \forall y \in \mathbb{R}^2 \setminus \overline{\hat{\Omega}}$. By (a unique) analytic continuation (see Theorem 4.1.4), one can extend w by zero in $\mathbb{R}^2 \setminus \overline{\Omega}$. Since w is a single layer potential over Γ , w is continuous on Γ and therefore, by continuity, $w = 0$ on Γ . Once again, using the fact that the single layer potential is harmonic in Ω , w satisfies the (interior) Laplace problem

$$\begin{cases} \Delta w = 0, & \text{in } \Omega \\ w(y) = 0, & \text{on } \Gamma \end{cases}$$

¹Here, Φ is used not only to represent the fundamental solution of the Laplace equation, but also the single layer potential S . This notation was used not only to emphasize that the fundamental solution centered in $y \in \hat{\Gamma}$ is in the space $H^{-\frac{1}{2}}(\Gamma)$ but also to remark that the action $\langle \Phi(\cdot - y), \varphi \rangle$ depends on y , contrary to the single layer potential in Definition 4.1.5.

which, by uniqueness, implies that $w = 0$ in Ω and consequently in \mathbb{R}^2 . Finally, we can conclude that $\varphi = 0$ in Γ by Proposition 4.1.6 since the normal derivate jump is zero.

Therefore, $N^\perp = \{0\}$ and by Lemma 2.1.10

$$\mathcal{S}(\Gamma, \hat{\Gamma}) \oplus \mathbb{R} = \{0\}^\perp$$

given that $H^{\frac{1}{2}}(\Gamma)$ is reflexive. Since $0 \in H^{\frac{1}{2}}(\Gamma)$ (and $0 \in H^{-\frac{1}{2}}(\Gamma)$) then $\mathcal{S}(\Gamma, \hat{\Gamma}) \oplus \mathbb{R}$ is dense in $H^{\frac{1}{2}}(\Gamma)$ and in $H^{-\frac{1}{2}}(\Gamma)$ (this is to be expected since $H^s(\Omega)$ is dense in $H^{-s}(\Omega)$ for $s > 0$). \square

Remark 4.1.10. Theorem 4.1.9 guarantees the existence of a sequence of density functions $\{\varphi_n\} \subset H^{\frac{1}{2}}(\Gamma)$ and a sequence of constants $\{c_n\} \subset \mathbb{R}$ such that the modified single-layer potential

$$\hat{\mathcal{S}}\varphi_n(y) = \int_{\Gamma} \Phi(x-y)\varphi_n(x)d\sigma(x) + c_n$$

converges to the Dirichlet boundary data g in $H^{\frac{1}{2}}(\Gamma)$, i.e.,

$$\|\hat{\mathcal{S}}\varphi_n|_{\Gamma} - g\|_{H^{\frac{1}{2}}(\Gamma)} \rightarrow 0, \quad n \rightarrow \infty.$$

Since $\hat{\mathcal{S}}\varphi_n$ is harmonic for each $n \in \mathbb{N}$, it allows us to approximate any interior Laplace Dirichlet BVP. Conversely, for any $\varphi \in H^{\frac{1}{2}}(\Gamma)$ and $c \in \mathbb{R}$, they define a BVP whose solution is given by the associated modified single-layer potential $\hat{\mathcal{S}}\varphi$, with boundary data determined by its restriction to Γ .

The density proof for the transmission/decomposition problem directly follows from Theorem 4.1.9 and the equivalence formulation presented in Theorem 3.3.2. In Chapter 5, we specifically consider the case $f_1 = f_2 = 1$ in equations (3.16). Thus, we introduce the source function

$$f = \begin{cases} \frac{1}{k_1}, & \text{in } \Omega_1 \\ \frac{1}{k_2}, & \text{in } \Omega_2 \end{cases} \quad (4.5)$$

and let $u \in H_0^1(\Omega)$ represent the associated unique weak solution to the Poisson equation with Dirichlet boundary conditions and a (discontinuous) source function f as in equation (3.17). According to Theorem 3.3.2, the restriction of u to each subdomain uniquely solves the weak form of

$$\begin{cases} -\Delta u_i = \frac{1}{k_i}, & \text{in } \Omega_i \\ u_1 - u_2 = 0, & \text{on } \gamma \\ k_1 \frac{\partial u_1}{\partial \mathbf{n}_1} + k_2 \frac{\partial u_2}{\partial \mathbf{n}_2} = 0, & \text{on } \gamma \\ u_i = 0, & \text{on } \Gamma_i \end{cases}, \quad \text{where } u = \begin{cases} u_1, & \text{in } \Omega_1 \\ u_2, & \text{in } \Omega_2 \end{cases} \quad (4.6)$$

and $u_i \in H^1(\Omega_i)$ for $i = 1, 2$.

Since $H^{\frac{1}{2}}(\partial\Omega_i)$ is the trace space of $H^1(\Omega_i)$, and the normal derivatives of u_i belong to the space $H^{-\frac{1}{2}}(\partial\Omega_i)$ (as seen in the final part of subchapter 2.3), one can apply Theorem 4.1.9 to each subdomain in equation (4.6). This allows us to find a sequence of density layers $\{\varphi_i^{(n)}\} \subset H^{\frac{1}{2}}(\partial\Omega_i)$ such that

$$\begin{aligned} \|\hat{\mathcal{S}}\varphi_i^{(n)}|_{\partial\Omega_i} - u_i\|_{H^{\frac{1}{2}}(\partial\Omega_i)} &\rightarrow 0, \quad n \rightarrow \infty, \\ \|M\varphi_i^{(n)}|_{\partial\Omega_i} - \frac{\partial u_i}{\partial n_i}\|_{H^{-\frac{1}{2}}(\partial\Omega_i)} &\rightarrow 0, \quad n \rightarrow \infty, \end{aligned}$$

where \hat{S} is defined in Remark 4.1.10, and M is the double-layer potential in Definition 4.1.5 (see Remark 4.1.15 for more details on how different boundary conditions can be handled). Consequently, given the equivalence between both problems, it is possible to approximate the solution u of the Poisson equation with a discontinuous source term using the MFS via the decomposition approach².

Finally, the discretization argument follows from the fact that for a set of source points $\mathcal{Y} = \{y_1, \dots, y_N\} \subset \mathbb{R}^2 \setminus \bar{\Omega}$, the fundamental solutions $\Phi(\cdot - y_1), \dots, \Phi(\cdot - y_N)$ are linearly independent on $\partial\Omega$ and, consequently, in Ω .

Theorem 4.1.11. *Let \mathcal{Y} be a set of source points, as defined above. Then, the restriction of the functions $\Phi(\cdot - y_1), \dots, \Phi(\cdot - y_N)$ to $\partial\Omega$ are linearly independent.*

Proof. Assume that $\tilde{u}(x) = \sum_{j=1}^N \alpha_j \Phi(x - y_j) = 0$, $\forall x \in \partial\Omega$. We prove that $\alpha_1 = \dots = \alpha_N = 0$. Since, by construction, \tilde{u} satisfies the Laplace equation and by assumption $\tilde{u}(x) = 0$, $\forall x \in \partial\Omega$, by the well-posedness of the interior Dirichlet problem, $\tilde{u} = 0$ in $\bar{\Omega}$. Again, by analytic continuation, $\tilde{u} = 0$ in $\mathbb{R}^2 \setminus \mathcal{Y}$. Applying the Laplace operator to \tilde{u} , by linearity

$$\sum_{j=1}^N \alpha_j \delta y_j = 0$$

which implies that $\alpha_1 = \dots = \alpha_N = 0$ by the linear independence of the Dirac deltas. \square

Now consider the operator $\mathcal{L} = -(\Delta + k^2)$, and assume that k is **not** an eigenfrequency of the Helmholtz equation in Ω (for the exterior problem, instead of using the term *eigenfrequency*, one says *scattering resonance*). The results presented for the fundamental solution of the Laplace Equation still hold for the fundamental solution of the Helmholtz equation. However, a different type of conditions at infinity must be considered, as discussed in [CK13].

Theorem 4.1.12 (Well-Posedness of the Exterior Dirichlet problem of the Helmholtz Equation). *Let Ω be a bounded and open subset of \mathbb{R}^2 and assume that k is positive. Then, there exists a unique solution $u \in C^2(\Omega^c) \cap C(\bar{\Omega}^c)$ of the exterior Dirichlet Helmholtz problem with boundary data $g \in C(\partial\Omega)$ given by*

$$\begin{cases} -\Delta u = k^2 u, & \text{in } \mathbb{R}^2 \setminus \bar{\Omega} \\ u = g, & \text{on } \partial\Omega \\ |x| \left(\frac{x}{|x|} \nabla u(x) - ik \right) u(x) = 0, & \text{for } |x| \rightarrow \infty. \end{cases}$$

Remark 4.1.13. *Just like the exterior Dirichlet problem for the Laplace Equation, the well-posedness of the exterior Helmholtz Problem depends on conditions at infinity. In this case, they are known as the*

²One important detail was overlooked: while the density result in 4.1.9 is independent of the MFS, by construction it is only applicable to harmonic functions. Nevertheless, one can always find a non-homogeneous solution and transform the problem into a homogeneous PDE by adjusting the boundary conditions accordingly. Chapter 5 presents a more detailed approach.

Sommerfeld Radiation Conditions and are expressed as

$$|x|^{\frac{d-1}{2}} \left(\frac{x}{|x|} \nabla u(x) - ik \right) u(x) = 0, \text{ as } |x| \rightarrow \infty,$$

where d represents the spatial dimension. It's worth noting that the single-layer potential defined as

$$\int_{\Gamma} \Phi_k(x-y) \varphi(x) d\sigma(x)$$

also satisfies the Sommerfeld Radiation Condition as $|y| \rightarrow \infty$.

Analogously to the Laplace problem, consider the space

$$\mathcal{S}(\Gamma, \hat{\Gamma}) = \text{span}\{\Phi_k(x-y)|_{x \in \Gamma} : y \in \hat{\Gamma}\}.$$

Again, like in Theorem 4.1.9, we point the reader to [Alv09], [Val08] and [AC05], where slightly different proofs are stated.

Theorem 4.1.14. Assume that k is positive and let Ω be an open and bounded set with C^2 boundary $\Gamma = \partial\Omega$ such that $\overline{\Omega} \subset \hat{\Omega} \subset \mathbb{R}^2$, where $\hat{\Omega}$ is an open and bounded set and $\hat{\Gamma} = \partial\hat{\Omega}$ is an admissible source set. Then, $\mathcal{S}(\Gamma, \hat{\Gamma})$ is dense in $H^{\frac{1}{2}}(\Gamma)$.

Proof. This proof follows the same steps as in the proof of Theorem 4.1.9. As before, let $E = H^{\frac{1}{2}}(\Gamma)$. For every (fixed) $y \in \hat{\Gamma}$, the map

$$\Phi_k(\cdot - y) : \varphi \mapsto \int_{\Gamma} \Phi_k(x-y) \varphi(x) d\sigma(x)$$

is linear and continuous in $H^{\frac{1}{2}}(\Gamma)$ and $\Phi_k(\cdot - y) \in H^{-\frac{1}{2}}(\Gamma)$. Let $N = \mathcal{S}(\Gamma, \hat{\Gamma})$ and

$$N^{\perp} = \{\varphi \in H^{\frac{1}{2}}(\Gamma) : \langle \psi, \varphi \rangle = 0, \psi \in N\}.$$

Once again, it suffices to prove that $N^{\perp} = \{0\}$, i.e., given $\varphi \in H^{\frac{1}{2}}(\Gamma)$ the implication

$$\forall y \in \hat{\Gamma}, \int_{\Omega} \Phi_k(x-y) \varphi(x) d\sigma(x) = 0 \implies \varphi(x) = 0, \forall x \in \mathbb{R}^2$$

holds and define

$$w(y) = \int_{\Gamma} \Phi_k(x-y) \varphi(x) d\sigma(x).$$

Given that w satisfies the Sommerfeld Radiation Conditions and, by assumption, $w(y) = 0$ in $\hat{\Gamma}$, then $w = 0$ in $\mathbb{R}^2 \setminus \Omega$ is the unique solution of the exterior Dirichlet problem of the Helmholtz equation

$$\begin{cases} -\Delta w = k^2 w, & \text{in } \mathbb{R}^2 \setminus \overline{\Omega} \\ w = 0, & \text{on } \partial\Omega \\ |y| \left(\frac{y}{|y|} \nabla w(y) - ik \right) u(x) = 0, & \text{for } |y| \rightarrow \infty, \end{cases}$$

since $k > 0$ is not a scattering resonance. By analytic continuation, one can extend w by zero to $\mathbb{R}^2 \setminus \overline{\Omega}$. The rest of the proof is the same as in the Theorem 4.1.9, using the fact that k is not an eigenfrequency of Ω , the interior Dirichlet problem is well-posed. \square

Remark 4.1.15. In both Theorem 4.1.9 and Theorem 4.1.14, the density proof can be extended to $H^s(\Gamma)$ for $s > \frac{1}{2}$. However, in practical applications, we are primarily interested in the case $s = \frac{1}{2}$. It's worth noting that when $s = 0$, there's no need to invoke the Hahn-Banach Theorem since $H^0(\Gamma) = L^2(\Gamma)$, which is a Hilbert Space. In such cases, we can rely on Corollary 2.2.3.

For situations involving general boundary conditions, the proofs presented above follow the same logical framework. One should consider the appropriate approximating set $\mathcal{S}(\Gamma, \hat{\Gamma})$ and the corresponding integral operator. For example, in the case of Neumann boundary conditions, the set $\mathcal{S}(\Gamma, \hat{\Gamma})$ would be defined as

$$\mathcal{S}(\Gamma, \hat{\Gamma}) = \text{span}\{\partial_n \Phi(x - y)|_{x \in \Gamma} : y \in \hat{\Gamma}\},$$

accompanied by the use of the double-layer potential $M\varphi$. It's important to note that $\partial_n u = g \in H^{-\frac{1}{2}}(\Gamma)$ in these scenarios.

Once again, the discretization argument relies on the linear independence of the functions $\Phi_k(\cdot - y_1), \dots, \Phi_k(\cdot - y_N)$, where $y_1, \dots, y_N \in \mathbb{R}^2 \setminus \overline{\Omega}$ are distinct source points. The proof follows the same logic as presented in Theorem 4.1.11 and from the fact that k is not an eigenfrequency of Ω .

Before stating the results regarding the convergence and stability of the MFS for the Laplace and Helmholtz equations, we address the issue of source point placement. Various methods for this purpose are discussed in [Alv09]. In this work, we adopt the approach outlined in point 2 of Definition 4.1.2 for the source points placement. To illustrate this method, consider $\Gamma = \partial\Omega$ and the equally spaced collocation points $x_1, \dots, x_M \in \Gamma$. We then approximate the outward normal vector $\tilde{\mathbf{n}}_i$ at the point x_i using the formula

$$\tilde{\mathbf{n}}_i = \frac{(x_i - x_{i-1})^\perp}{2} + \frac{(x_{i+1} - x_i)^\perp}{2},$$

with the orthogonal notation $z^\perp = (-z_2, z_1)$. Using this, we can further approximate the unit normal vector as $\mathbf{n}_i = \frac{\tilde{\mathbf{n}}_i}{|\tilde{\mathbf{n}}_i|}$, and define the source point y_i as

$$y_i = x_i + \eta \mathbf{n}_i,$$

where $\eta > 0$ (with its sign depending on the orientation of the boundary's parameterization) is a small coefficient controlling the distance between the boundary Γ and the artificial boundary $\hat{\Gamma}$. As we will discuss below, this coefficient significantly impacts the convergence of the MFS, with larger values of η potentially yielding better approximations. However, this approach is most effective for simple geometries, as it can increase the condition number of the matrix A , denoted by $\kappa(A)$.

4.2 Numerical approach for the Laplace Equation

Based on the results presented in the previous subsection, we can now proceed with the numerical solution of both the Laplace and Helmholtz equations for (Dirichlet, Neumann, . . .) boundary data g , pro-

vided we can determine the coefficients in the discretization of the single-layer potential. For simplicity, we will continue to assume Dirichlet boundary conditions. Let N denote the number of source points, and M represent the number of collocation points on the boundary, labeled as x_i with $i = 1, \dots, M$. We proceed by solving the discretized equation

$$\tilde{u}(x_i) = \sum_{j=1}^N \alpha_j \Phi(x_i - y_j) + \alpha_{N+1} = g(x_i)$$

with respect to the coefficients α_j . Defining $g_i := g(x_i)$, $i = 1, \dots, M$, notice that the equation above can be rewritten in the matrix form

$$\underbrace{\begin{bmatrix} \Phi(x_1, y_1) & \cdots & \Phi(x_1, y_N) & 1 \\ \vdots & \ddots & \vdots & \vdots \\ \Phi(x_M, y_1) & \cdots & \Phi(x_M, y_N) & 1 \end{bmatrix}}_A \underbrace{\begin{bmatrix} \alpha_1 \\ \vdots \\ \alpha_N \\ \alpha_{N+1} \end{bmatrix}}_{\alpha} = \underbrace{\begin{bmatrix} g_1 \\ \vdots \\ g_M \end{bmatrix}}_g \quad (4.7)$$

$M \times (N+1) \quad (N+1) \times 1 \quad M \times 1$

It is important to note that when $M < N + 1$, we have an under-determined system of equations. Consequently, the number of collocation points must be greater than the number of source points. This situation can be framed in two distinct ways:

- if $N + 1 = M$, we encounter an interpolation problem where we solve a linear system consisting of N equations with N unknowns;
- when $M > N + 1$, we must address a least-squares problem. This approach is adopted in this work as it avoids interpolation instabilities, enforces boundary conditions at specific points, and exhibits robustness, especially when dealing with irregular boundary data. Following numerous numerical experiments, as detailed in [Alv09], it was established that $M = 2N$ is a suitable choice for both the number of source and collocation points.

It's important to recall that various boundary conditions can be considered. For instance, when solving the Laplace equation with Neumann boundary conditions, the entries $\Phi(x_i, y_j)$ should be replaced with $\partial_{n_x} \Phi(x_i, y_j) = \nabla_x \Phi(x_i, y_j) \cdot \mathbf{n}_i$, where \mathbf{n}_i represents the unit normal vector at the boundary point x_i .

Now, we present some results concerning the convergence and stability of the MFS for the Laplace equation with Dirichlet boundary conditions. These results are specifically derived for a disk-shaped domain Ω with a circular artificial boundary $\hat{\Gamma} = \partial\hat{\Omega}$. Let ρ denote the radius of Ω , R the radius of $\hat{\Omega}$, and assume that $N = M$.

Theorem 4.2.1. *Assume that $R^N - \rho^N \neq 1$. Then,*

1. *the matrix A is non-singular;*
2. *if $R \neq 1$ and the boundary data g is real and analytic, then the exact solution u of the Laplace equation admits a harmonic extension to some neighborhood of $\overline{\Omega}$. Therefore, one may assume*

that u is harmonic in $0 \leq r \leq r_0$ for some $r_0 \geq \rho$. In this case, there exists $C > 0$ and $c \in (0, 1)$ which are independent of N and u such that

$$\sup_{x \in \Omega} |u(x) - \tilde{u}(x)| \leq Cc^N \sup_{|x| \leq r_0} |u(x)|.$$

Theorem 4.2.1 provides some insights into the MFS. Firstly, it's essential to note that this method exhibits *exponential convergence* concerning the number of source points, which is quite remarkable. In fact, the term c depends on the distance between Γ and the artificial boundary $\hat{\Gamma}$, controlled by the coefficient η , and is defined as

$$c = \begin{cases} \frac{\rho}{R}, & \text{if } r_0 > \frac{R^2}{\rho} \\ \sqrt{\frac{\rho}{R}}, & \text{if } r_0 < \frac{R^2}{\rho}. \end{cases}$$

However, one of the main drawbacks of the MFS is the ill-conditioning of the matrix A , along with the fact that this matrix is dense, making it unsuitable for the utilization of optimized sparse software solvers for the system (4.7). In particular, while larger values of the parameter η enable better numerical approximations, they also lead to an exponential increase³ in the condition number $\kappa(A)$, as documented in [CM81], [Kit88], and [Kit91].

Theorem 4.2.2. *In the conditions of the Theorem 4.2.1, the condition number $\kappa(A)$ can be estimated by*

$$\kappa(A) \sim \frac{\log R}{2} N \left(\frac{R}{\rho} \right)^{\frac{N}{2}}.$$

Another interesting point to note is the condition $R \neq 1$, which is directly related to the space $\mathcal{S}(\Gamma, \hat{\Gamma}) \oplus \mathbb{R}$ that was proven to be dense in $H^{\frac{1}{2}}(\Gamma)$ in Theorem 4.1.9. Suppose $R = 1$ and $\hat{\Omega}$ is a disk with radius R containing the origin. In such a case, if we exclude the constant basis function 1, then

$$\tilde{u}(0) = \sum_{j=1}^N \alpha_j \Phi(0 - y_j) = -\frac{1}{2\pi} \sum_{j=1}^N \alpha_j \log(R) = 0,$$

regardless of the choice of source points on $\hat{\Gamma}$. Consequently, it becomes impossible to approximate any non-zero harmonic function at the origin. However, this limitation is overcome when we include the basis function 1, as it was used to establish the density result. While this rarely affects the numerical approximations in the subsequent chapters, it is nevertheless included for the sake of consistency. This is why a column of ones was added to the matrix A .

4.2.1 An enrichment technique

Before diving into the numerical approach for the Helmholtz equation, we introduce some modifications to the classical MFS method presented in the previous subsection. There is another drawback in our

³It's important to note that the ill-conditioning of the matrix A is associated with the classical basis functions used in the MFS. Nonetheless, it is possible to derive basis functions that, after certain modifications, do not exhibit the same limitations and have a condition number $\kappa(A)$ of $\mathcal{O}(1)$. We refer to [Ant18b] and [Ant18a] for more information.

method: our basis functions are analytical and might lose precision when approximating functions that display singularities, for example near a corner if the domain is not smooth. In what follows we introduce an enrichment technique with particular solutions⁴ that allows for singularity treatment. In the same vein as in Proposition 3.2.3, consider a wedge-like domain with interior angle Θ .

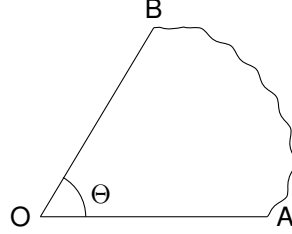


Figure 4.1: A wedge-like “shape” with an interior angle Θ .

Consider the Laplace equation in polar coordinates, given by

$$\left(\partial_r^2 + \frac{1}{r} \partial_r + \frac{1}{r^2} \partial_\theta^2 \right) u(r, \theta) = 0, \quad r > 0, \quad 0 \leq \theta \leq \Theta. \quad (4.8)$$

Then, by separation of variables $u(r, \theta) = R(r)T(\theta)$, one can find two different families of particular solutions given by

$$u(r, \theta) = (c_1 r^\alpha + c_2 r^{-\alpha}) \times (c_3 \cos(\alpha\theta) + c_4 \sin(\alpha\theta)), \quad \alpha > 0$$

or

$$u(r, \theta) = (c_1 \log(r) + c_2) \times (c_3 \theta + c_4),$$

where $c_1, c_2, c_3, c_4 \in \mathbb{C}$. To find α , one must take into account the amplitude of the angle Θ and the boundary conditions at each segment \overline{OA} and \overline{OB} . We summarize the asymptotic harmonic solutions of (4.8) in Appendix C.

To incorporate the singular behavior near a corner with less regularity and (possible) singularities⁵, first assume, without loss of generality, that the domain Ω has just one corner and that the solution of our BVP can be decomposed in regular and singular parts,

$$u(x) = u_R(x) + u_S(x), \quad x \in \overline{\Omega},$$

where u_R is the regular part approximated by the MFS basis functions and the singular part u_S is approximated by Fourier expansions using the families of particular solutions above, having the boundary

⁴ The terminology *particular solutions* agrees with the references [BT05], [AV10], and [BB08], and it does not refer to the solution of a non-homogeneous PDE, which is also called a *particular solution*. To avoid confusion, the latter will be referred to as a *non-homogeneous* solution.

⁵We discuss another matter related to terminology. In the literature, these types of corners are often referred to as “singular corners.” However, this terminology is problematic (as there is no such thing as a “singular corner”). Therefore, whenever we encounter such corners, we explicitly describe them as “less regular corners” or “corners with potential singularities”.

conditions into account. Let $\phi_s(r, \theta)$ be one of those expansions centered at the corner's tip, where s is the order of the expansion. Then, the numerical approximation can be written as

$$\tilde{u}(x) = \sum_{j=1}^N \alpha_j \Phi(x - y_j) + \alpha_{N+1} + \sum_{s=1}^P \beta_s \phi_s(r(x), \theta(x)), \quad x \in \bar{\Omega}. \quad (4.9)$$

Considering the collocation points $x_1, \dots, x_M \in \partial\Omega$, the linear system of equations (4.7) can be generalized to

$$\underbrace{\begin{bmatrix} A_1 & B_1 \end{bmatrix}}_{\substack{A \\ M \times (N+1+P)}} \begin{bmatrix} \alpha \\ \beta \end{bmatrix}_{(N+1+P) \times 1} = \begin{bmatrix} g \end{bmatrix}_{M \times 1}, \quad (4.10)$$

where the block matrix A_1 is the matrix A in (4.7) and the B_1 block matrix is given by

$$B_1 = \begin{bmatrix} \phi_1(r(x_1), \theta(x_1)) & \cdots & \phi_P(r(x_1), \theta(x_1)) \\ \vdots & \ddots & \vdots \\ \phi_1(r(x_M), \theta(x_M)) & \cdots & \phi_P(r(x_M), \theta(x_M)) \end{bmatrix}.$$

4.3 Numerical approach for the Helmholtz Equation

For the Helmholtz equation, the MFS convergence and stability results resemble the previous ones for the Laplace equation with Dirichlet boundary conditions. Once again, the results are stated for identical geometries as before, where Ω is the unit disk and the radius of $\hat{\Omega}$ is $R > 1$. Here it is assumed that the boundary data g can be analytically extended to the annulus $\{z \in \mathbb{C} : \frac{1}{\rho} < |z| < \rho\}$, where $\rho > 1$. The following result is due to [BB08].

Theorem 4.3.1. *Let $R > 1$ and N be an even number. Then the minimum boundary error achieved by the MFS in the unit disk satisfies*

$$\|g - \tilde{u}|_{\Gamma}\|_{L^2(\Gamma)} \leq \begin{cases} C\rho^{-\frac{N}{2}}, & \text{if } \rho < R^2 \\ C\sqrt{N}R^{-N}, & \text{if } \rho = R^2 \\ CR^{-N}, & \text{if } \rho > R^2 \end{cases}$$

where C is a constant that not depends on N .

To solve the Helmholtz equation with the MFS, one must start by computing the eigenvalues λ (or the eigenfrequencies k , with $\lambda = k^2$) first. In order to achieve that, recall that the BVP for the Helmholtz equation

$$\begin{cases} -\Delta u = k^2 u, & \text{in } \Omega \\ u = 0, & \text{on } \partial\Omega \end{cases} \quad (4.11)$$

is well-posed when k is not an eigenfrequency of Ω , and in that case the nullspace of the single layer potential operator

$$S_k \varphi(y) = \int_{\hat{\Gamma}} \Phi_k(x - y) \varphi(x) d\sigma(x)$$

is trivial. More precisely, one can prove the following result, e.g. [AA05].

Theorem 4.3.2. *If k is not an eigenfrequency of the interior Dirichlet problem, then $\dim(\ker(S_k)) = 0$.*

Proof. If k is not an eigenfrequency of Ω , then the interior problem is well posed which implies that $S_k\varphi(x) = 0, \forall x \in \bar{\Omega}$ since $S_k\varphi(x) = 0$ on $\partial\Omega$. By analytical continuation, $S_k\varphi(x) = 0, x \in \hat{\Omega}$. Since the single layer potential is continuous, then $S_k\varphi(x) = 0, x \in \hat{\Gamma}$. By the well-posedness of the exterior problem (notice that the single layer potential satisfies the Sommerfeld radiation conditions), then $S_k\varphi(x) = 0, \forall x \in \mathbb{R}^2$ and therefore $\varphi(x) = 0, \forall x \in \Gamma$, by the jump relations in Proposition 4.1.6. \square

Theorem 4.3.2 can be used to search for the eigenvalues/eigenfrequencies of the Laplace operator. By virtue of the discretization of the single layer potential (4.2), one should find the values k such that the nullspace of the matrix $A(k) = [\Phi_k(x_i - y_j)]_{M \times N}$ is not trivial. Like it was discussed in the previous section 4.2, that can be done in two different ways:

1. if $A(k)$ is a square matrix (with $M = N$), one can compute the determinant of $A(k)$. Since the components of $A(k)$ are complex numbers, then its determinant is also a complex number, and we consider its absolute value. In any case, instead of working with $|\det A(k)|$, since this value is very small, one must work with its logarithm and consider the function $d(k) = \log |\det A(k)|$;
2. if $A(k)$ is an $M \times N$ rectangular matrix, with $M > N$, one considers the smallest singular value, which we denote by $\sigma_N(k)$, where the singular values of $A(k)$ are assumed to be in decreasing order $\sigma_1(k) \geq \dots \geq \sigma_N(k)$. We emphasize that we only work with this case in the context of the Subspace Angle Technique presented in Appendix C.

To determine the eigenvalues/eigenfrequencies of the Laplace operator, it is necessary to locate the zeros of the functions $d(k)$ or $\sigma_N(k)$ in the first and second cases mentioned, respectively. This involves identifying the local minima of the functions $d(k)$ or $\sigma_N(k)$, which are expected to converge toward zero in highly regular domains.

To search for these roots, a simple direct search algorithm was developed to bracket the set of local minima in a given interval. The iterative algorithm used is based on the Golden Ratio Search already used in [AA05]. First, consider the graph of $\sigma_N(k)$ in a given interval $I = (a, b)$ (which likely has more than one local minima) and fix (a relatively large) step size h . Let $I_{M_0}^0 = \{a_0^0, \dots, a_{M_0}^0\}$ be the discretization of $I_{M_0}^0$ in M_0 points spaced by h in the zeroth iteration, and denote the set of local minimums of $I_{M_0}^0$ by $X_K^0 = \{x_0^0, \dots, x_K^0\} \subset I_{M_0}^0$, i.e., $\forall i = 1, \dots, K$ there exists $c^0, d^0 \in I_{M_0}^0$ such that $c^0 = x_i^0 - h, d^0 = x_i^0 + h$ and $x_i^0 < \min(c^0, d^0)$. Then, for each x_i^0 , $I_{M_0}^0$ is enlarged with the middle points between c^0 and x_i^0 , d^0 and x_i^0 , and it is denoted by $\tilde{I}_{M_1}^1$ (notice that $M_0 < M_1$)⁶. Finally, we sort $\tilde{I}_{M_1}^1$ in increasing order and repeat the process for a specified depth d . When the maximum depth is attained, one was able to successfully find small intervals which bracket *each local minimum* of σ_N in I , and it is now possible

⁶Given the nature of the algorithm, one can also consider the left adjacent point to c^0 , which we denote by $e_0 \in I_{M_0}^0$, compute and add their middle point to $\tilde{I}_{M_1}^1$

to apply a direct search method to find it to any desired precision: in this work, Brent's method was used [Bre71], although Golden Ratio Search is also possible. The general form of the algorithm is given in 4.1.

Algorithm 4.1: Direct Bracketing Algorithm

Set maximum depth d

Set step size h

Set bracketing interval $I = (a, b)$

begin

Discretize I into $I_{M_0}^0 = \{a_0^0, \dots, a_{M_0}^0\}$, where $a_{j+1} = a_j + h$ for each $j = 1, \dots, M_0 - 1$

Set $s = 0$

(Bracketing step)

while $s < d$ **do**

 Compute $X_{K_s}^s = \{x_0^s, \dots, x_{K_s}^s\}$, the set of local minima of $I_{M_s}^s$

 Let E be an empty array

foreach $x \in X_{K_s}^s$ **do**

 Consider the adjacent points to x given by $c, d \in I_{M_s}^s$ such that $c < x < d$

 Consider the left adjacent point to c , denoted by e

 Compute $\tilde{c} = \frac{c+x}{2}$

 Compute $\tilde{d} = \frac{d+x}{2}$

 Compute $\tilde{e} = \frac{e+c}{2}$

 Append \tilde{c} , \tilde{d} and \tilde{e} to E

 Let $\tilde{I}_{M_{s+1}}^{s+1} = I_{M_s}^s \cup E$

 Define $I_{M_{s+1}}^{s+1} = \text{sort}(\tilde{I}_{M_{s+1}}^{s+1})$

$s \leftarrow s + 1$

(Direct search step)

Let E be an empty array

foreach $x \in X_{K_d}^d$ **do**

 Consider the adjacent points to x given by $c, d \in I_{M_d}^d$ such that $c < x < d$

$\lambda = \text{Brent}(c, d)$

 Append λ to E

return E

Remark 4.3.3. Although the algorithm 4.1 is enough, we point out some problems and possible changes to consider. First, there are no guarantees regarding the eigenvalues found: this depends on the chosen

interval and the step. For example, if the first eigenvalue is not in the chosen interval, it will never be found. One may also find a “jump” if two eigenvalues are arbitrarily close, but the algorithm just found one of them: this is the case when an eigenvalue has a multiplicity bigger than one, which depends on the domain. However, this last case is easy to rule out if one considers the one parameter transformation between the domain Ω and the unitary disk \mathbb{D} given by

$$\Omega(t) = (1 - t)\mathbb{D} + t\Omega, \quad t \in (0, 1),$$

since the graph of the eigenvalues is continuous concerning t . Regarding the complexity of the algorithm, the objective is to find the minima of the function $\sigma_N(k)$ in the least amount of evaluations: a brute-force approach with a very small step is not feasible since each evaluation takes some time for big complex-valued matrices. However, we note that the algorithm can be improved by just considering the initial point a and “walking forward” with step size h . In that case, one could bracket each local minimum individually and only break to the main loop when the maximum depth was reached for each local minimum initially found. The loop would *break* when the number of eigenvalues found attains a prescribed value.

Finally, a posteriori estimate based on a result proved by Moler and Payne in [MP68] is stated.

Theorem 4.3.4. *Let \tilde{k} and $\tilde{u} \in C^2(\Omega) \cap C(\overline{\Omega})$ be an approximate eigenfrequency and eigenfunction which satisfy the following problem:*

$$\begin{cases} -\Delta \tilde{u} = \tilde{k}^2 u, & \text{in } \Omega \\ u = \xi(x), & \text{on } \Gamma. \end{cases}$$

Then, there exists an eigenfrequency k_n of (4.11) such that

$$\frac{|k_n - \tilde{k}|}{|k_n|} \leq \theta$$

where

$$\theta = \frac{\sqrt{|\Omega|} \|\xi\|_{L^\infty(\Gamma)}}{\|\tilde{u}\|_{L^2(\Omega)}}.$$

If, in addition, \tilde{u} and u is the normalized orthogonal projection of \tilde{u} onto the eigenspace of k_n , then

$$\|\tilde{u} - u\|_{L^2(\Omega)} \leq \frac{\theta}{\rho_n} \left(1 + \frac{\theta^2}{\rho_n^2}\right)^{\frac{1}{2}},$$

where

$$\rho_n = \min_{k_n \neq k_p} \frac{|k_p^2 - \tilde{k}^2|}{k_p^2}, \quad \text{for } p \in \mathbb{N}.$$

5

Numerical Results

In this chapter, the results found for the Dirac operator with infinite mass boundary conditions and the transmission problem are presented. For each problem, a numerical validation of the method is presented, in cases where closed-form solutions are available. Every simulation was implemented in Python 3.10.

5.1 Dirac equation simulations

Recall the system of equations given in (3.5)

$$\begin{bmatrix} m & -i(\partial_1 - i\partial_2) \\ -i(\partial_1 + i\partial_2) & -m \end{bmatrix} \begin{bmatrix} u_1(x) \\ u_2(x) \end{bmatrix} = \lambda \begin{bmatrix} u_1(x) \\ u_2(x) \end{bmatrix}, \quad (5.1)$$

which can be reduced to the Helmholtz equation with Cauchy-Riemann oblique boundary conditions

$$\begin{cases} -\Delta u_1 = (\lambda^2 - m^2)u_1, & \text{in } \Omega \\ i(\partial_1 + i\partial_2)u_1 + (\lambda + m)i(n_1 + in_2)u_1 = 0, & \text{on } \Gamma, \end{cases}$$

where $\Gamma = \partial\Omega$ as usual, and the function u_2 depends on the function u_1 through the following equality

$$u_2 = \frac{-i(\partial_1 + i\partial_2)u_1}{\lambda + m}.$$

5.1.1 Numerical validation of the method

In order to illustrate the MFS for the Dirac equation with infinite mass boundary conditions, we start by testing it for the unit disk. If $m = 0$, then as stated in Proposition 3.2.1, the first eigenvalue of problem (5.1) is $\lambda_1(\mathbb{D}) = 1.434695650819$, obtained as the smallest positive solution of the equation

$$J_0(\lambda_1(\mathbb{D})) = J_1(\lambda_1(\mathbb{D})).$$

In the numerical simulations presented below, 158 inner collocation points for the Subspace Angle Technique (see section C.2 in Appendix C) were considered¹ and the number of source points N was always half of the number of boundary points. Figure 5.1 shows the configuration used. The method described at the end of the subchapter 4.1, below Remark 4.1.15, was used to place the source points, with $\eta = 0.5$.

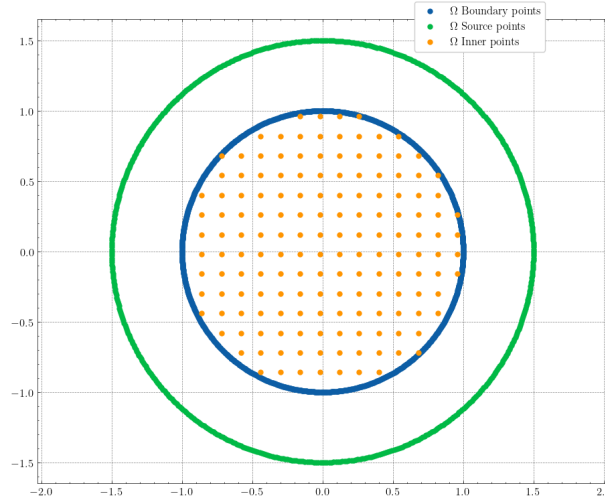


Figure 5.1: Configuration of the boundary, source, and inner points. The number of boundary collocation points used is 1200.

While in the other numerical simulations more eigenvalues are studied, in Table 5.1 only the first three eigenvalues are shown for the sake of brevity.

The results obtained using the bracketing algorithm 4.1 are plotted in Figure 5.2. For future reference, the first eigenfunction on the disk with $m = 0$ is shown in Figure 5.3, with the real and imaginary parts of the spinors u_1 and u_2 plotted. The functions in the plots are also normalized, i.e., $\|\mathbf{u}\|_{L^2(\mathbb{D})} = 1$.

¹In Figure 5.1, the inner collocation points were chosen in a lattice. However, one can place these points freely, in a lattice, or randomly. In fact, in some simulations, the inner points were placed using pseudo-random Halton sequences [Hal64].

Eigenvalues	N=1200	N=1000	N=800
$\tilde{\lambda}_1(\mathbb{D})$	1.4346956515	1.4346956481	1.4346956367
$\tilde{\lambda}_2(\mathbb{D})$	2.6298741163	2.6298741147	2.6298741276
$\tilde{\lambda}_3(\mathbb{D})$	3.1128644920	3.1128645083	3.1128645008
Absolute error: $ \lambda_1(\mathbb{D}) - \tilde{\lambda}_1(\mathbb{D}) $	$6,877 \times 10^{-10}$	$2,693 \times 10^{-9}$	$1,413 \times 10^{-8}$

Table 5.1: Eigenvalues for different values of N and the measured absolute error.

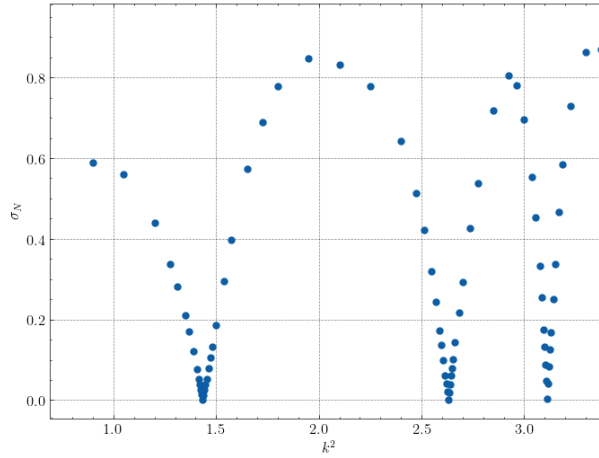


Figure 5.2: Results obtained by the direct search algorithm for the first three eigenvalues of the disk with $m = 0$.

In practice, more accurate approximations are achieved when smaller values of the smallest singular value σ_N of the matrix $Q(k)$ (studied in section C.2) are identified at each minimum.

5.1.2 Quadrilateral results

In this subsection, several numerical results regarding quadrilateral polygons are shown and discussed. First, numerical evidence for the Conjecture 3.2.7 is presented both for $m = 1$ and $m = 5$. Then, some simulations suggest that the conjectured Ashbaugh-Benguria Theorem 3.2.6 also holds for the Dirac operator with infinite mass boundary conditions. Finally, we also show that some disagreement between the spectrum of the Laplace and Dirac operators is already evident for the third eigenvalue, whose optimal shape is not the disk for some values of m , contrary to what is conjectured for the Laplacian (which is still an open problem).

Consider a rectangle with a width $a \geq 1$ and unit area, where the sides are a and $\frac{1}{a}$. Figures 5.4 and 5.5 illustrate the behavior of the first 5 eigenvalues for $m = 1$ and $m = 5$, respectively. Several interesting observations can be made:

1. The behavior of the spectrum remains qualitatively consistent for different values of m . Significantly, as m increases, the eigenvalues approach m with a diminishing gap, while remaining

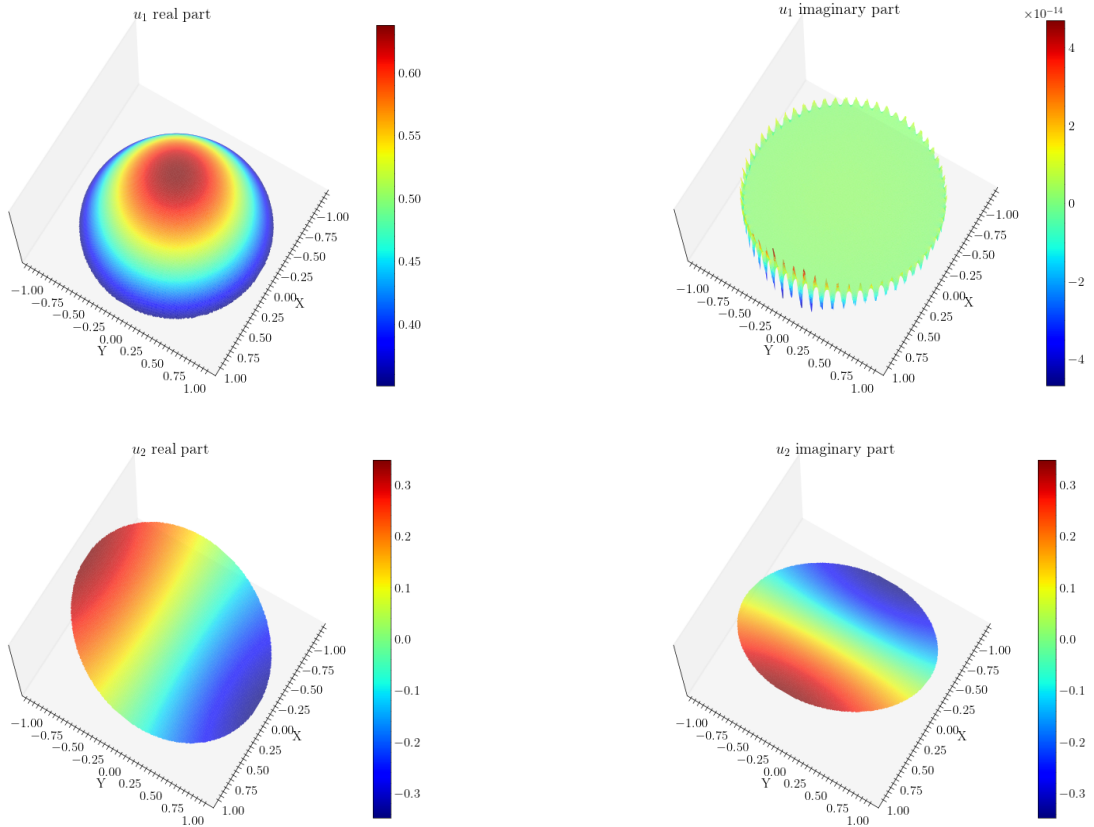


Figure 5.3: Plots of the real and imaginary parts of u_1 and u_2 of the first eigenfunction $\mathbf{u} = \begin{bmatrix} u_1 \\ u_2 \end{bmatrix}$. Observe that the imaginary part of u_1 is zero and the artifacts presented are due to precision lost.

greater than m . While this trend is discernible already in Figures 5.4 and 5.5, it becomes more apparent as m takes on even larger values. It is important to point out that the third eigenvalue is not globally minimized in the square for $m = 1$, but for some rectangle with width $a \approx 2.2$. However, this does not appear to hold for any mass $m \geq 0$ but only for some values of $m \leq m_{\text{crit}}$, where $1 \leq m_{\text{crit}} \leq 5$, i.e., for any mass $m \leq m_{\text{crit}}$ the global minimizer of the third eigenvalue is some (non-square) rectangle.

2. Starting from the third eigenvalue and beyond, certain spikes become evident in the plot. These spikes correspond to rectangular domains where the eigenvalue has a multiplicity of two. For instance, between the values 1 and 1.5, the third and fourth eigenvalues appear to coincide. This behavior becomes more frequent as the order of the eigenvalues increases.
3. By increasing the value of the parameter a , a linear growth in the eigenvalues magnitude is observed, with no change in their multiplicity. As a increases, the eigenvalues draw closer to each other, which is an expected outcome. This behavior arises as the rectangular domain transforms

into an unbounded line, giving rise to a continuous spectrum.

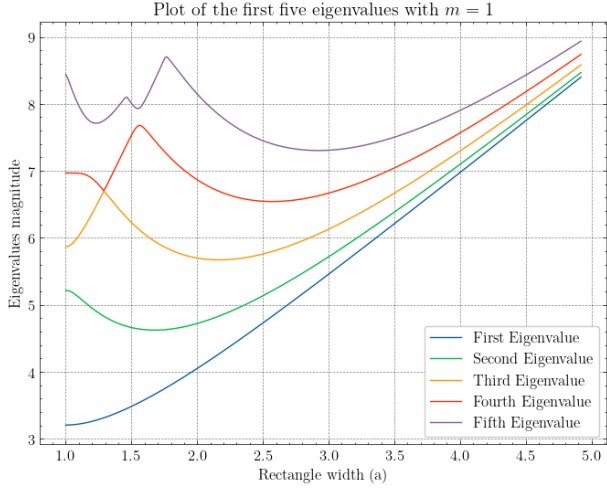


Figure 5.4: Behavior of the first five eigenvalues for rectangles with unit area, width a and $m = 1$.

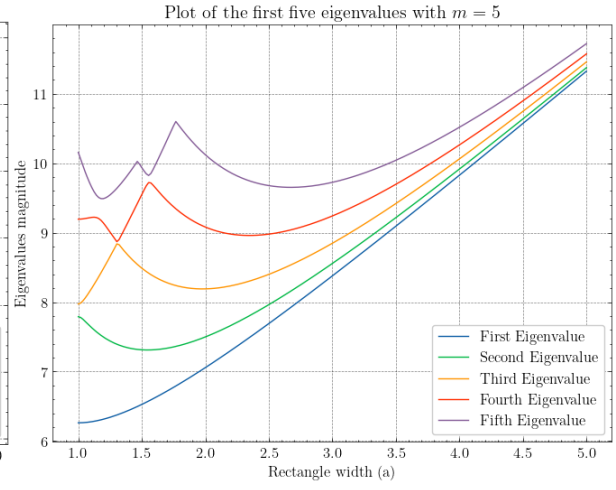


Figure 5.5: Behavior of the first five eigenvalues for rectangles with unit area, width a and $m = 5$.

In Figures 5.6 and 5.7 the results with fixed perimeter $L = 4$ are shown. While Conjecture 3.2.7 is stated for $a \in (0, 2)$ it is enough to consider $a \in (0, 1)$ given the symmetry of the problem and the fact that the perimeter is equal to 4. Note that the area of the rectangle may change when the perimeter is fixed and the rectangle width varies. The conclusions and remarks presented in points 1 and 2 for rectangles with fixed area are still valid. In this case, point 3 holds when a approaches zero.

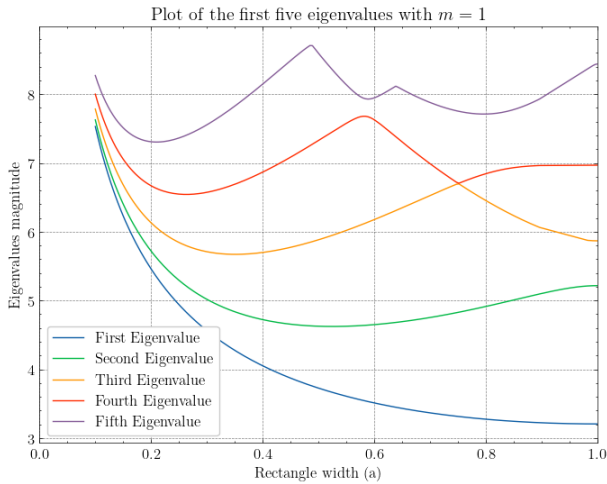


Figure 5.6: Behavior of the first five eigenvalues for rectangles with perimeter $L = 4$, width a and $m = 1$.

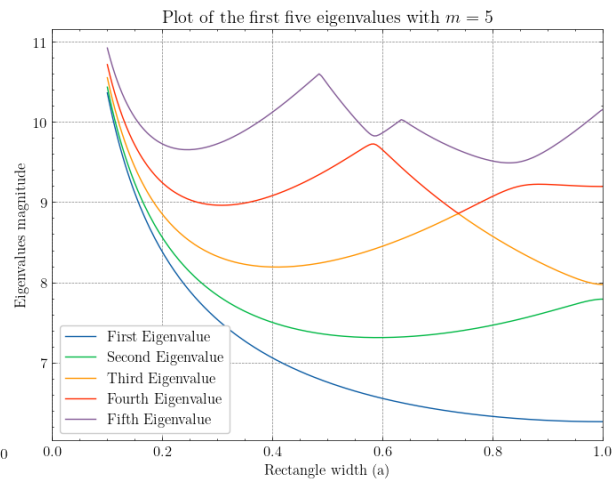


Figure 5.7: Behavior of the first five eigenvalues for rectangles with perimeter $L = 4$, width a and $m = 5$.

Given the results for rectangles with fixed area or perimeter, it is possible to state that the Conjecture 3.2.7 should hold, although it is not possible to ascertain that the results presented here hold for every m (as we saw before, the value of m has some discernible influence on the spectrum, which can already be seen for the third eigenvalue, although no difference was found for the first and second eigenvalues). In any case, it is known that the eigenvalues are continuous with domain perturbations (here these perturbations can be seen as stretching the rectangles), exactly what has been found in these numerical simulations.

To finish this subsection, we present the results for general quadrilaterals for $m = 1$. Since no (practical) parameterization can describe every quadrilateral, we have resorted to a random sampling of quadrilaterals and studied the results against rectangles and rhombi. Figure 5.8 presents the results of the numerical simulations. For the third eigenvalue, it is already possible to find some domains whose third eigenvalue is smaller than the eigenvalue of the unit disk. In Figures 5.9 and 5.10 the ratio between the first eigenvalues is studied, and the version of the Ashbaugh-Benguria presented in Theorem 3.2.6 appears to hold.

5.1.3 Results for triangles and general polygons

In this subsection, we tackle the Conjectures 3.2.8 stated in [Vu23]. At the end of the subsection, numerical evidence for Conjecture 3.2.9 is also presented. Instead of considering random triangles, this study can be done systematically given that, up to a congruence, three parameters completely define every triangle. The approach presented here is based on the work of Antunes and Freitas [AF11]. Consider the region R defined by

$$R = \{(x, y) \in \mathbb{R}^2 : x \geq 0, y > 0, (x+1)^2 + y^2 \leq 4\},$$

and its piecewise boundary $\partial R = \Gamma_0 \cup \Gamma_1 \cup \Gamma_2$, where

$$\Gamma_0 = \{(x, y) \in \mathbb{R}^2 : 0 \leq x \leq 1, y = 0\}$$

$$\Gamma_1 = \{(x, y) \in \mathbb{R}^2 : 0 \leq x < 1, y = \sqrt{4 - (x+1)^2}\}$$

$$\Gamma_2 = \{(x, y) \in \mathbb{R}^2 : x = 0, 0 < y < \sqrt{3}\}.$$

A triangle T is said to be *admissible* if its basis vertices are $(0, 0)$ and $(1, 0)$, and the third vertex coordinates² are (x, y) such that $(x, y) \in \overline{R}$. An isosceles triangle T is said to be *subequilateral* if $(x, y) \in \Gamma_1$ with aperture less than $\frac{\pi}{3}$, and *superequilateral* with aperture greater than $\frac{\pi}{3}$ such that $(x, y) \in \Gamma_2$; if $(x, y) = (0, \sqrt{3})$ then it is equilateral (obviously). The plot of the region R and its boundary ∂R is in Figure 5.11.

²Of course, one does not need to impose such constraints on the triangle: as said before, every triangle is unique up to congruence. Here, we just emphasize that it is enough to consider triangles in region R . Observe that this is just a way to exhaust numerically all possible triangles up to a congruence.

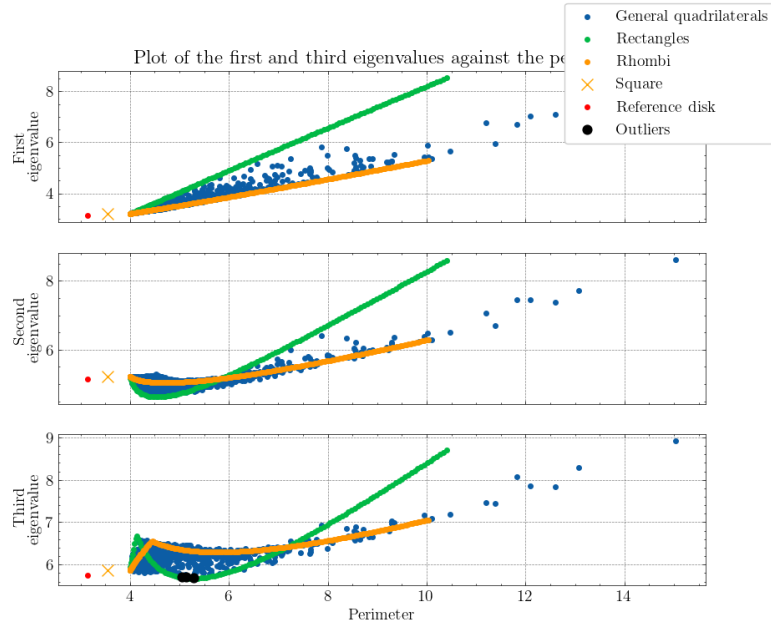


Figure 5.8: Plot of the first three eigenvalues against the perimeter for $m = 1$ for quadrilaterals. The “outliers” marked in black represent the domains in which the third eigenvalue is smaller than the third eigenvalue of the disk.

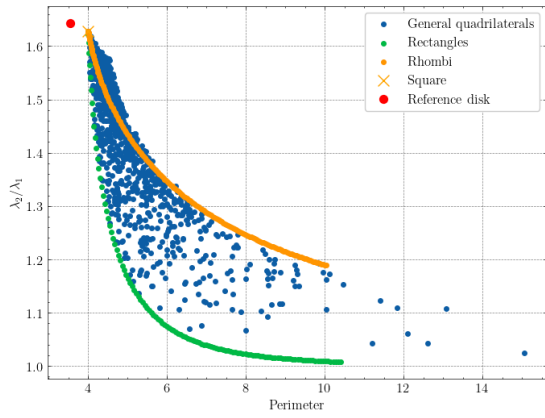


Figure 5.9: Ratio between the first two eigenvalues $\frac{\lambda_2}{\lambda_1}$ plotted against the perimeter for $m = 1$ for quadrilaterals, as in Figure 5.8.

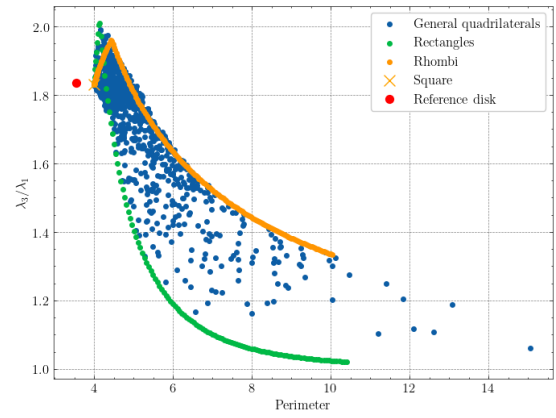


Figure 5.10: Ratio between the third and first eigenvalues $\frac{\lambda_3}{\lambda_1}$ plotted against the perimeter for $m = 1$ for quadrilaterals, as in Figure 5.8.

In Figure 5.12, we provide numerical evidence supporting Conjecture 3.2.8 with $m = 1$. It’s noteworthy how the eigenvalues of the superequilateral and subequilateral triangles define a (very thin) region

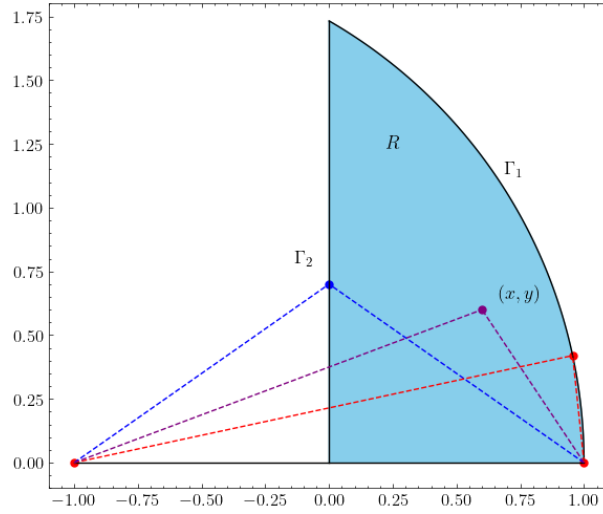


Figure 5.11: Configuration space of the admissible triangles. The dashed red line shows a subequilateral triangle; the dashed blue line a superequilateral triangle.

encompassing all other triangles with (x, y) vertices in R . Figure 5.13 numerically corroborates a version of the Ashbaugh-Benguria Theorem (see to Conjecture 3.2.6). Additionally, in Figure 5.14, we present a 3D plot of the first eigenvalue for each admissible triangle against the vertex coordinates (x, y) within \bar{R} . Finally, Figure 5.15 also showcases the first three eigenvalues for triangles with a fixed perimeter $L = 15$. This unconventional value was chosen due to the diminutive size of unit perimeter triangles, making the method implementation more challenging, prone to numerical errors, and the eigenvalues' amplitude too large. For instance, if we choose $L = \frac{6}{\sqrt[3]{3}}$, which corresponds to the perimeter of an equilateral triangle with unit area, the triangles with their third vertex (x, y) very close to the triangle's base $y = 0$ become extremely narrow and attain unusual large values because their area becomes exceedingly small.

In a manner similar to the conjecture regarding triangles with fixed area, the conjecture concerning triangles with fixed perimeter also seems to hold. Furthermore, it's worth noting that equilateral triangles minimize both the second and third eigenvalues.

While for quadrilaterals (and for smooth domains in the next subsection) only random domains could be considered, for the problem among triangles, one can consider *every* type of triangle by varying (x, y) in \bar{R} . Since the eigenvalues are continuous with respect to domain perturbations (in the next subsection, we will briefly formalize this concept using equation (5.2)), it means that it is very unlikely that the conjectures studied for triangles (at least for $m = 1$) do not hold, otherwise some jump would probably be found, for example in Figure 5.14.

To finish this subsection, numerical evidence for Conjecture 3.2.9 for $m = 1$ is presented in Figures 5.16, 5.17, 5.18 and 5.19. For the sake of brevity, we only present the results for the first eigenvalue, although similar results were found for the second and third eigenvalues. As it is possible to check, the

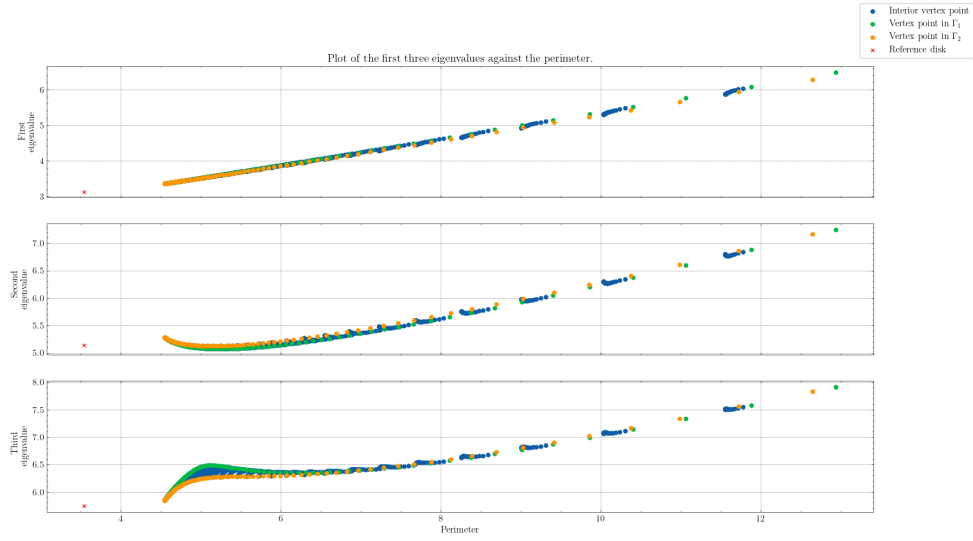


Figure 5.12: Plot of the first three eigenvalues against the perimeter for triangular domains.

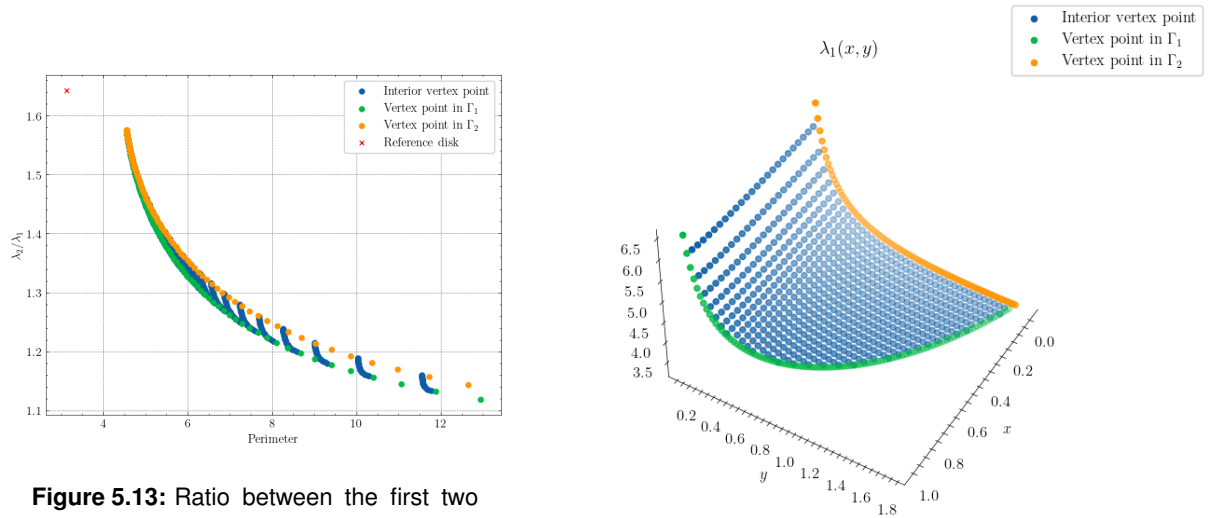


Figure 5.13: Ratio between the first two eigenvalues $\frac{\lambda_2}{\lambda_1}$ for triangular domains.

Figure 5.14: Plot of the first eigenvalue $\lambda_1(x, y)$ for each sample point $(x, y) \in R$ for triangular domains.

n -sided polygon with the least first eigenvalue is the regular polygon, with $n = 5, 6, 7, 8$.

5.1.4 Results in smooth domains

In this last subsection, the behavior of the spectrum in smooth (connected) domains with unit area is studied. Here, we fix $m = 1$. The reason is twofold: first, the shape of the domains can be arbitrary

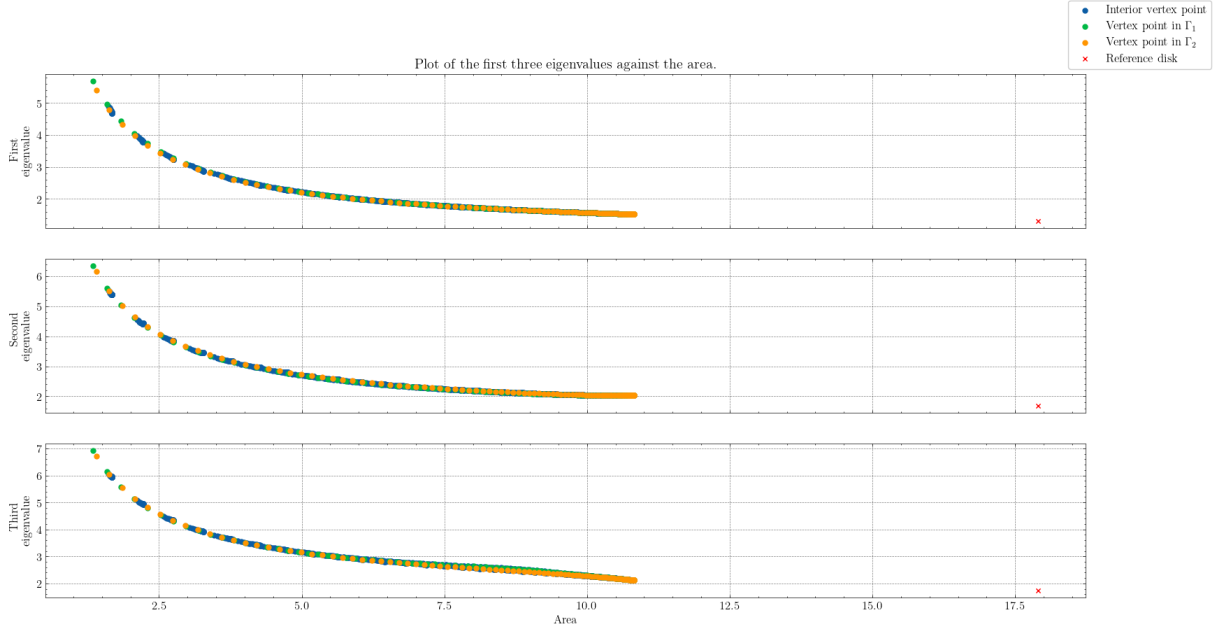


Figure 5.15: Plot of the first three eigenvalues against the area with perimeter $L = 15$ for triangular domains.

and the numerical approximations are more reliable; second, one can also consider the domain which minimizes the third eigenvalue.

In order to generate random smooth domains, periodic B-spline interpolation (e.g. [DBDB78] for details) for each component of a vector in \mathbb{R}^2 was used. One starts by generating randomly five points (using a uniform distribution), fitting a periodic B-spline on this points for each component, drawing the two-dimensional B-spline, and checking for auto-intersections³. If it does not auto-intersect, then it is a valid domain. Figure 5.20 presents an example.

The results correspond to the ones presented in sections 5.1.2 and 5.1.3. In Figure 5.21 a scatter plot of the first three eigenvalues as a function of the perimeter is shown. Once again, analogously to the Laplacian, Conjecture 3.2.5 appears to hold for the Dirac operator with infinite mass boundary conditions. As seen in Figure 5.8, some “outlier” domains have a third eigenvalue that is smaller than the third eigenvalue on the disk, which suggests that the minimizers of the third Dirac and Laplace eigenvalues do not coincide. Figures 5.22 and 5.23 are related to the ratio of the first eigenvalues and the spectral gap between them. Something analogous to the Ashbaugh-Benguria Theorem for the Laplacian also seems to hold for the Dirac operator.

Next, we search for the domain with the smallest third eigenvalue, and thus look for the minimizer of the functional

$$\mathcal{F}(\Omega) = \lambda_3(\Omega).$$

³Unfortunately, such sampling of smooth domains is not representative of the set of all smooth domains. For example, generating complex non-convex domains (like domains in the shape of a star) may be impossible.

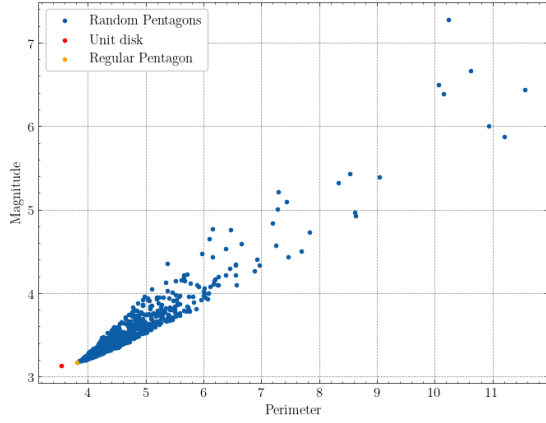


Figure 5.16: Numerical simulations in the first eigenvalue of general pentagons.

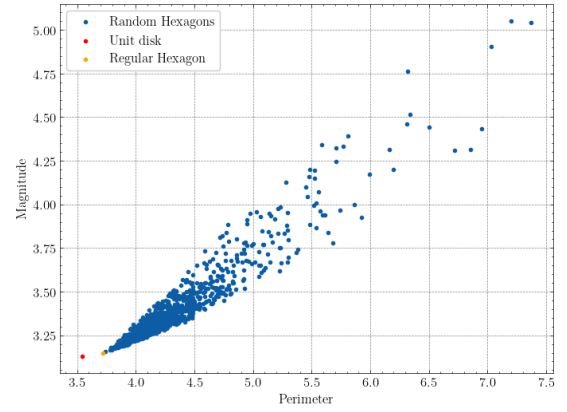


Figure 5.17: Numerical simulations in the first eigenvalue of general hexagons.

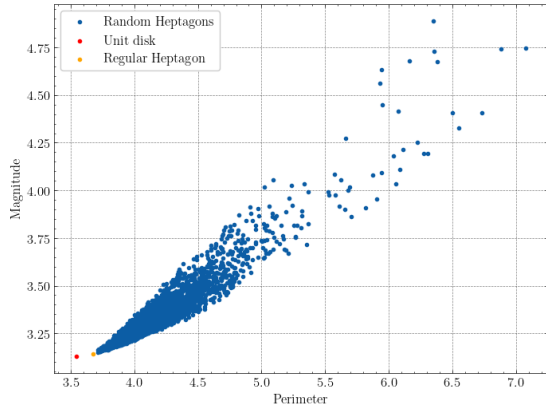


Figure 5.18: Numerical simulations in the first eigenvalue of general heptagons.

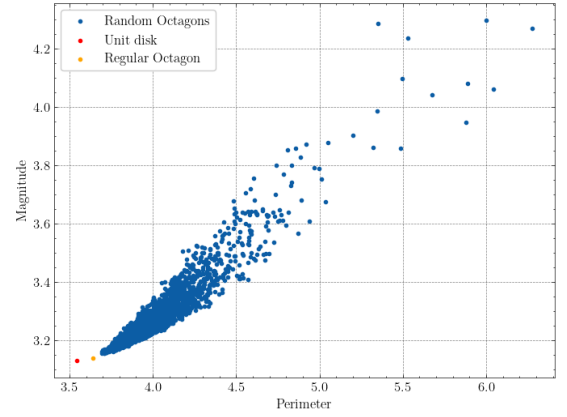


Figure 5.19: Numerical simulations in the first eigenvalue of general octagons.

In general, one can address minimization problems in Banach spaces using the notion of *Fréchet*-derivative. In shape optimization problems, for the eigenvalues of an elliptic operator, one can use the variational formula for its eigenvalues. For example, the variational formula (B.2) proved in Theorem B.0.4 can be used to derive some results for the Laplace-Dirichlet problem. In fact, let $\Omega_t = \varphi(t)(\Omega)$ be a small perturbation of Ω in the parameter t , where $\varphi(t)$ is a diffeomorphism for small values of t defined by

$$\varphi(t) = I + tW, \quad (5.2)$$

for some fixed vector field W and $\Omega_0 = \Omega$. Let $\lambda_k(t)$ be the k -th eigenvalue of the Laplace operator with Dirichlet boundary conditions on the domain Ω_t and $u_t^{(k)}$ its L^2 normalized eigenfunction in $H_0^1(\Omega_t)$. If

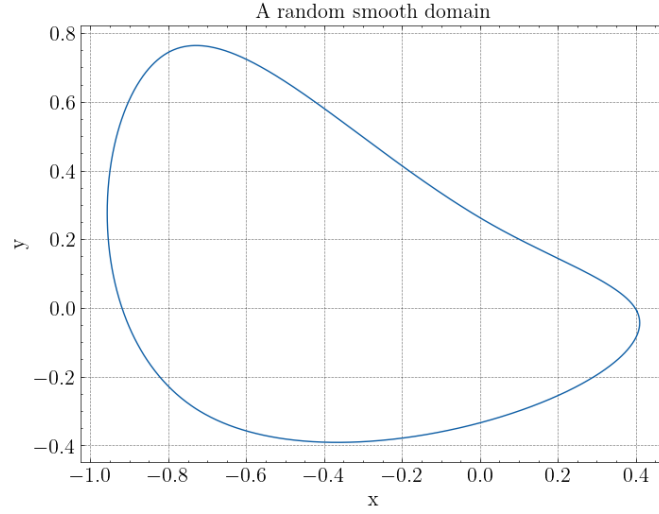


Figure 5.20: Smooth domain generated by B-splines.

λ_k has multiplicity one (if it is simple) and Ω is of class C^2 or convex, then

$$\lambda'_k(0) = - \int_{\partial\Omega} \left(\frac{\partial u_0^{(k)}}{\partial n} \right)^2 V \cdot n d\sigma. \quad (5.3)$$

For more details, we refer to [Hen06] and [Kat13]. Numerically, equation (5.3) can then be used in shape optimization problems for the Dirichlet Laplacian BVP, for example in gradient-based methods like gradient descent. As of the moment of writing, the author is not aware of any such closed-form for the derivative of the eigenvalues of the Dirac operator. Therefore, two different strategies were considered to solve the constrained minimization problem

$$\min_{\substack{\Omega \subset \mathbb{R}^2 \\ |\Omega|=1}} \mathcal{F}(\Omega). \quad (5.4)$$

Starting with a given domain Ω , \mathcal{F} can be minimized using the Broyden–Fletcher–Goldfarb–Shanno algorithm (BFGS) algorithm, e.g. see [And22], a quasi-Newton method that uses the local curvature of \mathcal{F} to find the descent direction given by an approximation of the Hessian matrix. As in most optimization techniques, we need, however, to compute the derivative of the objective function, since we are solving the equation $\mathcal{F}' = 0$. In our case, this can only be done numerically using, for example, finite differences. The second method is the multidimensional Nelder-Mead direct search method, which we also refer to [And22]. As in the bracketing algorithm used in finding the singularities on the graph of the smallest singular value, the Nelder-Mead method does not need any information on the derivative and relies solely on evaluations of the objective function \mathcal{F} to bracket the local minima, which we approximate using a heuristic strategy with a multidimensional simplex is used to approximate it.

To apply both the BFGS and the Nelder-Mead algorithms, one starts by parameterize the domain Ω_0 with the lowest third eigenvalue by a polar parameterization. This is achieved by considering a sample

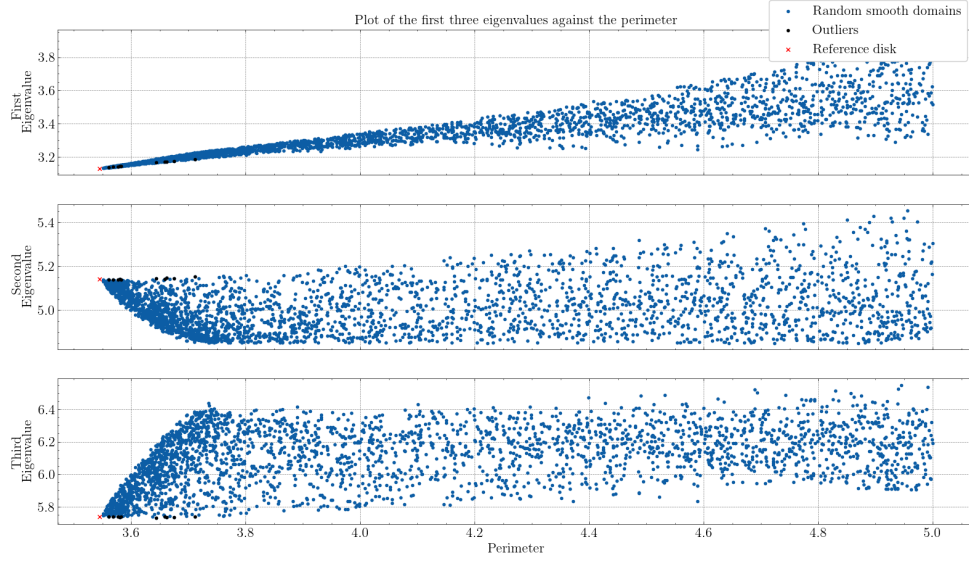


Figure 5.21: Magnitude of the first three eigenvalues plotted against the perimeter length in smooth domains. The “outliers” marked in black represent the domains in which the third eigenvalue is less than the third eigenvalue of the disk.

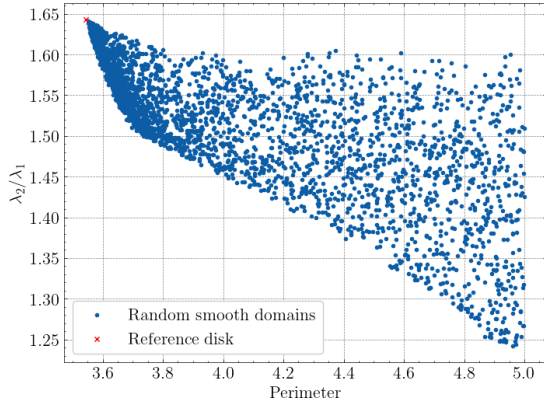


Figure 5.22: Ratio between the first two eigenvalues $\frac{\lambda_2}{\lambda_1}$ for smooth domains.

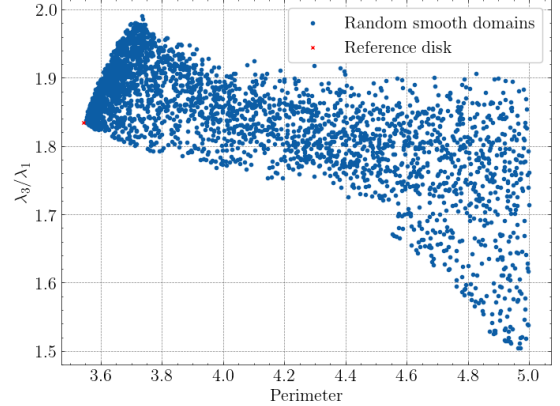


Figure 5.23: Ratio between the third and first eigenvalues $\frac{\lambda_3}{\lambda_1}$ for smooth domains.

of N boundary points from the domain, considering its polar coordinates, and finding the coefficients of the trigonometric interpolation. More precisely, let M be the order of the trigonometric interpolation. Assume that the radial part of each boundary point of Ω_0 can be parametrized by $r(\theta)$, where $\theta \in (0, 2\pi)$. In that case, one uses the approximation

$$r(\theta_i) \approx a_0 + \sum_{m=1}^M a_m \cos(m\theta_i) + \sum_{m=1}^M b_m \sin(m\theta_i),$$

where θ_i is the polar part of the sample point i with $i = 1, \dots, N$. Then, the system

$$\begin{bmatrix} 1 & \cos(1\theta_1) & \cos(2\theta_1) & \dots & \cos(M\theta_1) & \sin(1\theta_1) & \dots & \sin(M\theta_1) \\ \vdots & \vdots & \vdots & \vdots & \vdots & \vdots & \vdots & \vdots \\ 1 & \cos(1\theta_N) & \cos(2\theta_N) & \dots & \cos(M\theta_N) & \sin(1\theta_N) & \dots & \sin(M\theta_N) \end{bmatrix}_{N \times (2M+1)} \begin{bmatrix} a_0 \\ \vdots \\ b_M \end{bmatrix} = \begin{bmatrix} r(\theta_1) \\ \vdots \\ r(\theta_N) \end{bmatrix}$$

can be solved by least squares. Notice that problem (5.4) is now a finite-dimensional problem since every domain is a vector of coefficients in \mathbb{R}^{2M+1} . Of course, one must still scale the generated domain so that it has a unit area.

Figure 5.24 presents an (almost) optimal domain Ω^* which minimizes the third eigenvalue of the Dirac operator with infinite mass boundary conditions. This shape was obtained through the Nelder-Mead algorithm. The third eigenvalue of the problem in this domain is approximately $\lambda_3 \approx 5.63787728$ and the perimeter length of Ω^* is $L \approx 5.2650031$. In Figure 5.25 we validate our findings by plotting the (continuous) family of one-parameter transformations (known as the Minkowski sum) from the unit disk \mathbb{D} to Ω^* , given by

$$\Omega_t = (1 - t)\mathbb{D} + t\Omega^*, \quad 0 \leq t \leq 1.$$

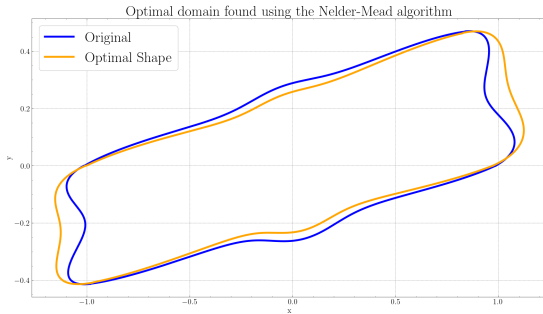


Figure 5.24: Optimal domain Ω^* (drawn in orange) and the initial domain (in blue) used in the first iteration of the Nelder-Mead algorithm.

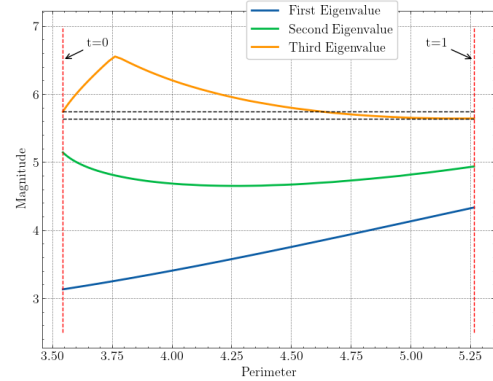


Figure 5.25: The first three eigenvalues in domains defined by the Minkowski sum Ω_t and plotted for the values of $t \in [0, 1]$ increasing from left to right.

As mentioned earlier, the BFGS method was also employed. However, this method did not yield meaningful results. We attribute this to the proximity of the initial domain to the global minimizer, leading to a natural loss of precision when calculating the gradient through finite differences. The combination of these issues, along with the finite (albeit accurate due to the smoothness of the domains being considered) numerical precision of the MFS, justifies the lack of convergence of the BFGS method.

Remark 5.1.1. One can not fail to point out a valid criticism to approach the minimization problem (5.4): since we only parametrized the radial part of the domain's boundary, we always end up with star-like shapes. Moreover, in our case, the order of the trigonometric interpolation was low, with $M = 4$. We note however that, by increasing the order of interpolation, the dimension of the optimization space also increases, and already in \mathbb{R}^9 it is very hard for a direct search method like Nelder-Mead to find a local minimum. The option to consider only the radial part, instead of both cartesian components, was also a way to reduce the dimensionality of the problem.

Finally, the normalized eigenfunction associated with the optimal third eigenvalue of domain Ω^* is shown in Figure 5.26.

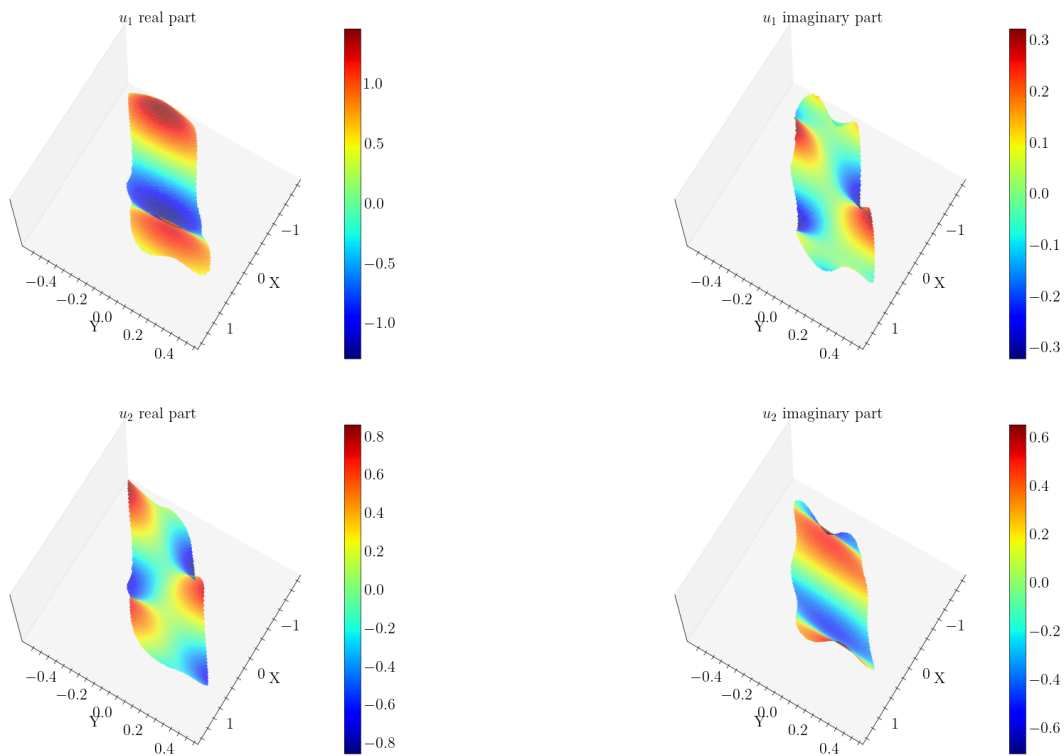


Figure 5.26: Real and imaginary parts of u_1 and u_2 of the third eigenfunction $\mathbf{u} = \begin{bmatrix} u_1 \\ u_2 \end{bmatrix}$ associated with the optimal domain Ω^* .

5.2 Transmission problem

We now recall the set of equations introduced in the subsection 3.3,

$$\begin{cases} -\nabla k_i (\nabla u_i) = f_i, & \text{in } \Omega_i \\ u_1 - u_2 = 0, & \text{on } \gamma \\ k_1 \frac{\partial u_1}{\partial \mathbf{n}_1} + k_2 \frac{\partial u_2}{\partial \mathbf{n}_2} = 0, & \text{on } \gamma \\ u_i = 0, & \text{on } \Gamma_i, \end{cases} \quad (5.5)$$

for $i = 1, 2$.

Problem 5.5 can be understood as a domain decomposition problem, where $\Omega \subset \mathbb{R}^2$ is divided into two non-overlapping regions Ω_1 and Ω_2 such that $\overline{\Omega} = \overline{\Omega_1} \cup \overline{\Omega_2}$. The interface between Ω_1 and Ω_2 is denoted by $\gamma = \partial\Omega_1 \cap \partial\Omega_2$ and the rest of the boundary of each domain by $\Gamma_i = \partial\Omega_i \setminus \gamma$, $i = 1, 2$. In what follows, the source functions f_i at each domain are taken to be constant⁴. Recall that $k_1 \geq k_2 > 0$ are constants and \mathbf{n}_i is the (normalized) outward normal to Ω_i , $i = 1, 2$, where we write $\mathbf{n} = \mathbf{n}_1 = -\mathbf{n}_2$ when \mathbf{n} is restricted to the interface.

The procedure presented here is based on [AC05] and [AMV21]. Given that $f_i = 1$, $i = 1, 2$, a solution of (5.5) can be found by taking the following steps:

1. Find a non-homogeneous solution (recall footnote 4 in Chapter 4) for the non-homogeneous problem

$$\begin{cases} -\Delta u_1^{NH} = \frac{1}{k_1} \\ -\Delta u_2^{NH} = \frac{1}{k_2}, \end{cases}$$

in \mathbb{R}^2 which does not necessarily satisfy the boundary and interface conditions in (5.5). This can easily be done, and

$$\begin{cases} u_1^{NH} = -\frac{x_1^2 + x_2^2}{4k_1} \\ u_2^{NH} = -\frac{x_1^2 + x_2^2}{4k_2} \end{cases}$$

are some possible non-homogeneous solutions;

2. Then we solve the homogeneous problem

$$\begin{cases} -\Delta u_i^H = 0, & \text{in } \Omega_i \\ u_1^H - u_2^H = u_2^{NH} - u_1^{NH}, & \text{on } \gamma \\ k_1 \frac{\partial u_1^H}{\partial \mathbf{n}_1} - k_2 \frac{\partial u_2^H}{\partial \mathbf{n}_1} = k_2 \frac{\partial u_2^{NH}}{\partial \mathbf{n}_1} - k_1 \frac{\partial u_1^{NH}}{\partial \mathbf{n}_1}, & \text{on } \gamma \\ u_i^H = -u_i^{NH}, & \text{on } \Gamma_i, \end{cases}$$

for u_1^H and u_2^H ;

3. Finally, the solution of (5.5) is $u_i = u_i^H + u_i^{NH}$.

⁴Like in article [GSV19], in this work we only considered $f_i = 1$. In any case, we will still have a jump in the material parameter k , if $k_1 \neq k_2$.

Remark 5.2.1. For general (possibly different) source functions, the steps above can also be used: however, it may not be possible to find a closed-form solution in the first step. In this case, the problem in step 1 must be solved numerically. A popular choice is to use Radial Basis Functions (RBFs), e.g. [GCK96], for example the thin plate spline

$$\varphi(r) = r^2 \log r,$$

and, for each subdomain Ω_i with $i = 1, 2$ find the coefficients $\alpha_j^{(i)}$ in $f_i(x_k^{(i)}) = \tilde{f}_i(x_k^{(i)}) = \sum_{j=1}^N \alpha_j^{(i)} \varphi_j(x_k^{(i)})$ using least square methods, where $x_k^{(i)}$ are collocation points for $k = 1, \dots, M^{(i)}$, \tilde{f}_i is an approximation for the source function f_i given by linear combinations of thin plate splines, $\varphi_j(x^{(i)}) = \varphi(|x^{(i)} - y_j|)$ and $y_j \in \mathbb{R}^2$, $j = 1, \dots, N$, is the RBF center, which is analogous to the concept of source points in the MFS. Finally, one can analytically solve for the Ψ_j functions in the polar Poisson equation $\frac{1}{r} \frac{\partial}{\partial r} (r \frac{\partial}{\partial r} \Psi_j) = \varphi_j$ with $j = 1, \dots, N$ in \mathbb{R}^2 , to recover the approximate non-homogeneous solutions u_1^{NH} and u_2^{NH} , given by

$$u_i^{NH}(x) = \sum_{j=1}^N \alpha_j^{(i)} \Psi_j(x - y_j^{(i)}).$$

In [AC05] and [AMV21] a different approach was suggested using the fundamental solutions of the Helmholtz equation instead of the classical RBFs; that method is known today as Kansa-MFS method.

In what follows, the numerical results illustrate the accuracy of the method in simply connected 2D domains. Let $N^{(i)}$ denote the number of source points at each domain and $N = N^{(1)} + N^{(2)}$. We denote the approximate solution by

$$\tilde{u} = \begin{cases} \tilde{u}_1, & \text{in } \Omega_1 \\ \tilde{u}_2, & \text{in } \Omega_2, \end{cases}$$

where

$$\begin{aligned} \tilde{u}_1(x) &= \sum_{j=1}^{N^{(1)}} \alpha_j^{(1)} \Phi(x - y_j^{(1)}) \\ \tilde{u}_2(x) &= \sum_{j=1}^{N^{(2)}} \alpha_j^{(2)} \Phi(x - y_j^{(1)}). \end{aligned}$$

Let $M^{(i)}$ be the number of boundary collocation points $x_m^{(i)}$ for each Ω_i and $M = M^{(1)} + M^{(2)}$. We also consider Q interface points $z_q \in \gamma$ with $q = 1, \dots, Q$. Then, the full block system is written as

$$\underbrace{\begin{bmatrix} \left[\Phi(x_m^{(1)} - y_j^{(1)}) \right]_{M^{(1)} \times N^{(1)}} & [0]_{M^{(1)} \times N^{(2)}} \\ [0]_{M^{(2)} \times N^{(1)}} & \left[\Phi(x_m^{(2)} - y_j^{(2)}) \right]_{M^{(2)} \times N^{(2)}} \\ \left[\Phi(z_q - y_j^{(1)}) \right]_{Q \times N^{(1)}} & \left[-\Phi(z_q - y_j^{(2)}) \right]_{Q \times N^{(2)}} \\ \left[k_1 \partial_n \Phi(z_q - y_j^{(1)}) \right]_{Q \times N^{(1)}} & \left[-k_2 \partial_n \Phi(z_q - y_j^{(2)}) \right]_{Q \times N^{(2)}} \end{bmatrix}}_A \underbrace{\begin{bmatrix} \alpha_j^{(1)} \\ \alpha_j^{(2)} \end{bmatrix}}_{\alpha} = \underbrace{\begin{bmatrix} \left[-u_1^{NH}(x_m^{(1)}) \right]_{M^{(1)} \times 1} \\ \left[-u_2^{NH}(x_m^{(2)}) \right]_{M^{(2)} \times 1} \\ \left[u_2^{NH}(z_q) - u_1^{NH}(z_q) \right]_{Q \times 1} \\ \left[k_2 \partial_n u_2^{NH}(z_q) - k_1 \partial_n u_1^{NH}(z_q) \right]_{Q \times 1} \end{bmatrix}}_b \quad (5.6)$$

where the dimensions of the matrix A are $(M^{(1)} + M^{(2)} + 2Q) \times (N^{(1)} + N^{(2)})$.

Most of the examples below do not have an analytical solution: only in the section 5.2.1, when we test the results against a known solution, we can compute the actual error everywhere. In the other cases, we only check for consistency errors which measure how accurately the interface and boundary conditions are satisfied:

- $\|\tilde{u}_i - 0\|_{L^2(\Gamma_i)}$, $i = 1, 2$: boundary collocation error;
- $e_\gamma^0 = \|\tilde{u}_1 - \tilde{u}_2\|_{L^2(\gamma)}$, $i = 1, 2$: L^2 error of \tilde{u} across γ ;
- $e_\gamma^1 = \|k_1 \partial_n \tilde{u}_1 - k_2 \partial_n \tilde{u}_2\|_{L^2(\gamma)}$, $i = 1, 2$: L^2 error of $\partial_n \tilde{u}$ across γ .

From a numerical point of view, let \mathcal{I} be the sample of test points. The L^2 norm is discretized into the Root Mean Squared Error (RMSE), which is equivalent to the l^2 norm, and is given by

$$\|u - \tilde{u}\|_2 = \sqrt{\frac{1}{\#\mathcal{I}} \sum_{z \in \mathcal{I}} |u(z) - \tilde{u}(z)|^2}.$$

For every result below the number of sample test points is 5 times larger than the sample used to find the coefficients of the MFS, and we fix $k_2 = 1$ since the ratio $\frac{k_1}{k_2}$ is responsible for the behavior of the solutions near the interface.

5.2.1 Numerical validation of the method

First, we start by testing the numerical algorithm for the unit disk \mathbb{D} , with $k_1 = k_2 = 1$. From Theorem 3.3.2, we know that the system of differential equations (5.5) is equivalent to the Poisson equation

$$\begin{aligned} -\Delta u &= 1, \text{ in } \mathbb{D} \\ u &= 0, \text{ on } \partial\mathbb{D}, \end{aligned} \tag{5.7}$$

and is easy to see that the exact solution of Equation (5.7) is given in polar coordinates by $u(r, \theta) = \frac{1-r^2}{4}$.

The absolute error between the approximate solution and the exact solution can then be calculated for each domain point. The sample points to compute the absolute error were generated in a uniform grid and were also used to plot Figure 5.28. The method described at the end of the subchapter 4.1, below Remark 4.1.15, was used to place the source points, where the coefficient η that controls the distance between the boundary Γ and the artificial boundary $\hat{\Gamma}$ is 0.3.

The numerical results presented in Tables 5.2 and 5.3 are not yet optimal. When considering a larger value of η , the results increase by more than two orders of magnitude, but this also leads to a significant increase in the already very high condition number of matrix A in the system (5.6) (see Table 5.3), as expected. Despite this, the results show great promise, which was anticipated due to the domain's smoothness.

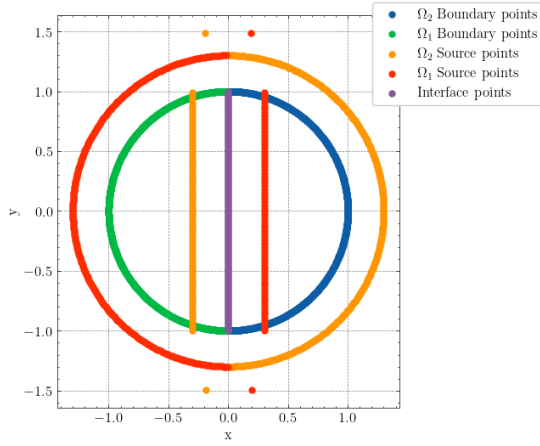


Figure 5.27: Configuration of the boundary, source, and interface points. Each domain has 600 boundary points, 377 source points and the common interface has 100 points.

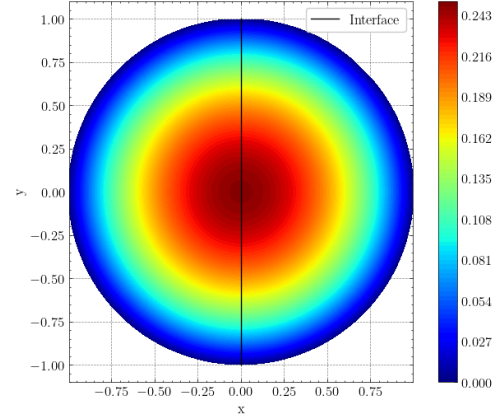


Figure 5.28: Numerical approximation of the solution u of the BVP (5.7) using the configuration presented in Figure 5.27. The colorbar shows the values of u .

Boundary/Interface Points	Boundary Error		Total Error	
	Domain 1	Domain 2	Domain 1	Domain 2
600/150	9.759×10^{-12}	9.541×10^{-12}	1.465×10^{-11}	1.439×10^{-11}
500/100	3.667×10^{-11}	3.945×10^{-11}	9.382×10^{-11}	9.310×10^{-11}
412/100	3.721×10^{-11}	5.036×10^{-11}	9.652×10^{-11}	9.584×10^{-11}

Table 5.2: Numerical errors at the boundaries $\partial\Omega_1$ and $\partial\Omega_2$ and in the domains Ω_1 and Ω_2

As mentioned previously, the MFS yields better results in highly regular domains, even when considering curved geometries. However, increasing the number of boundary and interface collocation points improves the accuracy of the solution. It is important to note that a larger number of points also makes the condition number grow, making solving the problem accurately more challenging.

5.2.2 Results for the rectangle

In this subchapter, we focus on a rectangular domain $[-1, -0.5] \times [1, 0.5]$ with a vertical interface along the line $x = 0$. We aim to study the problem for $k_1 \neq k_2$, where $k_2 = 1$ is fixed. The results presented in Table 5.4 for each value of k were obtained using 600 boundary points and 404 source points in each domain, with 150 interface points and $\eta = 0.08$.

Figures 5.29, 5.30, and 5.31 display the numerical approximations for different k_1 values. Notice

Boundary/Interface Points	Interface e_γ^0 Error	Interface e_γ^1 Error	Condition number
600/150	6.945×10^{-11}	1.841×10^{-11}	2.528×10^{19}
500/100	3.910×10^{-10}	1.100×10^{-10}	2.382×10^{18}
412/100	4.035×10^{-10}	1.342×10^{-10}	7.597×10^{17}

Table 5.3: Numerical errors at the interface γ . The condition number of the matrix is also presented.

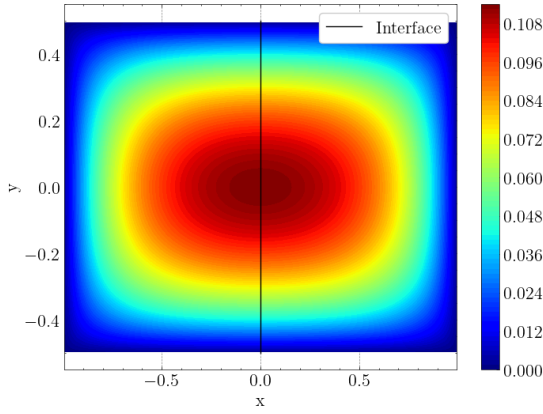


Figure 5.29: Numerical simulation with $k_1 = 1$.

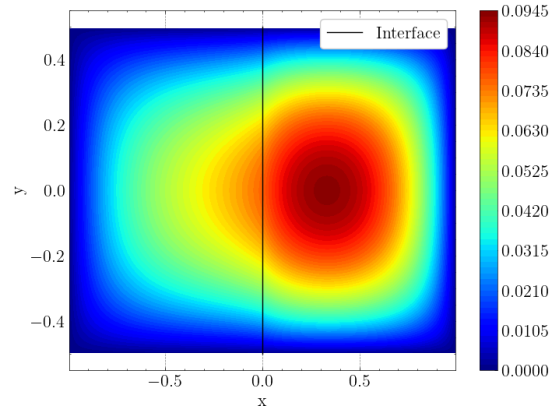


Figure 5.30: Numerical simulation with $k_1 = 2$.

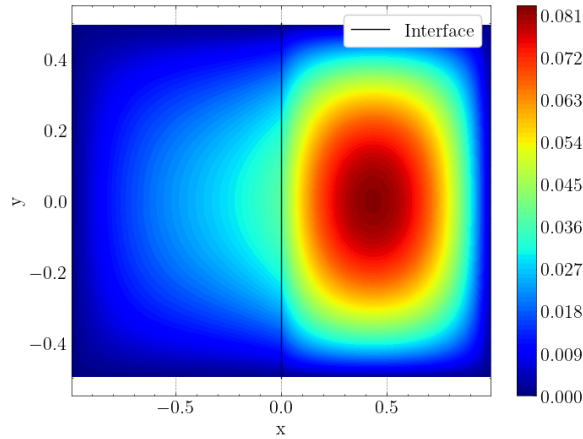


Figure 5.31: Numerical simulation with $k_1 = 5$.

Numerical approximations of the BVP for a rectangular domain with different k_1 values.

that as k_1 increases, the symmetry of the solution is disrupted, causing a shift from Ω_1 (the left domain) to Ω_2 (the right domain). Although these results are slightly less accurate than the previous ones due to reduced domain regularity, they still maintain a high level of accuracy. It's worth mentioning that when k_1 and k_2 have different values, the method's accuracy decreases, as expected, since the material

k_1 value	Boundary Error		Interface Errors		Condition number
	Domain 1	Domain 2	e_γ^0	e_γ^1	
1	7.775×10^{-8}	7.779×10^{-8}	4.732×10^{-9}	7.589×10^{-9}	2.331×10^{13}
2	4.398×10^{-8}	8.614×10^{-8}	2.499×10^{-6}	7.868×10^{-8}	3.623×10^{13}
5	2.181×10^{-8}	1.036×10^{-7}	3.838×10^{-6}	1.551×10^{-7}	8.182×10^{13}

Table 5.4: Consistency errors on the boundary and at the interface γ .

parameter changes at the interface, reducing the solution's regularity.

Notice that the condition number of the coefficient matrix A in (5.6) for the rectangle is smaller than the one presented in Table 5.3 for the unit disk. This is a consequence of a smaller value of η (we recall that in this section we took $\eta = 0.08$ and in the numerical validation section $\eta = 0.3$), which in this case appears to be optimal since increasing its value decreases the overall accuracy.

5.2.3 Results for an L-shape domain with basis functions enrichment

In the previous subsection, a domain with corners was analyzed. However, it still preserved some regularity, and the MFS with classical basis functions was able to capture the behavior of the solution around the corners, for more details on the corner behavior, see Remark C.1.1 in Appendix C. In this subsection, we are going to study the case of an L-shaped, nonconvex domain whose solutions are less regular due to the corners. Two different interfaces will be considered: first, the interface along the line $x = 0$; then, along the symmetry axis of the domain Ω , i.e. along the line $y = x + \frac{1}{2}$.

Consider the L-shaped given in Figure 5.32. The left and right subdomains are denoted by Ω_1 and Ω_2 , respectively. The number of interface points is 300, and the number of source points for each domain is 428. The number of boundary collocation points for Ω_1 and Ω_2 is 710 and 639, respectively.

In Table 5.5, the results without resorting to enrichment are presented. It is evident that the method yields poorer results due to the lower regularity of the solution in the re-entrant corner. Particularly, the error along the interface (mainly the lack of continuity) is significantly higher compared to previous cases, even when considering more collocation points on the interface. It appears that the shape of the domain poses more challenges than the discontinuous source function when considering different values for the material parameters k_1 and k_2 . In Figure 5.33, it is even possible to see that there already exists some small jump near the edges of the interface.

One of the major problems for the method is the behavior of the solution near the re-entrant corner of Ω , which in Ω_1 corresponds to a corner of π radians where different boundary conditions meet (the problem much resembles the *Motz-problem* in [Mot47], which is used as a benchmark in the study

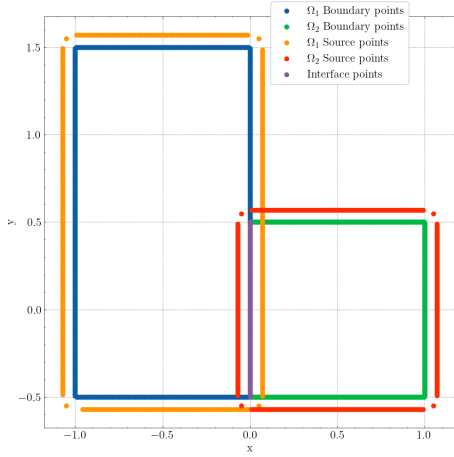


Figure 5.32: L-shaped domain with a vertical interface. Configuration of the boundary, source, and interface points.

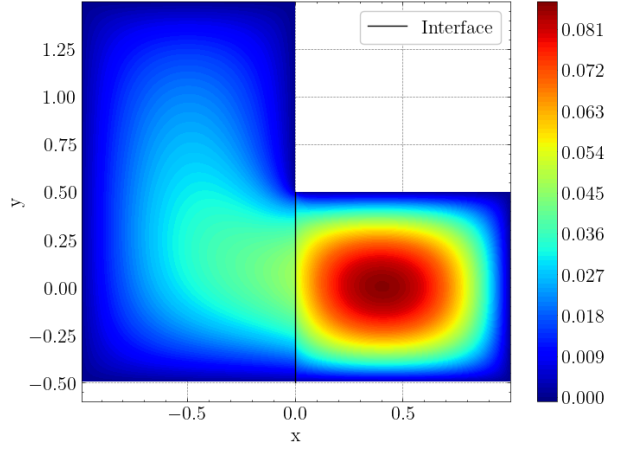


Figure 5.33: Numerical approximation of the transmission problem in an L-shaped domain with interface along $x = 0$ and $k_1 = 5$.

k_1 value	Boundary Error		Interface Errors		Condition number
	Domain 1	Domain 2	e_γ^0	e_γ^1	
1	7.853×10^{-5}	1.155×10^{-4}	2.916×10^{-3}	2.155×10^{-5}	5.587×10^{12}
2	8.152×10^{-5}	1.350×10^{-4}	3.835×10^{-3}	1.149×10^{-5}	8.161×10^{12}
5	7.079×10^{-5}	1.378×10^{-4}	4.085×10^{-3}	5.411×10^{-5}	1.776×10^{13}

Table 5.5: Consistency errors on the boundary and in the interface γ

of numerical methods for PDEs which present singularities, for example in [AV10]). In this case, we consider Dirichlet-Neumann particular solutions presented in C.1 centered in the corner which imposes less regularity on the solution. Notice that for Ω_2 these types of particular solutions are not added to the set of basis functions since the interface edges make a right angle with the adjacent edges. Therefore, we only consider particular solutions that describe the behavior of the solution in the π radians corner with a possible singularity. Let

$$v_{p_1}(r, \theta) = \beta_{p_1} r^{\alpha_{p_1}} \sin(\beta_{p_1}(\theta - \theta_1)) \quad (5.8)$$

where

$$\beta_{p_1} = \frac{(p_1 + \frac{1}{2})\pi}{\Theta},$$

$\theta_1 = \frac{\pi}{2}$, $\Theta = \pi$ is the total angle amplitude, and where the polar coordinates r and θ , centered in the corner, are given by

$$r(x, y) = \sqrt{x^2 + y^2}, \quad \theta(x, y) = \begin{cases} \text{atan2}(y, x), & \text{if } \text{atan2}(y, x) > 0 \\ \text{atan2}(y, x) + 2\pi, & \text{if } \text{atan2}(y, x) \leq 0, \end{cases}$$

where the function $\text{atan2}(y, x)$ computes the \arctan of $\frac{y}{x}$ taking into account which quadrant the point (x, y) is in, and it is given by

$$\text{atan2}(y, x) = \begin{cases} \arctan\left(\frac{y}{x}\right) & \text{if } x > 0, \\ \arctan\left(\frac{y}{x}\right) + \pi & \text{if } x < 0 \text{ and } y \geq 0, \\ \arctan\left(\frac{y}{x}\right) - \pi & \text{if } x < 0 \text{ and } y < 0, \\ \frac{\pi}{2}, & \text{if } x = 0 \text{ and } y > 0, \\ -\frac{\pi}{2}, & \text{if } x = 0 \text{ and } y < 0, \\ \text{undefined}, & \text{if } x = 0 \text{ and } y = 0. \end{cases}$$

See the open standard [Jon10] for more details. By differentiating Equation (5.8) in cartesian coordinates and returning back to polar coordinates we find that

$$\nabla v_{p_1}(r, \theta) = \left(-\frac{(2\pi p_1 + \pi)^2 r^{\frac{2\pi p_1 + \pi}{2\Theta}} \sin\left(\theta + \frac{\pi(p_1 + \frac{1}{2})(s-\theta)}{\Theta}\right)}{4\Theta^2 r}, \frac{(2\pi p_1 + \pi)^2 r^{\frac{2\pi p_1 + \pi}{2\Theta}} \cos\left(\theta + \frac{\pi(p_1 + \frac{1}{2})(s-\theta)}{\Theta}\right)}{4\Theta^2 r} \right).$$

Finally, considering the truncated expansion

$$\phi(r, \theta) = \sum_{p_1=0}^{P_1} \delta_{p_1} v_{p_1}(r, \theta), \quad (5.9)$$

where P_1 is the number of particular solutions added and δ_{p_1} are the coefficient to be found using least squares. Expanding the matrix in (5.6), it becomes

$$\begin{bmatrix} \left[\Phi(x_m^{(1)} - y_j^{(1)}) \right] & [0] & [\phi(r(x_m), \theta(x_m))] \\ [0] & \left[\Phi(x_m^{(2)} - y_j^{(2)}) \right] & [0] \\ \left[\Phi(z_q - y_j^{(1)}) \right] & \left[-\Phi(z_q - y_j^{(2)}) \right] & [\phi(r(z_q), \theta(z_q))] \\ \left[k_1 \partial_n \Phi(z_q - y_j^{(1)}) \right] & \left[-k_2 \partial_n \Phi(z_q - y_j^{(2)}) \right] & [k_1 \partial_n \phi(r(z_q), \theta(z_q))] \end{bmatrix}$$

Table 5.7 presents the results after applying the enrichment technique for the previously considered k_1 values. In expansion (5.9), different numbers of terms were considered. After some simulations, it became clear that choosing $P_1 > 2$ would not achieve better results for positive p_1 values. On the other hand, negative values of p_1 were considered. Interestingly, when adding particular solutions for the exterior problem, better results were achieved. Not only did the error decrease at the boundary Γ_i of each domain, but better results were also achieved on the interface.

To finish this subsection, we present an L-shaped domain where the interface is drawn along its axis of symmetry. In this case, notice that there are two corners which imposes less regularity on the solution, both with $\frac{3}{4}\pi$ radians⁵. In Figure 5.34, we present the configuration with Ω_1 extending further up and Ω_2 further right. The number of interface points and source points for each domain is still 300 and 428, respectively. We also chose 628 boundary collocation points for both domains. Table 5.8 summarizes the results without considering particular solutions.

p_1 values	k_1 value	Boundary Error		Interface Errors		Condition number
		Domain 1	Domain 2	e_γ^0	e_γ^1	
0, 1	1	2.965×10^{-5}	7.907×10^{-5}	2.94×10^{-3}	2.624×10^{-5}	5.584×10^{12}
	2	2.203×10^{-5}	6.657×10^{-5}	1.86×10^{-3}	2.068×10^{-5}	8.156×10^{12}
	5	2.203×10^{-5}	6.657×10^{-5}	1.86×10^{-3}	2.068×10^{-5}	8.156×10^{12}
-1, 0, 1	1	8.627×10^{-6}	4.132×10^{-5}	7.68×10^{-4}	6.876×10^{-6}	5.585×10^{12}
	2	7.333×10^{-6}	2.791×10^{-5}	6.01×10^{-4}	2.555×10^{-5}	8.157×10^{12}
	5	4.271×10^{-6}	1.118×10^{-5}	2.69×10^{-4}	4.166×10^{-5}	1.775×10^{13}
-2, -1, 0, 1	1	3.898×10^{-6}	5.975×10^{-6}	1.44×10^{-3}	2.505×10^{-6}	4.156×10^{14}
	2	2.584×10^{-6}	2.514×10^{-6}	9.69×10^{-4}	1.048×10^{-5}	4.156×10^{14}
	5	1.119×10^{-6}	6.838×10^{-7}	4.89×10^{-4}	1.106×10^{-5}	4.156×10^{14}

Table 5.7: Consistency errors on the boundary and at the interface γ after enriching the basis with particular (angular) solutions.

k_1 value	Boundary Error		Interface Errors		Condition number
	Domain 1	Domain 2	e_γ^0	e_γ^1	
1	1.812×10^{-4}	2.060×10^{-4}	7.305×10^{-3}	8.018×10^{-5}	1.050×10^{10}
2	1.398×10^{-4}	9.729×10^{-5}	5.986×10^{-4}	5.505×10^{-5}	1.646×10^{10}
5	7.096×10^{-5}	3.030×10^{-5}	1.528×10^{-3}	4.348×10^{-5}	3.730×10^{10}

Table 5.8: Consistency errors on the boundary and at the interface γ .

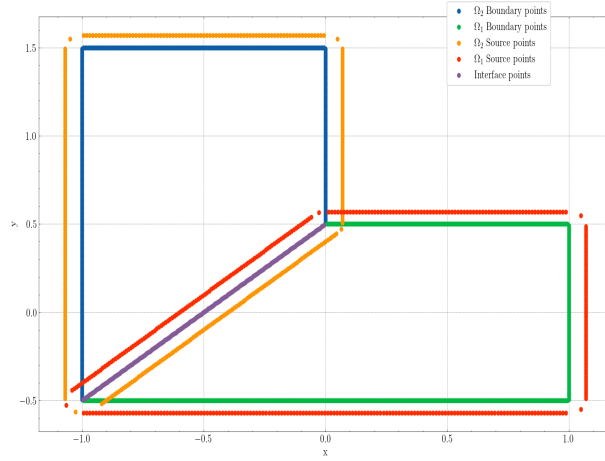


Figure 5.34: L-shaped domain with the interface on the symmetry axis. Configuration of the boundary, source, and interface points.

Since particular solutions will be added at the corner which imposes less regularity on the solution in Ω_2 , one should now consider Neumann-Dirichlet particular solutions centered in such corner (check section C.1 in Appendix C for more details). These particular solutions have the form

$$w_{p_2}(r, \theta) = \beta_{p_2} r^{\beta_{p_2}} \cos(\beta_{p_2}(\theta - \theta_2)),$$

where the β_{p_2} coefficients are the same as in (5.8), $\Theta = \frac{3}{4}\pi$ and $\theta_2 = \frac{5}{4}\pi$. Notice that Θ is the same in both domains. The (polar) gradient of w is now

$$\nabla w(r, \theta)_{p_2} = \left(\frac{(2\pi p_2 + \pi)^2 r^{\frac{2\pi p_2 + \pi}{2\Theta}} \cos\left(\theta + \frac{\pi(p_2 + \frac{1}{2})(s - \theta)}{\Theta}\right)}{4\Theta^2 r}, \frac{(2\pi p_2 + \pi)^2 r^{\frac{2\pi p_2 + \pi}{2\Theta}} \sin\left(\theta + \frac{\pi(p_2 + \frac{1}{2})(s - \theta)}{\Theta}\right)}{4\Theta^2 r} \right).$$

Table 5.10 shows the results obtained when particular solutions are added to both domains. Once again, negative values of p_2 were considered. Without intending to show too much data (because we would have to account for every combination of p_1 and p_2 values), we fix $p_2 = 0, 1$. The reason for this choice is that better results are achieved when increasing the number of particular solutions in the domain where the diffusion coefficient is higher. Since we are only varying k_1 , we can fix the p_2 values.

⁵The other two corners have an angle of $\frac{\pi}{4}$ radians which cause no problem for the classical MFS basis functions.

p_1 values	k_1 value	Boundary Error		Interface Errors		Condition number
		Domain 1	Domain 2	e_γ^0	e_γ^1	
0, 1	1	3.107×10^{-7}	2.100×10^{-7}	1.158×10^{-5}	1.019×10^{-7}	1.054×10^{10}
	2	1.061×10^{-7}	6.892×10^{-7}	6.366×10^{-5}	7.065×10^{-8}	1.648×10^{10}
	5	1.207×10^{-7}	1.141×10^{-6}	9.544×10^{-5}	9.487×10^{-8}	3.732×10^{10}
-1, 0, 1	1	3.319×10^{-7}	2.026×10^{-7}	1.813×10^{-5}	1.048×10^{-7}	1.054×10^{10}
	2	1.676×10^{-7}	3.166×10^{-7}	8.375×10^{-6}	7.951×10^{-8}	1.647×10^{10}
	5	9.871×10^{-8}	4.807×10^{-7}	1.549×10^{-6}	5.285×10^{-8}	3.732×10^{10}
-2, -1, 0, 1	1	3.070×10^{-7}	2.415×10^{-7}	1.610×10^{-5}	9.893×10^{-8}	5.659×10^{12}
	2	1.762×10^{-7}	2.670×10^{-7}	8.385×10^{-6}	8.480×10^{-8}	5.656×10^{12}
	5	9.761×10^{-8}	3.201×10^{-7}	1.993×10^{-6}	6.049×10^{-8}	5.655×10^{12}

Table 5.10: Consistency errors on the boundary and at the interface γ after adding particular (angular) solutions to the classical MFS basis.

Again, we found the same surprising results as before, that is, with negative values for p_1 we achieve better approximations, particularly when $k_1 \neq k_2 = 1$. An interesting observation was made when both p_1 and p_2 had negative values. In that case, the numerical solution exploded in both domains. Intuitively, it seems that one cannot consider particular solutions for the exterior problem in both domains. On the other hand, one may consider $p_1 = p_2 = 0, \dots, P$, where $P = P_1 = P_2$, for $P > 1$ (P may be as large as 8, for example, with 16 particular solutions being added in total) and the results can be as good as the ones presented in Table 5.10 for $p_1 = -2, -1, 0, 1$, but only if $k_1 = k_2 = 1$; otherwise, the approximation on the interface gets worse.

Figures 5.35 and 5.36 show the absolute value of the errors for each interface point, with $k_1 = 2$ and the p values for the particular solutions are $p_1 = -2, -1, 0, 1$ and $p_2 = 0, 1$. As expected, both errors peak near the endpoints of the interface, in particular near the re-entrant corner.

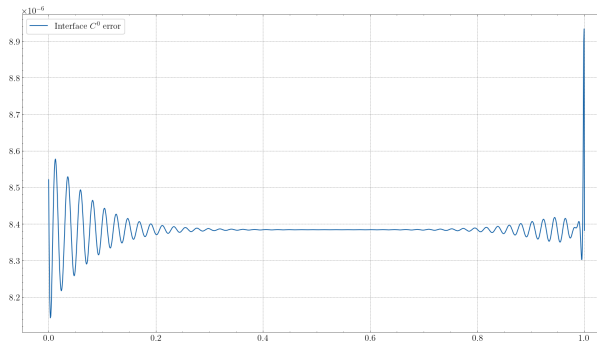


Figure 5.35: Interface ϵ_γ^0 error.

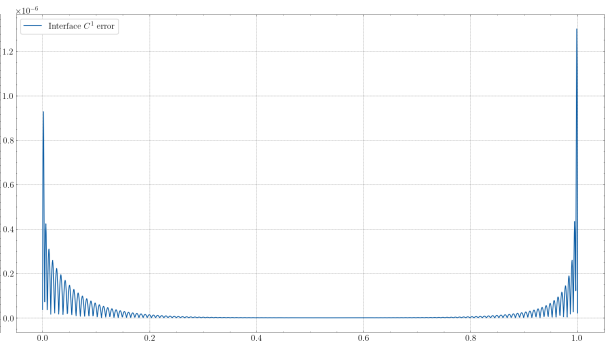


Figure 5.36: Interface ϵ_γ^1 error.

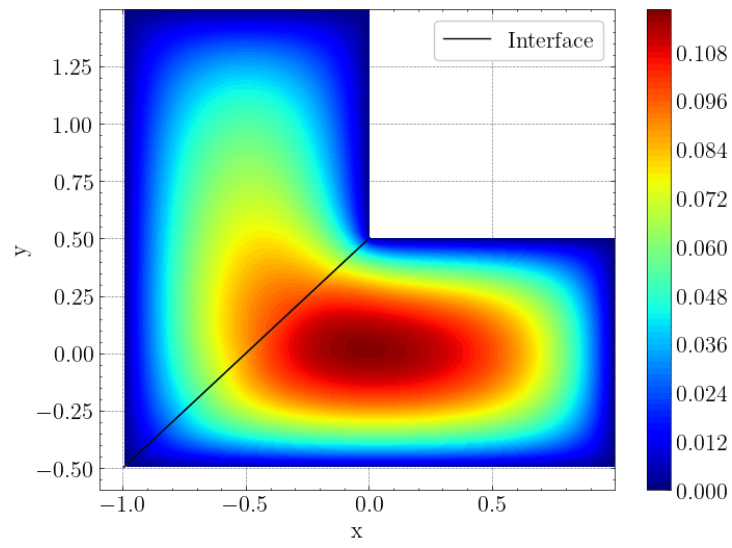


Figure 5.37: Absolute value of the interface errors and numerical approximation for $k_1 = 2$, $p_1 = -2, -1, 0, 1$ and $p_2 = 0, 1$.

6

Conclusions

In this dissertation, the Method of Fundamental Solutions (MFS) was used within the context of the Dirac operator with infinite mass boundary conditions, as well as in transmission problems involving the diffusion equation. Besides presenting the theoretical foundations of the MFS, this work also aimed at contributing to the comprehension of the method's capabilities and limitations through the applications.

In regard to the Dirac operator, the extension of the proof on the absence of separation of variables in polar coordinates near a corner's tip is interesting from a numerical point of view. Although anticipated, this extension complicates the use of specific solutions near a corner. Numerical simulations proved valuable in validating previous conjectures and generating new ones, both reaffirming the MFS's efficacy in addressing specific challenges and solidifying its practical usefulness for the numerical approximation of Partial Differential Equations. Numerical evidence supporting the generalizations of the Faber-Krahn inequality and the Ashbaugh-Benguria Theorem, both in polygonal and in smooth domains was given, further enhancing the veracity of these conjectures. Additionally, an unexpected behavior of the third eigenvalue in the Dirac operator's spectrum was revealed, signaling potential disparities with respect to the behavior of the Laplace operator, even at the beginning of the spectrum. It is also worth noticing that such a finding only appears to be valid for some mass ranges, also indicating the spectrum's dependence

on the mass m .

The application of the Method of Fundamental Solutions with particular solutions to transmission problems is also significant since it is the first study that introduces the use of particular solutions to better describe the solution's behavior near corners in these types of PDEs. Although this technique was previously employed for other types of PDEs, its application to transmission problems represents a novel advancement, expanding the practical utility of the method.

Nonetheless, numerous questions remain unanswered, setting the stage for future work. The spectrum of the Dirac operator, alongside its distinct behavior compared to the Laplace operator, requires further investigation. This includes the behavior of the second eigenvalue and the shape of the optimal domain for various eigenvalues. Future explorations may uncover valuable insights that can be useful for such theoretical problems, advancing our understanding of spectral geometry. Is the optimal shape for the second eigenvalue still two disjoint balls with the same volume, and does this insight provide a basis for understanding higher eigenvalues? Can the Method of Fundamental Solutions be adapted to handle topological changes, like connectedness, and how can the behavior of eigenvalues in such cases be predicted? Notice that for the third eigenvalue, we still do not know if the optimal shape is even connected. If it is not, then the shape presented in this work is not the optimal one. For the Laplacian, these topological questions can be addressed using Theorem 3.1.7, but is there any analogous result for the Dirac operator with infinite mass boundary conditions?

Similarly, the transmission problem presents its own set of questions and problems when using the Method of Fundamental Solutions. A result that is not addressed in this work concerns a potential *a posteriori* error estimate. Such an estimate would aim to bound, both from above and from below, the error between an exact solution and a numerical solution by an error estimator depending only on the discrete solution and (possibly) the data. Is it possible to use different particular solutions whose behavior better adapts to the problem? How can these particular solutions be tailored to yield more accurate results on the interface between domains? Addressing these issues could further refine the Method of Fundamental Solutions and broaden its applicability.

This dissertation represents a step towards finding more accurate numerical methods for complex Partial Differential Equations, with the potential to bring new insights into the investigation of the behavior of their solutions. Our objective remains to continue this study, tackle these problems, and adapt these methods to push the boundaries of the already achieved results.

Bibliography

- [AA05] Carlos JS Alves and Pedro RS Antunes. The method of fundamental solutions applied to the calculation of eigenfrequencies and eigenmodes of 2d simply connected shapes. *CMC-TECH SCIENCE PRESS*, 2(4):251, 2005.
- [AA13] Carlos JS Alves and Pedro RS Antunes. The method of fundamental solutions applied to some inverse eigenproblems. *SIAM Journal on Scientific Computing*, 35(3):A1689–A1708, 2013.
- [ABLOB21] Pedro RS Antunes, Rafael D Benguria, Vladimir Lotoreichik, and Thomas Ourmières-Bonafos. A variational formulation for Dirac operators in bounded domains. applications to spectral geometric inequalities. *Communications in Mathematical Physics*, 386(2):781–818, 2021.
- [AC05] CJS Alves and CS Chen. A new method of fundamental solutions applied to nonhomogeneous elliptic problems. *Advances in Computational Mathematics*, 23:125–142, 2005.
- [AF03] Robert A Adams and John JF Fournier. *Sobolev spaces*. Elsevier, 2003.
- [AF11] Pedro RS Antunes and Pedro Freitas. On the inverse spectral problem for Euclidean triangles. *Proceedings of the Royal Society A: Mathematical, Physical and Engineering Sciences*, 467(2130):1546–1562, 2011.
- [Alv09] Carlos JS Alves. On the choice of source points in the method of fundamental solutions. *Engineering Analysis with Boundary Elements*, 33(12):1348–1361, 2009.
- [AMV21] Carlos JS Alves, Nuno FM Martins, and Svilen S Valtchev. Domain decomposition methods with fundamental solutions for Helmholtz problems with discontinuous source terms. *Computers & Mathematics with Applications*, 88:16–32, 2021.
- [And22] Neculai Andrei. *Modern Numerical Nonlinear Optimization*, volume 195. Springer Nature, 2022.

- [Ant18a] Pedro RS Antunes. A numerical algorithm to reduce ill-conditioning in meshless methods for the Helmholtz equation. *Numer. Algorithms*, 79(3):879–897, 2018.
- [Ant18b] Pedro RS Antunes. Reducing the ill conditioning in the method of fundamental solutions. *Advances in Computational Mathematics*, 44:351–365, 2018.
- [ASR88] Milton Abramowitz, Irene A Stegun, and Robert H Romer. Handbook of mathematical functions with formulas, graphs, and mathematical tables, 1988.
- [AU10] Wolfgang Arendt and Karsten Urban. *Partielle differenzialgleichungen*. Springer, 2010.
- [AV10] Pedro RS Antunes and Svilen S Valtchev. A meshfree numerical method for acoustic wave propagation problems in planar domains with corners and cracks. *Journal of Computational and Applied Mathematics*, 234(9):2646–2662, 2010.
- [BB08] Alex H Barnett and Timo Betcke. Stability and convergence of the method of fundamental solutions for Helmholtz problems on analytic domains. *Journal of Computational Physics*, 227(14):7003–7026, 2008.
- [BB22] Benjamin Bogosel and Dorin Bucur. On the polygonal Faber-Krahn inequality. *arXiv preprint arXiv:2203.16409*, 2022.
- [BFSVDB17] Rafael D Benguria, Søren Fournais, Edgardo Stockmeyer, and Hanne Van Den Bosch. Spectral gaps of Dirac operators describing graphene quantum dots. *Mathematical Physics, Analysis and Geometry*, 20:1–12, 2017.
- [BK22] Philippe Briet and David Krejčířík. Spectral optimization of Dirac rectangles. *Journal of Mathematical Physics*, 63(1):013502, 2022.
- [Bog85] Alexander Bogomolny. Fundamental solutions method for elliptic boundary value problems. *SIAM Journal on Numerical Analysis*, 22(4):644–669, 1985.
- [Bor20] David Borthwick. *Spectral Theory: Basic Concepts and Applications*, volume 284. Springer Nature, 2020.
- [Bre71] Richard P. Brent. An algorithm with guaranteed convergence for finding a zero of a function. *The computer journal*, 14(4):422–425, 1971.
- [Bré11] Haim Brézis. *Functional analysis, Sobolev spaces and partial differential equations*, volume 2. Springer, 2011.
- [BT05] Timo Betcke and Lloyd N Trefethen. Reviving the method of particular solutions. *SIAM review*, 47(3):469–491, 2005.

- [Buc12] Dorin Bucur. Minimization of the k -th eigenvalue of the Dirichlet laplacian. *Archive for Rational Mechanics and Analysis*, 206(3):1073–1083, 2012.
- [CH08] Richard Courant and David Hilbert. *Methods of mathematical physics: partial differential equations*. John Wiley & Sons, 2008.
- [CK13] David Colton and Rainer Kress. *Integral equation methods in scattering theory*. SIAM, 2013.
- [CM81] Søren Christiansen and E Meister. Condition number of matrices derived from two classes of integral equations. *Mathematical Methods in the Applied Sciences*, 3(1):364–392, 1981.
- [CWHM17] Simon N Chandler-Wilde, David P Hewett, and Andrea Moiola. Sobolev spaces on non-Lipschitz subsets of \mathbb{R}^n with application to boundary integral equations on fractal screens. *Integral Equations and Operator Theory*, 87(2):179–224, 2017.
- [CZ10] Goong Chen and Jianxin Zhou. *Boundary element methods with applications to nonlinear problems*, volume 7. Springer Science & Business Media, 2010.
- [DBDB78] Carl De Boor and Carl De Boor. *A practical guide to splines*, volume 27. springer-verlag New York, 1978.
- [Dir28] Paul Adrien Maurice Dirac. The quantum theory of the electron. *Proceedings of the Royal Society of London. Series A, Containing Papers of a Mathematical and Physical Character*, 117(778):610–624, 1928.
- [EG15] Lawrence Craig Evans and Ronald F Gariepy. *Measure theory and fine properties of functions*. CRC press, 2015.
- [Eva22] Lawrence C Evans. *Partial differential equations*, volume 19. American Mathematical Society, 2022.
- [FK08] Pedro Freitas and David Krejčířík. A sharp upper bound for the first Dirichlet eigenvalue and the growth of the isoperimetric constant of convex domains. *Proceedings of the American Mathematical Society*, 136(8):2997–3006, 2008.
- [GCK96] Michael A Golberg, Ching-Shyang Chen, and SR Karur. Improved multiquadric approximation for partial differential equations. *Engineering Analysis with boundary elements*, 18(1):9–17, 1996.
- [Gey07] Giuseppe Geymonat. Trace theorems for sobolev spaces on Lipschitz domains. necessary conditions. In *Annales mathématiques Blaise Pascal*, volume 14, pages 187–197, 2007.

- [GSO21] Javier Gómez-Serrano and Gerard Orriols. Any three eigenvalues do not determine a triangle. *Journal of Differential Equations*, 275:920–938, 2021.
- [GSV19] Tom Gustafsson, Rolf Stenberg, and Juha Videman. Error analysis of Nitsche’s mortar method. *Numerische Mathematik*, 142:973–994, 2019.
- [GTGT77] David Gilbarg, Neil S Trudinger, David Gilbarg, and NS Trudinger. *Elliptic partial differential equations of second order*, volume 224. Springer, 1977.
- [GWW92] Carolyn Gordon, David Webb, and Scott Wolpert. Isospectral plane domains and surfaces via Riemannian orbifolds. *Inventiones mathematicae*, 110(1):1–22, 1992.
- [Hal64] John H Halton. Algorithm 247: Radical-inverse quasi-random point sequence. *Communications of the ACM*, 7(12):701–702, 1964.
- [HB00] Antoine Henrot and Dorin Bucur. Minimization of the third eigenvalue of the Dirichlet laplacian. *Proceedings of the Royal Society of London. Series A: Mathematical, Physical and Engineering Sciences*, 456(1996):985–996, 2000.
- [Hen06] Antoine Henrot. *Extremum problems for eigenvalues of elliptic operators*. Springer Science & Business Media, 2006.
- [Hen17] Antoine Henrot. *Shape optimization and spectral theory*. De Gruyter Open, 2017.
- [HM17] David P Hewett and Andrea Moiola. A note on properties of the restriction operator on sobolev spaces. *Journal of Applied Analysis*, 23(1):1–8, 2017.
- [Hör15] Lars Hörmander. *The analysis of linear partial differential operators I: Distribution theory and Fourier analysis*. Springer, 2015.
- [Jon10] Larry Jones. Wg14 n1539 committee draft iso/iec 9899: 201x, 2010.
- [Kac66] Mark Kac. Can one hear the shape of a drum? *The american mathematical monthly*, 73(4P2):1–23, 1966.
- [Kat13] Tosio Kato. *Perturbation theory for linear operators*, volume 132. Springer Science & Business Media, 2013.
- [Kit88] Takashi Kitagawa. On the numerical stability of the method of fundamental solution applied to the Dirichlet problem. *Japan Journal of Applied Mathematics*, 5:123–133, 1988.
- [Kit91] Takashi Kitagawa. Asymptotic stability of the fundamental solution method. *Journal of Computational and Applied Mathematics*, 38(1-3):263–269, 1991.

- [KLL19] David Krejčířík, Simon Larson, and Vladimir Lotoreichik. Problem list of the aim workshop, 2019.
- [Kra26] Edgar Krahn. Über minimaleigenschaften der kugel in drei und mehr dimensionen. (*No Title*), 1926.
- [Kre13] R. Kress. *Linear Integral Equations*. Applied Mathematical Sciences. Springer New York, 2013.
- [LL00] Zi-Cai Li and Tzon-Tzer Lu. Singularities and treatments of elliptic boundary value problems. *Mathematical and Computer Modelling*, 31(8-9):97–145, 2000.
- [LM12] Jacques Louis Lions and Enrico Magenes. *Non-homogeneous boundary value problems and applications: Vol. 1*, volume 181. Springer Science & Business Media, 2012.
- [LOB19] Vladimir Lotoreichik and Thomas Ourmières-Bonafos. A sharp upper bound on the spectral gap for graphene quantum dots. *Mathematical Physics, Analysis and Geometry*, 22:1–30, 2019.
- [Mot47] H Motz. The treatment of singularities of partial differential equations by relaxation methods. *Quarterly of Applied Mathematics*, 4(4):371–377, 1947.
- [MP68] CB Moler and LE Payne. Bounds for eigenvalues and eigenvectors of symmetric operators. *SIAM Journal on Numerical Analysis*, 5(1):64–70, 1968.
- [Nec11] Jindrich Necas. *Direct methods in the theory of elliptic equations*. Springer Science & Business Media, 2011.
- [NN12] Raghavan Narasimhan and Yves Nievergelt. *Complex analysis in one variable*. Springer Science & Business Media, 2012.
- [PS51] George Pólya and Gábor Szegő. *Isoperimetric inequalities in mathematical physics*. Number 27. Princeton University Press, 1951.
- [QV99] Alfio Quarteroni and Alberto Valli. *Domain decomposition methods for partial differential equations*. Number BOOK. Oxford University Press, 1999.
- [Reu06] S Yu Reutskiy. The method of fundamental solutions for Helmholtz eigenvalue problems in simply and multiply connected domains. *Engineering Analysis with Boundary Elements*, 30(3):150–159, 2006.
- [RS75] Michael Reed and Barry Simon. *II: Fourier Analysis, Self-Adjointness*, volume 2. Elsevier, 1975.

- [Rud91] W. Rudin. *Functional Analysis*. International series in pure and applied mathematics. McGraw-Hill, 1991.
- [Sal16] Sandro Salsa. *Partial differential equations in action: from modelling to theory*, volume 99. Springer, 2016.
- [Smy09] Yiorgos-Sokratis Smyrlis. Applicability and applications of the method of fundamental solutions. *Mathematics of computation*, 78(267):1399–1434, 2009.
- [Tav] Hugo Tavares. Partial differential equations, lecture notes. https://ulisboa-my.sharepoint.com/:b:/g/personal/ist27898_tecnico_ulisboa_pt/EfizUpSVmCRCo0Nst2a-sacBDwFrkPuh9w8A55EU9BoFmA?e=kY5B2R. Accessed: 28-4-2023.
- [Val08] Svilen Valtchev. *Numerical Analysis of Methods with Fundamental Solutions for Acoustic and Elastic Wave Propagation Problems*. PhD thesis, Universidade Técnica de Lisboa, Instituto Superior Técnico, 2008.
- [Vu23] Tuyen Vu. Spectral inequality for Dirac right triangles. *arXiv preprint arXiv:2302.13040*, 2023.
- [WK94] Sven Andreas Wolf and Joseph Bishop Keller. Range of the first two eigenvalues of the laplacian. *Proceedings of the Royal Society of London. Series A: Mathematical and Physical Sciences*, 447(1930):397–412, 1994.
- [Wlo87] Joseph Wloka. *Partial differential equations*. Cambridge University Press, 1987.
-



Some details on regular domains and Sobolev spaces

This appendix serves as a resource to complement Chapter 2 by providing additional insights into domain regularity and Sobolev spaces on manifolds. While these subjects were not covered in Chapter 2, they play an important role in the formalization and understanding of the broader context of this work, for example when defining layer potentials in Chapter 4. We refer to [Sal16], [Nec11], and [Wlo87] for more details on this Appendix.

Until otherwise indicated, let $\Omega \subset \mathbb{R}^d$ be an open and bounded set, with $d \geq 2$ and boundary $\partial\Omega$. First, we formalize the notion of C^k and Lipschitz domains.

Definition A.0.1. *The boundary $\partial\Omega$ is of class C^k (or the domain Ω is of class C^k) if for each $x \in \partial\Omega$ there exists a system of coordinates $(\mathbf{y}', y_d) = (y_1, \dots, y_{d-1}, y_d)$ with origin at x , a ball $B(x)$ and a function φ defined in a neighbourhood $U \subset \mathbb{R}^{d-1}$ of $\mathbf{y}' = \mathbf{0}'$, such that*

$$\varphi \in C^k(U), \varphi(\mathbf{y}') = \mathbf{0}'$$

and

- $\partial\Omega \cap B(x) = \{(\mathbf{y}', y_d) : y_d = \varphi(\mathbf{y}'), \forall \mathbf{y}' \in U\};$
- $\Omega \cap B(x) = \{(\mathbf{y}', y_d) : y_d > \varphi(\mathbf{y}'), \forall \mathbf{y}' \in U\}.$

On the other hand, the boundary $\partial\Omega$ is Lipschitz (or the domain Ω is Lipschitz) if φ is a Lipschitz function on U , i.e.,

$$p, q \in U \implies |\varphi(p) - \varphi(q)| \leq L|p - q|$$

for some $L > 0$.

In order to formalize the notion of Sobolev spaces in manifolds (which is used in Theorem 2.3.10 and when presenting layer potentials), we state Lemma A.0.2.

Lemma A.0.2 (Partition of Unity). *Let $K \subset \mathbb{R}^d$ be a compact set and U_1, \dots, U_N be an open covering of K , i.e., $K \subset \bigcup_{i=1}^N U_i$ (such covering exists since K is compact). Then, there exists functions $\theta_1, \dots, \theta_N$ (said to be a partition of unity subordinated to the decomposition of $\partial\Omega$) such that*

- for every $i = 1, \dots, N$, $\theta_i \in \mathcal{D}(U_i)$ and $0 \leq \theta_i \leq 1$;
- for every $x \in K$, $\sum_{i=1}^N \theta_i(x) = 1$.

Assume that Ω is (at least) a Lipschitz domain. Let $g : \partial\Omega \rightarrow \mathbb{R}$ and the balls B_1, \dots, B_N be an open covering of $\partial\Omega$ centered at points of Γ . Then, by Lemma A.0.2, there exists a partition of unity $\theta_1, \dots, \theta_N$ subordinated to $\partial\Omega$ such that the function g can be written as

$$g = \sum_{i=1}^N g_i$$

where $g_i = \theta_i g$ for each $i = 1, \dots, N$. Since $\partial\Omega \cap B_i$ is the graph of an (at least) Lipschitz function $\varphi_i(\mathbf{y}')$, by the local parametrization we have

$$g_i(x) = \theta_i(x)g(x) = \theta_i(\varphi(\mathbf{y}'))g(\varphi(\mathbf{y}')) = \tilde{g}_i(\mathbf{y}'), \quad \mathbf{y}' \in U_i$$

for any $x \in \partial\Omega \cap B_i$ and U_i is a neighbourhood of \mathbf{y}' . Thus, for $s \geq 0$ we say that $g \in H^s(\partial\Omega)$ if

$$\|g\|_{H^s(\partial\Omega)}^2 = \sum_{i=1}^N \|\tilde{g}_i\|_{H^s(U_i)}^2 < \infty.$$

Note that norm $\|g\|_{H^s(\partial\Omega)}^2$ depends on the cover and partition of unity. However, norms corresponding to different parametrizations of Γ and partitions of unity are all equivalent.

B

Spectral Decomposition of the Laplace operator

In this appendix, we make a brief study regarding the Laplace operator in a bounded domain $\Omega \subset \mathbb{R}^d$ with Lipschitz boundary. The main results presented here are mostly consequences of the Spectral Theorem 2.2.15. Firstly, recall the Divergence Theorem, e.g. [EG15].

Theorem B.0.1 (Divergence Theorem). *Let $\Omega \subset \mathbb{R}^d$ defined as above. Then,*

$$\int_{\Omega} \operatorname{div} \phi dx = \int_{\partial\Omega} \phi \cdot \mathbf{n} d\sigma,$$

where \mathbf{n} denotes the exterior unitary normal and the $(d-1)$ -surface element is given by

$$d\sigma = \sqrt{1 + |\nabla \varphi_i|^2} dy'$$

where φ is the local parametrization given in Definition A.0.1. Although φ is only a Lipschitz function, by Rademacher Theorem (see Chapter 1 in [Sal16]) φ is differentiable almost everywhere.

A key consequence of the Divergence Theorem is the *Green's Formulas*.

Corollary B.0.2 (Green's Formulas). *In this same conditions of the Theorem B.0.1, let $u, v \in H^2(\Omega)$. Then,*

1. $\int_{\Omega} \Delta u dx = \int_{\partial\Omega} \frac{\partial u}{\partial n} d\sigma;$
2. $\int_{\Omega} \Delta uv dx = - \int_{\Omega} \nabla u \cdot \nabla v dx + \int_{\partial\Omega} \frac{\partial u}{\partial n} v d\sigma;$
3. $\int_{\Omega} \Delta uv - u \Delta v dx = \int_{\partial\Omega} \frac{\partial u}{\partial n} v - \frac{\partial v}{\partial n} u d\sigma.$

The study of the spectrum of the Laplace operator is of major importance in this work. We will only state and prove a classical result which can also be found in numerous textbooks, see [Bré11], [AU10], [CH08] or [Bor20]. While we assume null Dirichlet boundary conditions, we notice that the Neumann case is analogous.

Definition B.0.3. *Consider the Helmholtz equation with null Dirichlet boundary conditions*

$$\begin{cases} -\Delta u(x) = \lambda u(x), & x \in \Omega, \\ u(x) = 0, & x \in \partial\Omega. \end{cases} \quad (\text{B.1})$$

One says that $\lambda \in \mathbb{R}$ is an eigenvalue of the equation (B.1) if there exists an eigenfunction $u \neq 0$ belonging to the function spaces $C^2(\Omega) \cap C(\overline{\Omega})$.

Theorem B.0.4. *There exists a Hilbert basis $(u_n)_{n \in \mathbb{N}}$ of $L^2(\Omega)$ consisting of eigenfunctions u_n of $-\Delta$, i.e., for each $n \in \mathbb{N}$ there exists a pair eigenvalue/eigenfunction (λ_n, u_n) such that*

$$-\Delta u_n = \lambda_n u_n$$

where the sequence of eigenvalues can be ordered in increasing order and $\lambda_n \rightarrow \infty$, $n \rightarrow \infty$. Furthermore, define $E_n = \text{span}\{u_1, \dots, u_n\}$ and the Rayleigh Quotient

$$R(u) = \frac{\|\nabla u\|_{L^2(\Omega)}^2}{\|u\|_{L^2(\Omega)}^2}.$$

Then,

$$\lambda_n = \min_{\substack{u \in E_{n-1}^\perp \\ u \neq 0}} R(u) = \max_{\substack{u \in E_n \\ u \neq 0}} R(u). \quad (\text{B.2})$$

Proof. For each $f \in L^2(\Omega)$, consider the problem

$$\begin{cases} -\Delta u(x) = f, & \text{in } \Omega \\ u = 0, & \text{on } \partial\Omega \end{cases}$$

with the associated variational form

$$\int_{\Omega} \nabla u \cdot \nabla v = \int_{\Omega} f v, \quad \forall v \in H_0^1(\Omega). \quad (\text{B.3})$$

Using Lax-Milgram Theorem 2.2.7, it is straightforward to prove that the variational form (B.3) admits a unique weak solution $u \in H_0^1(\Omega)$ and the operator

$$\begin{aligned} T : L^2(\Omega) &\rightarrow L^2(\Omega) \\ f &\mapsto u \end{aligned}$$

is well-defined. To prove that T is a compact operator, using Poincaré and Cauchy-Schwarz inequalities one notices that

$$\alpha \|u\|_{H^1(\Omega)}^2 \leq \int_{\Omega} |\nabla u|^2 = \int_{\Omega} f u \leq \|f\|_{L^2(\Omega)} \|u\|_{L^2(\Omega)} \leq \|f\|_{L^2(\Omega)} \|u\|_{H^1(\Omega)} \implies \|u\|_{H^1(\Omega)} \leq C \|f\|_{L^2(\Omega)}$$

where $\alpha, C > 0$. The above result can be written as

$$\|Tf\|_{H^1(\Omega)} \leq C \|f\|_{L^2(\Omega)}, \quad \forall f \in L^2(\Omega)$$

and by Theorem 2.3.6, T is a compact operator. To check that T is self-adjoint it suffices to consider the weak variational form of the null Dirichlet boundary problems

$$-\Delta u = f \quad -\Delta v = g$$

for $f, g \in L^2(\Omega)$ and apply Green's formulas. It is also easy to see that $(Tf, f)_{L^2(\Omega)} \geq 0, \forall f \in L^2(\Omega)$ since

$$\int_{\Omega} (Tf)f = \int_{\Omega} u f = \|\nabla u\|_{L^2(\Omega)}^2 \geq 0.$$

Applying the Spectral Theorem 2.2.15 to T , there exists a Hilbert basis $(u_n)_{n \in \mathbb{N}}$ such that

$$Tu_n = \mu_n u_n$$

for $\mu_n \in \mathbb{R}$, $\mu_n \rightarrow 0$ as $n \rightarrow \infty$. In particular, taking $f = \lambda_n u_n$, where $\lambda_n = \frac{1}{\mu_n}$, one can write

$$-\Delta u_n = \lambda_n u_n,$$

or in the integral form

$$\int_{\Omega} |\nabla u|^2 = \lambda_n \int_{\Omega} u^2,$$

with $\lambda_1 \leq \lambda_2 \leq \dots \rightarrow \infty$. To check the variational form (B.2), let $u \in E_{n-1}^\perp$. Then,

$$\begin{aligned} \|\nabla u\|_{L^2(\Omega)}^2 &= (\nabla u, \nabla u)_{L^2(\Omega)} = \left(\sum_{m \geq n} (u, u_m)_{L^2(\Omega)} \nabla u_m, \nabla u \right)_{L^2(\Omega)} \\ &= \sum_{m \geq n} (u, u_m)_{L^2(\Omega)} (\nabla u_m, \nabla u)_{L^2(\Omega)} \\ &= \sum_{m \geq n} \lambda_m (u, u_m)_{L^2(\Omega)} (u_m, u)_{L^2(\Omega)} \\ &\geq \lambda_n \sum_{m \geq n} |(u, u_m)_{L^2(\Omega)}|^2 \\ &= \lambda_n \|u\|_{L^2(\Omega)}^2 \end{aligned}$$

where we used the bilinearity of the inner product, the fact that the sequence λ_n is non-decreasing, and Parseval's identity. It is easy to check that the equality is only attained if and only if u is in the eigenspace of λ_k . This proves that

$$\lambda_n = \min_{\substack{u \in E_{n-1}^\perp \\ u \neq 0}} R(u).$$

The other case is analogous. □

Remark B.0.5. Observe that (B.0.4) only guarantees that the eigenfunctions u_n belong to $H_0^1(\Omega)$. To achieve the regularity stated in Definition (B.0.3), certain conditions on Ω should be imposed. For example, if Ω is an open set of class C^2 , then $u_n \in C^\infty(\overline{\Omega})$ when Ω is smooth.

Corollary B.0.6 (Homogeneity). Let $\alpha > 0$. Consider the set

$$\alpha\Omega = \{\alpha x \in \mathbb{R}^d : x \in \Omega\},$$

i.e., $\alpha\Omega$ is a dilation of Ω by a factor of scale α . Then, for all $n \in \mathbb{N}$,

$$\alpha^2 \lambda_n(\alpha\Omega) = \lambda_n(\Omega),$$

where $\lambda_n(\alpha\Omega)$ is the n -th eigenvalue of (B.1) on the domain $\alpha\Omega$ (and analogously for $\lambda_n(\Omega)$).

Proof. The proof is an easy consequence of the variational description (B.2). Let $\varphi(x) = \alpha x$ and $\alpha\Omega = \varphi(\Omega)$. Then,

$$\lambda_n(\alpha\Omega) = \min_{\substack{u \in E_{n-1}^\perp \\ u \neq 0}} \frac{\int_{\varphi(\Omega)} |\nabla u(x)|^2 dx}{\int_{\varphi(\Omega)} |u(x)|^2 dx} = \min_{\substack{u \in E_{n-1}^\perp \\ u \neq 0}} \frac{\int_{\Omega} |\nabla u(\alpha x)|^2 dx}{\int_{\Omega} |u(\alpha x)|^2 dx},$$

via a change of variables (the Jacobian determinant of the linear transformation φ vanished from consideration as we are dealing with a ratio). Let $v(x) = u(\alpha x)$. Then,

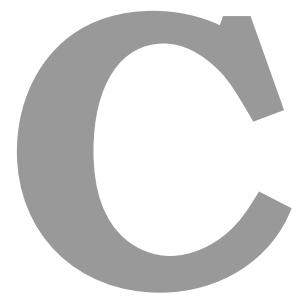
$$\nabla v(x) = \alpha \nabla u(\alpha x)$$

and

$$\alpha^2 \lambda_n(\alpha\Omega) = \min_{\substack{u \in E_{n-1}^\perp \\ u \neq 0}} \frac{\int_{\Omega} |\alpha \nabla u(\alpha x)|^2 dx}{\int_{\Omega} |u(\alpha x)|^2 dx} = \min_{\substack{v \in E_{n-1}^\perp \\ v \neq 0}} \frac{\int_{\Omega} |\nabla v(x)|^2 dx}{\int_{\Omega} |v(x)|^2 dx} = \lambda_n(\Omega).$$

□

Remark B.0.7. Notice that, unlike the homogeneity property stated in Corollary B.0.6 for the Laplace operator, a similar property does not hold for the Dirac operator with infinite mass boundary conditions unless $m = 0$ is considered in the variational form presented in Proposition 3.2.1.



Some useful insights to the Method of Fundamental Solutions

This appendix presents some useful results and techniques that can be used to increase the accuracy of the Method of Fundamental Solutions. Firstly, we present the behavior of the Laplace equation's solutions in polar coordinates near a corner's tip, supplementing the subsection 4.2.1. Such considerations were the basis for the results presented in 5.2. Then, the Subspace Angle Technique is also presented, which was used in 5.1 to tackle the ill-conditioning of the MFS for the Dirac equation with infinite mass boundary conditions.

C.1 Behavior of the Laplace equation's solutions near a corner.

In this subsection, the behavior of the Laplace equation's solutions near a corner is summarized for different boundary conditions. For more details, we point the reader to [\[LL00\]](#).

- For Dirichlet-Dirichlet boundary conditions given by $u(r, 0) = A, u(r, \Theta) = B$, then $\alpha_k = \frac{k\pi}{\Theta}$ and

$$u(r, \theta) = A(B - A) \frac{\theta}{\Theta} + \sum_{k=0}^{\infty} \alpha_k r^{\alpha_k} \sin(\alpha_k \theta);$$

- For Dirichlet-Neumann boundary conditions given by $u(r, 0) = A, \partial_n u(r, \Theta) = B$, then $\alpha_k = \frac{(k + \frac{1}{2})\pi}{\Theta}$ and

- If $\Theta \neq \frac{\pi}{2}, \frac{3\pi}{2}$,

$$u(r, \theta) = A + \frac{B}{\cos(\Theta)} r \sin(\theta) + \sum_{k=0}^{\infty} \alpha_k r^{\alpha_k} \sin(\alpha_k \theta);$$

- If $\Theta = \frac{\pi}{2}, \frac{3\pi}{2}$,

$$u(r, \theta) = A + (-1)^{l+1} \frac{Br}{\Theta} (\log(r) \sin(\theta) + \theta \cos(\theta)) + \sum_{k=0}^{\infty} \alpha_k r^{\alpha_k} \sin(\alpha_k \theta),$$

with $l = 0$ if $\Theta = \frac{\pi}{2}$ and $l = 1$ if $\Theta = \frac{3\pi}{2}$;

- For Neumann-Dirichlet boundary conditions given by $\partial_n u(r, 0) = A, u(r, \Theta) = B$, then $\alpha_k = \frac{(k + \frac{1}{2})\pi}{\Theta}$ and

- If $\Theta \neq \frac{\pi}{2}, \frac{3\pi}{2}$,

$$u(r, \theta) = B - Ar \sin(\theta) + \frac{A \sin(\Theta)}{\cos(\Theta)} r \cos(\theta) + \sum_{k=0}^{\infty} \alpha_k r^{\alpha_k} \cos(\alpha_k \theta);$$

- If $\Theta = \frac{\pi}{2}, \frac{3\pi}{2}$,

$$u(r, \theta) = B - \frac{Ar}{\Theta} (\log(r) \cos(\theta) - \theta \sin(\theta)) - Ar \sin(\theta) + \sum_{k=0}^{\infty} \alpha_k r^{\alpha_k} \cos(\alpha_k \theta);$$

- For Neumann-Neumann boundary conditions given by $\partial_n u(r, 0) = A, \partial_n u(r, \Theta) = B$, then $\alpha_k = \frac{k\pi}{\Theta}$ and

- If $\Theta \neq \pi, 2\pi$,

$$u(r, \theta) = -Ar \sin(\theta) - \frac{B + A \cos(\Theta)}{\sin(\Theta)} r \cos(\theta) + \sum_{k=0}^{\infty} \alpha_k r^{\alpha_k} \cos(\alpha_k \theta);$$

- If $\Theta = \pi, 2\pi$,

$$u(r, \theta) = -Ar \sin(\theta) + \frac{(-1)^l B - A}{\Theta} r (\log(r) \cos(\theta) - \theta \sin(\theta)) + \sum_{k=0}^{\infty} \alpha_k r^{\alpha_k} \cos(\alpha_k \theta);$$

with $l = 0$ if $\Theta = \pi$ and $l = 1$ if $\Theta = 2\pi$.

Remark C.1.1. Observe that if the wedge domain is rotated by some angle θ_1 (see Figure (C.1)) one can consider the translation $\theta^* = \theta - \theta_1$, where θ^* is the angle on the “correct” wedge domain, see Figure (4.1).

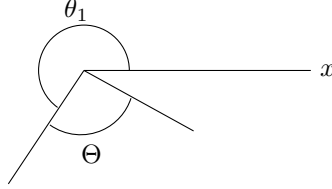


Figure C.1: Rotation of the wedge domain.

In applications, we are mostly concerned with Dirichlet-Neumann and Neumann-Dirichlet boundary conditions. Just like stated above, some of these boundary conditions have different expansions for the angles $\Theta = \frac{\pi}{2}$ and $\Theta = \frac{3\pi}{2}$. However, we are only concerned with the expansion

$$v(r, \theta) = \sum_{k=0}^{\infty} \alpha_k r^{\alpha_k} \psi(\alpha_k \theta)$$

where $\psi = \sin$ or $\psi = \cos$. In these cases, if we neglect the other terms, for the special angle $\Theta = \frac{\pi}{2}$ above we would find that $\alpha_k \in \mathbb{N}$. Without going into much depth in singularity analysis, then its partial derivative $\partial_r v(r, \theta)$ would be of the form

$$\partial_r v(r, \theta) = \sum_{k=0}^{\infty} \alpha_k^2 r^{\alpha_k - 1} \psi(\alpha_k \theta)$$

where $\alpha_k - 1 \in \mathbb{N}$ for every integer k . In general, if $\alpha_k \in \mathbb{N}$ for some angle Θ then all of its derivatives are continuous and $v(r, \theta)$ is analytical. More precisely, there is no singularity in these cases nor regularity loss. Therefore, one does not need to enrich the set of basis functions since the fundamental solutions correctly reproduce the behavior near the corner's tip.

Note that in the expansions provided above, the term $r^{-\alpha_k}$ is absent. This omission is a consequence of addressing an interior problem. It's worth highlighting that when dealing with the exterior problem, the terms r^{α_k} are substituted with $r^{-\alpha_k}$, adhering to the asymptotic conditions necessary for establishing the well-posedness of the exterior problem.

C.2 The Subspace Angle Technique

One of the drawbacks of the MFS is the ill-conditioning of the system. In this subsection we introduce the so-called *Subspace Angle Technique*, first presented in [BT05]. Intuitively, there are two problems at play: firstly, while the MFS only needs the boundary data to approximate the solution of the BVP, the exponential growth of the condition number against its exponential convergence can be seen has

the lack of information given by the collocation points on the boundary, which is not enough to decide if an approximate eigenfunction is spurious; secondly, while we proved the linear independence of the basis functions, in practice the columns of the matrix $A(k)$ are almost linear dependent if its number is too large (in fact, this is, once again, associated with the distance from the boundary to the artificial boundary).

To solve the first problem, we add additional interior points in order to over-determine the system; and for the second problem, we construct an orthonormal basis of the column space of $A(k)$, denoted by $\mathcal{C}(A(k))$, using the QR factorization of $A(k)$. Let M_B be the number of boundary points and M_I the number of interior points, such that $M = M_B + M_I$. Then, by adding some interior points, matrix $A(k)$ can be extended to

$$A(k) = \begin{bmatrix} A_B(k) \\ A_I(k) \end{bmatrix},$$

where the indices B and I correspond to the block matrices with the boundary and interior collocation points, respectively. To generate an orthonormal basis of the column space of $A(k)$, consider the QR factorization of $A(k)$, given by $A(k) = Q(k)R(k)$, where $Q(k)$ is a unitary complex (possible non-rectangular) matrix. By partitioning $Q(k)$ in the boundary and interior collocation points, we also have

$$Q(k) = \begin{bmatrix} Q_B(k) \\ Q_I(k) \end{bmatrix},$$

and each unit vector $u \in \mathcal{C}(A(k))$ has the form

$$u = \begin{bmatrix} u_B \\ u_I \end{bmatrix} = Q(k)v = \begin{bmatrix} Q_B(k) \\ Q_I(k) \end{bmatrix} v \quad (\text{C.1})$$

for some $v \in \mathbb{R}^2$, $\|v\| = 1$. Assuming homogeneous Dirichlet boundary conditions, we are interested in non-trivial solutions $v \in \mathbb{R}^2$ to problem (C.1) when $u \approx 0$ at the boundary, i.e., to solve the constrained minimization problem

$$\min_{v \in \mathbb{R}^2, \|v\|=1} \|Q_B(k)v\|.$$

The above problem is easy to solve and has a closed-form solution which can be found using Lagrange multipliers. The solution \tilde{v} is the right singular vector of $Q_B(k)$ associated with the smallest singular value σ_N and

$$\sigma_N(k) = \|Q_B(k)\tilde{v}\|.$$

Let $\tilde{u} = Q(k)\tilde{v}$. By taking the norm on both sides of equation (C.1), one can write

$$1 = \|\tilde{u}\|^2 = \left\| \begin{bmatrix} Q_B(k) \\ Q_I(k) \end{bmatrix} \tilde{v} \right\|^2 = \sigma_N^2(k) + \|Q_I(k)\tilde{v}\|^2. \quad (\text{C.2})$$

Notice how equation (C.2) can be used to eliminate spurious solutions: since $0 < \sigma_N < 1$, if $\sigma_N \approx 1$, then $Q_I(k)\tilde{v} \approx 0 \implies u_I \approx 0$ which is an incorrect solution (is zero on the interior and does not satisfy the boundary constraints); on the other hand, if $\sigma_N \approx 0$, then we found an eigenfunction which is small on the boundary points and whose interior is not null.

The name Subspace Angle Technique comes from the fact that σ_N is related to the angle between the subspaces $\mathcal{C}(A(k))$ and \mathcal{G}_0 , the space of vectors that are zero at boundary points¹. The angle $\phi(k) = \angle(\mathcal{C}(A(k)), \mathcal{G}_0)$ between both subspaces is defined by

$$\cos \phi(k) = \sup_{\substack{u \in \mathcal{C}(A(k)), \|u\|=1 \\ v \in \mathcal{G}_0, \|v\|=1}} (u, v),$$

and one can prove (cf. [BT05]) that

$$\sigma_N = \sin \phi(k).$$

Therefore, the discrete problem has a non-trivial solution (i.e., λ is an eigenvalue of the Laplace operator) if and only if $\mathcal{C}(A(k))$ and \mathcal{G}_0 have a non-trivial intersection (i.e., $\phi(k) = l\pi$, $l \in \mathbb{Z}$).

Remark C.2.1. *While the construction above assumed homogeneous Dirichlet boundary conditions, it can be easily generalized to any type of homogeneous boundary conditions \mathcal{B} by considering the appropriate A matrix.*

Remark C.2.2. *Neither the enrichment technique with particular solutions nor the Subspace Angle Technique are specific methods only applicable to the Laplace equation and the Helmholtz equation, respectively. They can be used for both equations at the same time. For example, in [AV10], both methods were used to study the spectrum of the Laplace operator in domains with corners and cracks.*

¹ \mathcal{G}_0 can be seen as the discretization of the functions which satisfy the boundary conditions but not the Helmholtz equation.



On Bessel Functions

In this appendix, we present some theory of Bessel functions, which naturally arise in the study of the Helmholtz equation in polar coordinates, and play a crucial role in proving Proposition 3.2.3. We begin by presenting some of their properties and relationships, followed by the proof of the fundamental solution of the Laplace operator. Much of the content in this appendix draws from the classical reference [ASR88] and from [CZ10].

Let $\nu \in \mathbb{C}$. Bessel functions are the solutions $y(x)$ of the differential equation

$$x^2 \frac{\partial^2 y}{\partial x^2} + x \frac{\partial y}{\partial x} + (x^2 - \nu^2)y = 0. \quad (\text{D.1})$$

Since equation (D.1) is a second-order linear differential equation, its two linearly independent solutions are the Bessel functions of first kind and second kind, J_ν and Y_ν , respectively. The Bessel function of first kind can be represented by the series

$$J_\nu(z) = \left(\frac{1}{2}z\right)^\nu \sum_{k=0}^{\infty} \frac{\left(-\frac{1}{4}z^2\right)^k}{k! \Gamma(\nu + k + 1)},$$

where $\Gamma(z) = \int_0^\infty t^{z-1} e^{-t} dt$ is the special Gamma function. For the Bessel function of second kind, series expansions are only available for non-negative integers ν . For non-integers the relation (D.2)

holds

$$Y_\nu(z) = \frac{J_\nu(z) \cos(\nu\pi) - J_{-\nu}(z)}{\sin(\nu\pi)}, \quad (\text{D.2})$$

where the right-hand side is replaced by its limiting value if ν is an integer or zero.

Both functions are holomorphic through the complex plane cut along the negative real axis. If $\nu \in \mathbb{N}$, then J_ν is an entire function, i.e., holomorphic in the whole complex plane. In any other cases, both Bessel functions display a singularity on the origin: if $\nu > 0$ then $J_\nu(0) = 0$, but it is not differentiable at the origin. Figures D.1 and D.2 show the Bessel functions of first and second kinds. The plots were created using Wolfram Mathematica 13.3.1.0.

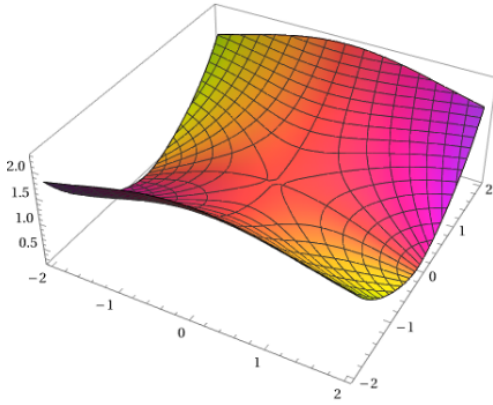


Figure D.1: Complex plot of the absolute value of the Bessel function $J_\nu(z)$ with $\nu = 0$ in the complex plane from $-2-2i$ to $2+2i$. The plots are colored by the argument of the function and the colorbar shows its variation from $-\pi$ to π .

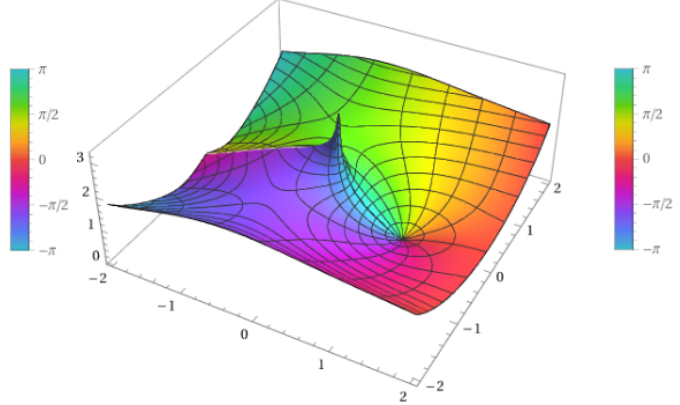


Figure D.2: Complex plot of the absolute value of the Bessel function $Y_\nu(z)$ with $\nu=0$ in the complex plane from $-2-2i$ to $2+2i$. The plots are colored by the argument of the function and the colorbar shows its variation from $-\pi$ to π .

A particularly important Bessel function in this work was the Bessel functions of third kind, known as Hankel functions $H_\nu^{(1)}(z), H_\nu^{(2)}(z)$. Those functions are also known as the Hankel function of first and second kind, respectively, and are defined using the $J_\nu(z)$ and $Y_\nu(z)$ Bessel functions:

$$H_\nu^{(1)}(z) = J_\nu(z) + iY_\nu(z)$$

$$H_\nu^{(2)}(z) = J_\nu(z) - iY_\nu(z),$$

and therefore also satisfy equation (D.1).

Figures D.3 and D.4 show the Hankel functions of first and second kinds and Proposition D.0.1 presents the asymptotic expansions for small and large arguments of $H_\nu^{(1)}(z)$ and $H_\nu^{(2)}(z)$.

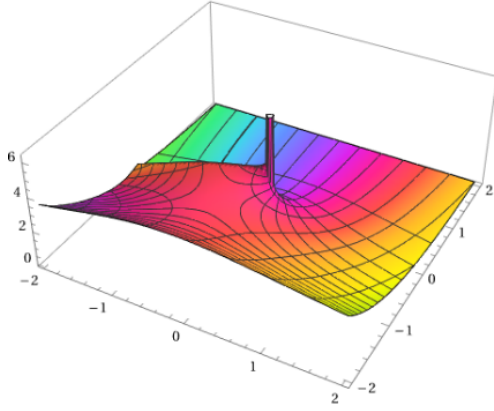


Figure D.3: Complex plot of the absolute value of the Hankel function $H_\nu^{(1)}(z)$ with $\nu = 0$ in the complex plane from $-2 - 2i$ to $2 + 2i$. The plots are colored by the argument of the function and the colorbar shows its variation from $-\pi$ to π .

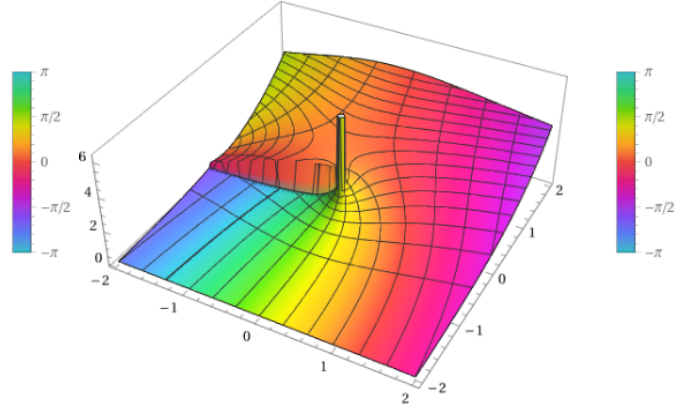


Figure D.4: Complex plot of the absolute value of the Hankel function $H_\nu^{(2)}(z)$ with $\nu=0$ in the complex plane from $-2 - 2i$ to $2 + 2i$. The plots are colored by the argument of the function and the colorbar shows its variation from $-\pi$ to π .

Proposition D.0.1. Let $\nu \in \mathbb{C}$. The limiting forms of the Hankel functions $H_0^{(1)}(z)$ and $H_0^{(2)}(z)$ for a small argument z take the form,

$$H_\nu^{(1)}(z) \sim \begin{cases} -\frac{2\pi}{i} \log z, & \nu = 0 \\ \frac{1}{i\pi} \Gamma(\nu) \left(\frac{1}{2}z\right)^{-\nu}, & \nu \neq 0 \end{cases}$$

and

$$H_\nu^{(2)}(z) \sim \begin{cases} \frac{2\pi}{i} \log z, & \nu = 0 \\ -\frac{1}{i\pi} \Gamma(\nu) \left(\frac{1}{2}z\right)^{-\nu}, & \nu \neq 0, \end{cases}$$

when $z \rightarrow 0$ and $\text{Re}\{\nu\} \geq 0$. On the other hand, the asymptotic expansions for large arguments are

$$H_\nu^{(1)}(z) \sim \sqrt{\frac{2}{\pi z}} e^{i(z - \frac{1}{2}\nu\pi - \frac{1}{4}\pi)}, \text{ if } -\pi < \arg z < 2\pi$$

$$H_\nu^{(2)}(z) \sim \sqrt{\frac{2}{\pi z}} e^{-i(z - \frac{1}{2}\nu\pi - \frac{1}{4}\pi)}, \text{ if } -2\pi < \arg z < \pi$$

when $|z| \rightarrow \infty$.

Before presenting the proof of the Helmholtz equation's fundamental solution, some recurrence relations are stated, which were used in the proof of Proposition 3.2.3.

Proposition D.0.2. Let \mathcal{Z}_ν denote $J_\nu, Y_\nu, H_\nu^{(1)}$ or $H_\nu^{(2)}$ for any $\nu \in \mathbb{C}$. The following recurrence relations hold:

$$\begin{aligned}\mathcal{Z}_{\nu-1}(z) + \mathcal{Z}_{\nu+1}(z) &= \frac{2\nu}{z} \mathcal{Z}_\nu(z) \\ \mathcal{Z}_{\nu-1}(z) - \mathcal{Z}_{\nu+1}(z) &= 2 \frac{d\mathcal{Z}_\nu(z)}{dz} \\ \frac{d\mathcal{Z}_\nu(z)}{dz} &= \mathcal{Z}_{\nu-1}(z) - \frac{\nu}{z} \mathcal{Z}_\nu(z) \\ \frac{d\mathcal{Z}_\nu(z)}{dz} &= -\mathcal{Z}_{\nu+1}(z) + \frac{\nu}{z} \mathcal{Z}_\nu(z).\end{aligned}$$

In particular,

$$\frac{d\mathcal{Z}_0(z)}{dz} = -\mathcal{Z}_1(z).$$

Let $k \in \mathbb{C}$ such that $\text{Im}\{k\} \geq 0$ and $\Phi_k(x)$ be the fundamental solution of the Helmholtz equation, i.e.,

$$-(\Delta \Phi_k(x) + k^2 \Phi_k(x)) = \delta_0(x). \quad (\text{D.3})$$

First, one proves that equation (D.3) is invariant under rotations.

Lemma D.0.3. Let $\Phi_k(x)$ be a solution of equation (D.3). Then, $\Phi_k(Rx)$ is also a solution, where R is a rotation (orthogonal) matrix, such that $R^T = R^{-1}$.

Proof. The proof is straightforward and only uses the chain rule. Let $\psi(x) = \Phi_k(Rx)$. Then,

$$\begin{aligned}\nabla \psi(x) &= R^T \nabla \Phi_k(Rx) \\ \Delta \psi(x) &= R^T R \Delta \Phi_k(Rx) = \Delta \Phi_k(Rx)\end{aligned}$$

by the orthogonality property of matrix R . Since R is a bijective map from \mathbb{R}^2 to \mathbb{R}^2 , the claim follows. \square

Proposition D.0.4. The function $\Phi_k : \mathbb{R}^d \setminus \{0\} \rightarrow \mathbb{R}$ given by

$$\Phi_k(x) = \begin{cases} \frac{i}{4} H_0^{(1)}(k\|x\|), & d = 2 \\ \frac{e^{ik\|x\|}}{4\pi\|x\|}, & d = 3 \end{cases}$$

is the fundamental solution of the Helmholtz equation (D.3).

Proof. Let $x \in \mathbb{R}^d \setminus \{0\}$ and Φ_k be the solution of

$$\Delta \Phi_k(x) + k^2 \Phi_k(x) = 0. \quad (\text{D.4})$$

Considering equation (D.4) in polar coordinates, by Lemma D.0.3 it suffices to consider the radial part of equation

$$\frac{1}{r^{d-1}} \frac{d}{dr} \left(r^{d-1} \frac{d\Phi_k(r)}{dr} \right) + k^2 \Phi_k(r) = 0 \iff \frac{d}{dr} \left(r^{d-1} \frac{d\Phi_k(r)}{dr} \right) + k^2 r^{d-1} \Phi_k(r) = 0. \quad (\text{D.5})$$

Through the change of variables $\Phi_k(r) = r^{1-\frac{d}{2}}\psi(r)$, the equation (D.5) above can be written as

$$\frac{d}{dr} \left(r \frac{d\psi(r)}{dr} \right) + \left(k^2 r - \frac{\left(\frac{1}{2}d - 1\right)^2}{r} \right) \psi(r) = 0,$$

and after differentiating the first term and multiplying by r one finds that

$$r^2 \frac{d^2\psi(r)}{dr^2} + r \frac{d\psi(r)}{dr} + \left((kr)^2 - \left(\frac{1}{2}d - 1\right)^2 \right) \psi(r) = 0.$$

Making another change of variables $\rho = kr$ one obtains the equation (D.1)

$$\rho^2 \frac{d^2\psi(\rho)}{d\rho^2} + \rho \frac{d\psi(\rho)}{d\rho} + \left(\rho^2 - \left(\frac{1}{2}d - 1\right)^2 \right) \psi(\rho) = 0,$$

whose solution (in the complex numbers) is given by the Hankel functions (or order $\frac{1}{2}d - 1$)

$$\psi(\rho) = AH_{\frac{1}{2}d-1}^{(1)}(\rho) + BH_{\frac{1}{2}d-1}^{(2)}(\rho),$$

where $A, B \in \mathbb{C}$ and

$$\Phi_k(r) = r^{1-\frac{d}{2}} \left(AH_{\frac{1}{2}d-1}^{(1)}(kr) + BH_{\frac{1}{2}d-1}^{(2)}(kr) \right).$$

Since Φ_k must satisfy the radiation conditions 4.1.13 and $\text{Im}\{k\} \geq 0$, it implies that $B = 0$ by Proposition D.0.1 and

$$\Phi_k(r) = r^{1-\frac{d}{2}} AH_{\frac{1}{2}d-1}^{(1)}(kr).$$

To find A , one integrates equation (D.3) on the ball $B_\epsilon(0)$, apply the Divergence Theorem B.0.1 and by Proposition D.0.1

$$\int_{\partial B_\epsilon(0)} \frac{\partial \Phi_k}{\partial n} d\sigma \rightarrow -1, \epsilon \rightarrow 0.$$

On the other hand

$$\int_{\partial B_\epsilon(0)} \frac{\partial \Phi_k}{\partial n} d\sigma = |\partial B_1(0)| \epsilon^{d-1} \Phi'_k(\epsilon)$$

which implies that

$$|\partial B_1(0)| \epsilon^{d-1} \Phi'_k(\epsilon) \rightarrow -1, \epsilon \rightarrow 0. \quad (\text{D.6})$$

From Proposition D.0.2, equation (D.6) above can be written as

$$-Ak |\partial B_1(0)| \epsilon^{\frac{d}{2}} H_{\frac{d}{2}}^{(1)}(k\epsilon) \rightarrow -1, \epsilon \rightarrow 0,$$

which is asymptotically equal to

$$Ak |\partial B_1(0)| \frac{i 2^{\frac{d}{2}} \Gamma(\frac{d}{2})}{\pi} \rightarrow -1, \epsilon \rightarrow 0$$

by Proposition D.0.1, and

$$A = \frac{i \pi 2^{-\frac{d}{2}} k^{\frac{(d-2)}{2}}}{\Gamma(\frac{d}{2}) |\partial B_1(0)|}.$$

Since $|\partial B_1(0)| = \frac{2\pi^{\frac{d}{2}}}{\Gamma(\frac{1}{2}d)}$, and for $d = 3$

$$H_{\frac{1}{2}}^{(1)}(z) = \frac{1}{i} \sqrt{\frac{2}{\pi}} \frac{e^{iz}}{\sqrt{z}},$$

the fundamental solution of the Helmholtz equation is given by

$$\Phi_k(r) = \begin{cases} \frac{i}{4} H_0^{(1)}(kr), & d = 2 \\ \frac{e^{ikr}}{4\pi r}, & d = 3. \end{cases}$$

□

Figures D.5 and D.6 show the real and imaginary part of the fundamental solution $\frac{i}{4} H_0^{(1)}(kr)$, respectively.

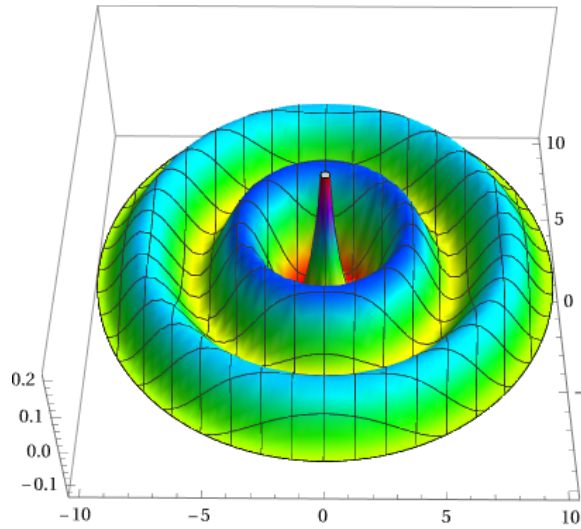


Figure D.5: Plot of the real part of $\Phi_k(r)$ with $k = 1.5$ in the disk of radius 10.

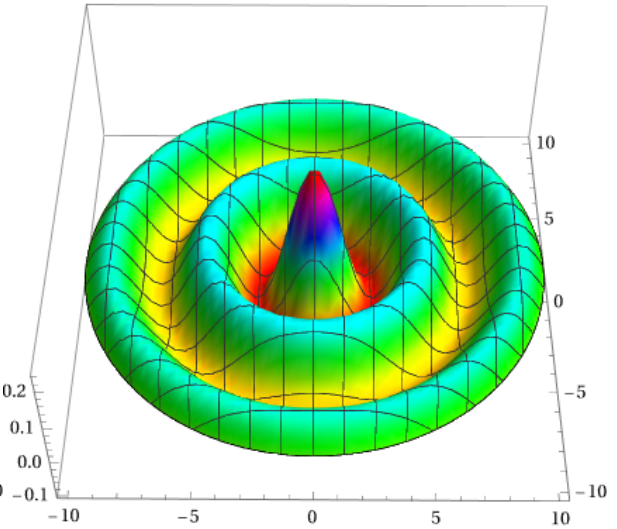


Figure D.6: Plot of the imaginary part of $\Phi_k(r)$ with $k = 1.5$ in the disk of radius 10.